

CORROSION INITIATION AND PROPAGATION ON CORROSION RESISTANT
ALLOYS EMBEDDED IN CONCRETE BY ACCELERATED CHLORIDE
TRANSPORT

by

Francisco Gutierrez Tellez

A Thesis Submitted to the Faculty of
The College of Engineering and Computer Science
in Partial Fulfillment of the Requirements for the Degree of
Master of Science

Florida Atlantic University

Boca Raton, FL

August 2013

CORROSION INITIATION AND PROPAGATION ON CORROSION RESISTANT
ALLOYS EMBEDDED IN CONCRETE BY ACCELERATED CHLORIDE
TRANSPORT

by

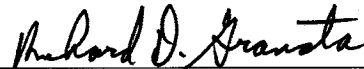
Francisco Gutierrez

This thesis was prepared under the direction of the candidate's thesis advisor, Dr. Francisco Presuel-Moreno, Department of Ocean & Mechanical Engineering, and has been approved by the members of his supervisory committee. It was submitted to the faculty of the College of Engineering and Computer Science and was accepted in partial fulfillment of the requirements for the degree of Master of Science.

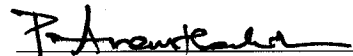
SUPERVISORY COMMITTEE:



Francisco Presuel-Moreno, Ph.D.
Thesis Advisor



Richard Granata, Ph.D.



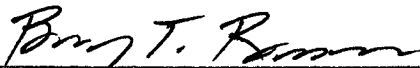
P. Ananthakrishnan, Ph.D.



Javad Hashemi, Ph.D.
Chair, Department of Ocean & Mechanical Engineering



Mohammad Ilyas, Ph.D.
Interim Dean, College of Engineering and Computer Science



Barry T. Rosson, Ph.D.
Dean, Graduate College

July 18, 2013
Date

ACKNOWLEDGEMENTS

I would like to express my sincere thanks and appreciation to my advisor Dr. Francisco Presuel-Moreno for his invaluable direction, profound patience and constant encouragement during the entire course of this research project.

I would also like to thank the members of my graduate committee for their guidance and suggestions, especially Dr. Granata and Dr. Ananthakrishnan.

I acknowledge the Florida Department of Transportation for financial support and preparation of the specimens for this project, and Outokumpu for providing the corrosion resistant alloys.

I would like to thank all my colleagues from the Marine Materials and Corrosion Laboratory at FAU for their help.

Last but not least, I would like to deeply thank my lovely wife Mena, my mother Camila, and my beautiful family for their support, encouragement and most of all their understanding throughout my study. For them I dedicate this thesis.

ABSTRACT

Author: Francisco Gutierrez
Title: Corrosion Initiation and Propagation on Corrosion Resistant Alloys
Embedded In Concrete by Accelerated Chloride Transport
Institution: Florida Atlantic University
Advisor: Dr. Francisco Presuel-Moreno
Degree: Master of Science
Year: 2013

Two duplex stainless steels rebars: UNS32304SS and UNS32101SS, were selected to investigate the corrosion initiation and propagation in reinforced concrete specimens. The investigation is divided in two phases with two different methods to accelerate the transport of chlorides through the concrete and initiate corrosion in a short period of time. After corrosion had initiated and propagated for some time; selected specimens were terminated for visual examination. On specimens selected for autopsy, the rebars in the top row showed corrosion to various degrees. Corrosion had propagated to such extent on the terminated specimens that the specimen showed cracks. Stray current might have caused accelerated corrosion on rebars where corrosion had initiated. Based on chloride concentrations measured at the rebar trace, corrosion initiated: on S32101 rebars on average at 7.9 kg/m^3 , and S32101 rebars on average at 6.0 kg/m^3 . The findings suggest that S32304 rebars corroded at a slower than S32101.

CORROSION INITIATION AND PROPAGATION ON CORROSION RESISTANT
ALLOYS EMBEDDED IN CONCRETE BY ACCELERATED CHLORIDE
TRANSPORT

LIST OF TABLES	viii
LIST OF FIGURES	ix
1.1 Research Background.....	1
1.2 Research Objective.....	3
2 LITERATURE REVIEW	4
2.1 Stainless Steel.....	4
2.2 Mechanism of Corrosion Steel/Concrete	7
2.3 Factors Affecting the Propagation of Corrosion	9
2.4 Accelerated Corrosion Test.....	11
2.5 Migration Ions Transport	12
3 APPROACH.....	14
3.1 Specimens and Materials.....	14
3.2 Chloride Transport Methods	18
3.3 Method during Phase I	18
3.4 Phase II Electric Field Method.....	19

3.5	Linear Polarization Resistance (LPR) and Electrochemical Impedance Spectroscopy (EIS)	22
3.6	Autopsy of Terminated Specimen.....	23
3.7	Chloride Analysis.....	26
4	RESULTS/DISCUSSION	27
4.1	Phase I	27
4.2	Phase II.....	28
4.2.1	Potentials Measurements upon Electric Field Removal	28
4.2.2	Solution Resistance -Electrochemical Impedance Spectroscopy (EIS) Measurements.....	33
4.2.3	Linear Polarization Resistance (LPR) and Electrochemical Impedance Spectroscopy (EIS) Measurements	36
4.2.4	Observed Surface Cracks	41
4.3	Specimens Terminated and Dissected.....	47
4.3.1	Specimen 1-1 Termination and Dissection	47
4.3.2	Specimen 1-2 Termination and Dissection	51
4.3.3	Specimen 2-1 Termination and Dissection	54
4.3.4	Specimen 2-2 Termination and Dissection	57
4.4	Chloride Analysis.....	61
4.5	Chloride Threshold of Austenitic and Duplex Stainless Steels.....	62
4.6	Localized corrosion penetration causing concrete cover to cracks	66
5	CONCLUSION	73
6	APPENDIX A. FIGURES & TABLES.....	74
7	APPENDIX B.....	100

REFERENCE.....	102
----------------	-----

LIST OF TABLES

Table 1 Common types of stainless steel used as reinforcement.....	4
Table 2 Chemical elements on steel and its properties	5
Table 3 PREN Numbers of different stainless steel.....	6
Table 4 Projected Chloride at the rebar depth ($d=2.54$ cm) for different reinforcement [2]	7
Table 5 Mix design	14
Table 6 Reinforcement chemical composition	16
Table 7 Chloride concentration at rebar trace (kg/m^3) and chloride by weight cementitious percentage (WC%) for Batch 1-1 and Batch 1-2	63
Table 8 Chloride concentration at rebar trace (kg/m^3) and chloride by weight cementitious percentage (WC%) for Batch 2-1 and Batch 2-2	63
Table 9 Critical Chloride Threshold Value for different authors and steels by Weight by cement (WC) %	65
Table 10 Mass loss approximation and parameters	68
Table 11 values for different equations and parameters	71
Table 12 Applied voltage schedule.....	74

LIST OF FIGURES

Figure 1 Schematic illustrations of the initiation and propagation stage in reinforced concrete [1]	2
Figure 2 Schematic representation of the electrochemical reaction steel/concrete	8
Figure 3 Schematic representation of pitting corrosion of steel in concrete.....	9
Figure 4 schematic representation of the migration test	13
Figure 5 Specimen at cast	15
Figure 6 Sample schematic, dimensions and specifications	17
Figure 7 Picture of the specimen	17
Figure 8 OCP measurement components.....	19
Figure 9 High humidity chamber.....	20
Figure 10 Electric field set up.....	21
Figure 11 Cores cuts and dimensions	24
Figure 12 Schematic illustration of the concrete sectioning for specimens as listed in dissection steps 4 and 5 above.....	26
Figure 13 Batch 1 & batch 2 potential measurements over time for Phase I.....	28
Figure 14 Plots symbols clarification	31

Figure 15 Batch 1 samples OCP measurements over time for Phase II	31
Figure 16 Batch 2 samples OCP measurements over time for Phase II	33
Figure 17 solution resistance plot over time for samples batch 1-1 and 1-2	35
Figure 18 Solution resistance plot over time for samples batch 2-1 and 2-2.....	36
Figure 19 R_p -meas- R_s over time for Phase II plots of samples Batch 1-1 and 1-2	39
Figure 20 Batch 2 samples R_p -meas- R_s over time for Phase II.....	41
Figure 21 Diagram of the crack evolution over time for specimen batch 1-1	42
Figure 22 Lateral cracks pictures for specimen Batch 1-1	43
Figure 23 Diagram of the crack evolution over time for specimen batch 2-1	44
Figure 24 final crack picture of specimen batch 1-2.....	45
Figure 25 final crack picture of specimen batch 2-2.....	47
Figure 26 Autopsy and visual examination of batch 1-1	49
Figure 27 Close-up picture of sample batch 1-1B rebar before and after cleaning	51
Figure 28 Autopsy and visual examination of batch 1-2	53
Figure 29 Close-up picture of sample batch 1-2B rebar before and after cleaning	54
Figure 30 Autopsy and visual examination of batch 2-1	56
Figure 31 Close-up picture of sample batch 2-1B rebar before and after cleaning	57
Figure 32 Specimen batch 2-2 termination rebar and autopsy picture	59
Figure 33 Close-up picture of sample batch 2-2 B before and after cleaning	60

Figure 34 Close-up picture of sample batch 2-2 A before and after cleaning	60
Figure 35 Chloride profile for specimens batch 1-1 and 2-1	62
Figure 36 Observed length L and value explanation process for specimen 1-1 rebar C.....	69
Figure 37 Observed length L and value explanation process for specimen 2-2 rebar B.....	70
Figure 38 Plot of the Xcrit values for equations (1), (2) and experimental results as a function of C/L ratio.....	72
Figure 39 Open Circuit Potential (OCP) Measurements of Phase I – Batch 1 Samples	75
Figure 40 Open Circuit Potential Measurements (OCP) of Phase I – Batch 2 Samples	76
Figure 41 OCP measurements over time for batch 1 samples at Phase II	77
Figure 42 OCP measurements over time for batch 2 samples at Phase II	78
Figure 43 Solution Resistance over time for samples batch 1 phase II	79
Figure 44 Solution Resistance over time for samples batch 2 phase II	80
Figure 45 Rp_meas-Rs over time for batch 1 samples at Phase II	81
Figure 46 Rp_meas-Rs over time for batch 2 samples at Phase II	82
Figure 47 Crack by inspection day for batch 1 and 2	83
Figure 48 Autopsy and visual examination of bottom rebars batch 1-1	93

Figure 49 Close-up picture of sample batch 1-1A rebar before and after cleaning	93
Figure 50 Close-up picture of sample batch 1-1C rebar before and after cleaning	94
Figure 51 Autopsy and visual examination of bottom rebars batch 1-2	95
Figure 52 Close-up pictures before and after cleaning for batch 1-2	96
Figure 53 Autopsy and visual examination of bottom rebars batch 2-1	97
Figure 54 Close-up pictures before and after cleaning for batch 2-1	97
Figure 55 Pictures Autopsy bottom rebars for batch 2-2	99

INTRODUCTION

1.1 Research Background

Corrosion of the reinforcing steel due to chloride ions is a major problem that bridges and other structures face when exposed to marine environments. There are two periods that model the service life of a reinforced concrete structure: 1) time to corrosion initiation, (once a critical chloride threshold concentration (C_T) is exceeded) and 2) corrosion propagation stage [1] [2]. The time to corrosion initiation of corrosion resistant alloys (CRAs) embedded in concrete is expected to be significantly longer than for carbon steel. The prolonged time to corrosion initiation is due to the high C_T of these alloys. CRAs have the property of resisting higher concentration of chloride reaching the surface of the reinforcement before corrosion initiates; than typical reinforcing steel alloys used (such as carbon steel [1] [2]). Once C_T is exceeded corrosion initiates. Then, the corrosion propagation stage begins.

Corrosion propagation stage is usually assumed to last a few years (typically five years). This duration applies to carbon steel rebar embedded in concrete of moderate durability. It is unknown how long would the propagation stage would last for CRAs or how corrosion would spread during the propagation stage. Most experimental work has

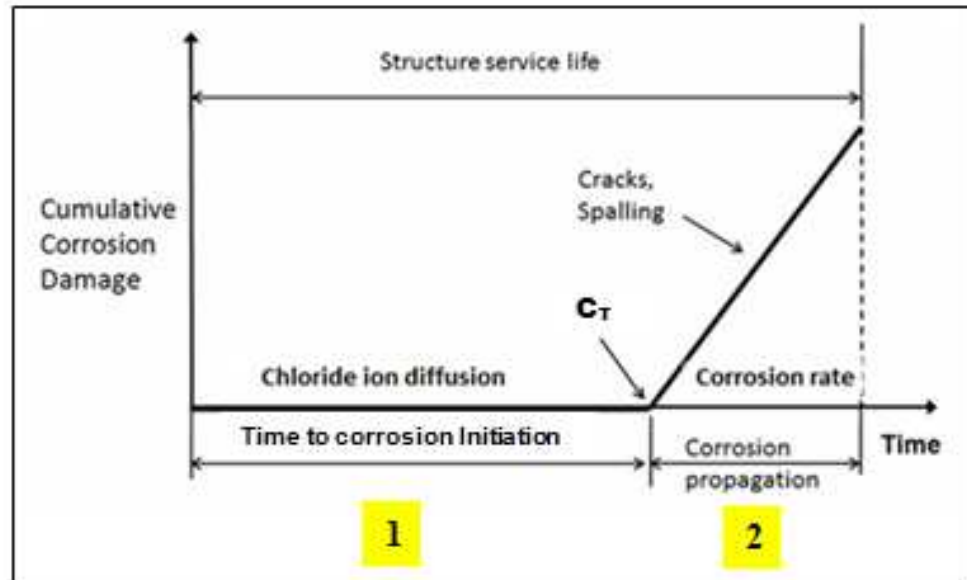


Figure 1 Schematic illustrations of the initiation and propagation stage in reinforced concrete [1]

been done to determine the time to corrosion initiation and chloride threshold with the specimens terminated shortly after corrosion has initiated. Several authors have investigated corrosion of the CRAs as an alternative to carbon steel reinforcement as an approach to achieve bridge repair-free service life in excess of 75 years. Currently a couple of US state DOTs (Virginia and Oregon) require CRAs rebars be used in new bridge construction exposed to aggressive chlorides environments. Previous studies [1] [2] [3] have identified duplex stainless steel and austenitic stainless steel (with high PREN and with Ni and Mo) as alloys with a high chloride threshold. One of the methods developed to determine the chloride threshold concentration was to do an anodic potential hold (+200 mV_{sce}) on the studied alloy while exposed to simulated pore solution with chlorides [4] [5] Tests in solution provided comparable ranking of the different alloys. However, not enough time was usually allowed during initial immersion in simulated

pore solution for a mature/thick passive layer to form before adding the chlorides. A mature passive layer is expected to be present on CRAs embedded in concrete when the chlorides ions arrive. Based on previous studies, that reported chloride thresholds, a relative high chloride concentration was usually first added to the solution when the more corrosion resistant alloys were exposed. In recent years the use of corrosion resistant alloys (e.g. duplex stainless steels) has been suggested as a way to achieve a long maintenance-free service life [3]. Two corrosion resistance alloys (CRA) duplex stainless steels rebars: UNS32304 and UNS32101 embedded in concrete were selected in this study to investigate corrosion initiation and corrosion propagation stages.

1.2 Research Objective

The project objectives are as follows:

1. To develop methods that allows the initiation of corrosion via accelerated chloride transport in a short period of time.
2. To better understand the corrosion propagation stage in CRAs reinforcements embedded in concrete.
3. To autopsy and determine the extent of corrosion during the early period of the propagation stage.

2 LITERATURE REVIEW

2.1 Stainless Steel

Stainless steel is currently being considered during the design of new structures as reinforcement for the most critical areas of reinforced concrete structures (such as tidal zone and splash zone, in partially submerged structures or external areas in bridges) to improve the structural durability [1] [3] [6]. The two most common types of stainless steel used as reinforcement are:

Table 1 Common types of stainless steel used as reinforcement

Stainless steel group	Example EN Grades	Example US Grades	Example UNS Grades
Austenitic	1.4301	304	S30400
	1.4436	316	S31600
Duplex	1.4462	2205	S31803/S32205
	1.4362	2304	S32304
	1.4162	2101	S32101

When comparing duplex stainless steel to other austenitic stainless steel, lean duplex alloys have been found to have higher mechanical strength, equal or better corrosion (not

for all grades) resistance when exposed to environments containing chloride, and a cost efficient material [3] [6] when compared to austenitic and high grade duplex. Different types of stainless steel may have different properties depending on the alloy chemical elements, composition and manufacturing process [3] [6] [7]. Table 2 shows the composition and some properties by element of stainless steel [6].

Table 2 Chemical elements on steel and its properties

Element	Property
Chromium (Cr)	makes it stainless
Nickel (Ni)	increases formability and weld ability
Molybdenum (Mo)	increases corrosion resistance
Nitrogen (N)	increases strength and corrosion resistance
Copper (Cu)	increases corrosion resistance
Carbon (C)	decreases corrosion resistance, increases strength
Titanium (Ti)	reduces the negative effects of carbon
Sulfur (S)	for better machinability and weld ability
Manganese (Mn)	may substitute Nickel (austenite stabilizer)
Silicon (Si)	increase the resistance to oxidation

A measurement of the corrosion resistance of stainless steel containing nickel is called PREN (Pitting Resistance Equivalent Number) and can be expressed by the following formula:

$$\text{PREN} = \% \text{Cr} + 3.3(\% \text{Mo}) + 16(\% \text{N})$$

This parameter could be used as a reference when choosing an adequate alloy to use in construction. The higher the alloy PREN number is, the better its resistance to pitting corrosion [7]. Table 3 lists some PREN numbers as a function of the element concentration in stainless steel alloys.

Table 3 PREN Numbers of different stainless steel

Stainless steel group	Example UNS Grades	Cr	Mo	N	PREN Number
Austenitic	S30400	17.5 -19.5	NS	0.11	17.5 – 20.8
	S31600	16.5– 18.5	2.0 – 2.5	0.11	23.1 -28.7
Duplex	S31803/S32205	21.0– 23.0	2.5 – 3.5	0.10 – 0.22	30.8 -38.1
	S32304	22.0– 24.0	0.1 – 0.6	0.05 – 0.20	23.1 – 29.2
	S32101	21.0– 22.0	0.1 – 0.8	0.20 – 0.25	24.5 – 28.6

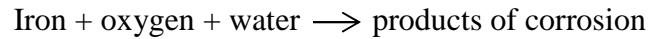
Table 4 shows the exposure time and the chloride concentration at the rebar depth reported for different reinforcement types; these values are taken from concrete exposed outdoors to weekly wet/dry cycles with 15% NaCl. No corrosion was observed on any of these at these concentrations.

Table 4 Projected Chloride at the rebar depth (d=2.54 cm) for different reinforcement [2]

Reinforcement Type	Exposure Time, days	[Cl ⁻], kg/m ³
316	1,726	13.9
304	440	10.2
2304	929	12.5

2.2 Mechanism of Corrosion Steel/Concrete

The electrochemical corrosion process of steel embedded in concrete can be illustrated by the following reactions in the presence of chloride ions in the solution [8] [9].



This is an electrochemical reaction and is composed by four processes [9] [8] (see Figure 2):

- I. The oxidation of iron (anodic process) that liberates the electrons in the metallic phase and gives rise to the formation of iron ions ($\text{Fe} \longrightarrow \text{Fe}^{2+} + 2 \text{e}^-$) whose hydrolysis produce acidity ($\text{Fe}^{2+} + 2\text{H}_2\text{O} \longrightarrow \text{Fe}(\text{OH})_2 + 2\text{H}^+$)
- II. The reduction of oxygen (cathodic process) that consumes the electrons produced in I and produces alkalinity : $\text{O}_2 + 2\text{H}_2\text{O} + 4 \text{e}^- \longrightarrow 4\text{OH}^-$
- III. The transport of electrons within the metal from the anodic regions where they become available, to the cathodic regions where they are consumed (since the electrons carry a negative charge, this gives rise to a nominal electrical current flowing in the opposite direction)

IV. Finally, in order for the circuit to be complete the flow of current inside the concrete electrolyte from the anodic regions to the cathodic regions, transport of ions in the pore solution takes place.

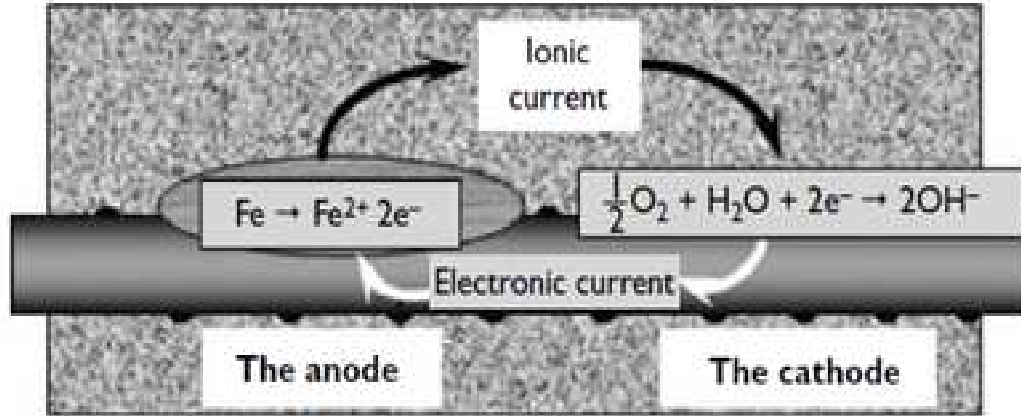


Figure 2 Schematic representation of the electrochemical reaction steel/concrete

These four processes complement each other which are to say that they occur at the same time. Steel reinforced concrete is a durable construction materials as the passive layer is formed at the steel surface, which is promoted by the concrete pore solution high alkaline environment ($\text{pH} = 12.5 - 13.5$) [1] [2]. However, when concrete is carbonated or chloride penetrates the concrete and reaches/exceeds the C_T at the rebar surface corrosion would initiate. The form of corrosion in stainless steel alloys resulting from the attack of chloride is usually pitting corrosion. The C_T that initiates pitting corrosion for this alloys structures is affected by many factors [10] [11]. The main factors are the concrete pH, i.e. the concentration of Hydroxyl ions in the pore solution, the ratio of Cl^-/OH^- , the potential of the steel and the presence of voids at the steel/concrete interface, and environmental conditions (e.g. relative humidity, temperature). Areas no longer protected

by the passive film act as anodes (active zone) with respect to the surrounding still passive areas where the cathodic reaction (primarily the oxygen reduction reaction (ORR) takes place). It has been reported that the ORR is slower in stainless steel alloys [12]. Figure 3 shows the morphology of the pitting attack.

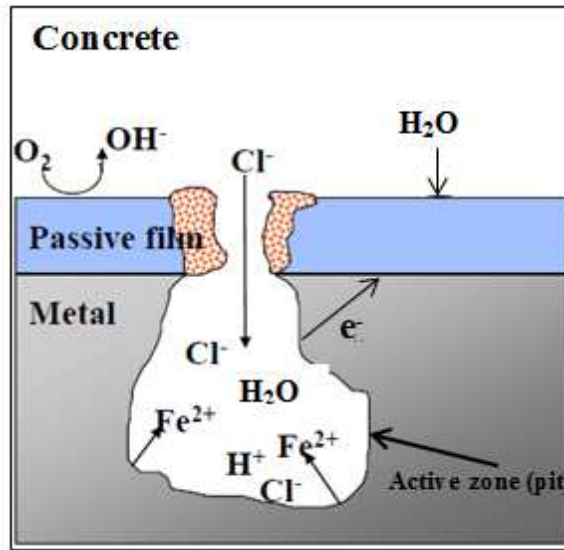


Figure 3 Schematic representation of pitting corrosion of steel in concrete

2.3 Factors Affecting the Propagation of Corrosion

The C_T of the steel depends on several factors ranging from the concrete characteristics to the alloys composition. One of the key factors is to find out the C_T of the alloys. This can be done by monitoring the open circuit potential (OCP) and its variation to more negative values. [9] [11] [13]. This fact implies that the best way of defining the C_T value may be a set of values in function of the steel potential when tested in simulated pore solution [11] [13] [14]. Factors affecting the corrosion propagation

period include: concrete porosity and interconnectivity of the pore system, concrete cover, degree of saturation, availability of water, availability of oxygen, resistivity (last three parameters both in the concrete), corrosion rate, environmental characteristics [15], characteristics of the alloy and its chemical composition. [9] [11] [12] The corrosion rate of steel in concrete can be limited by the concrete resistivity which is controlled by w/c, moisture content, and pozzolanic materials such as fly ash. Fly Ash usually reduces the porosity with time as hydration and the pozzolanic reaction progresses. It is widely understood that the corrosion rate of the submerged or fully saturated reinforced concrete is lower compared to atmospherically exposed reinforced concrete due to low oxygen concentration of the former. Previous studies have confirmed that the corrosion rate is reduced in such conditions due to insufficient supply of oxygen to the steel [9] [16]. More recently, Hussain investigated the coupled effect of oxygen and moisture on the corrosion of reinforcing steel in concrete [9] [16]. The results reported by Hussain revealed that the diffusion of oxygen is a vital limiting factor for corrosion of the rebar only when the reinforced concrete structure is either submerged or in a high RH environment with a dense concrete cover and low w/c ratio. Moreover, it is known that the ORR is slower in stainless steel alloys than on carbon steel.

Several manufacturers are producing CRAs reinforcements because of its corrosion resistant property. The C_T of this type of rebars is high, consequently it would take more time to reach this value (C_T) and corrode when comparing to carbon steel in concrete. Many researchers have investigated reinforcements embedded in concrete until the C_T take place in the steel and then terminate the specimens shortly afterward, leaving the corrosion propagation stage uninvestigated. Few researchers have investigated the

corrosion propagation stage on the duplex stainless steels rebars; most experiments have been done with rebars embedded in mortar as the geometry of the samples, or rebars submerged in solution [3] [13] [17] [2] . This research is using different geometry (simulated bridge deck) and with rebars embedded in concrete.

2.4 Accelerated Corrosion Test

To analyze and investigate the propagation stage, it would be necessary to shorten the time to corrosion initiation via accelerated chloride transport methods [10] [13] [18], among others have proposed methods to determine chloride threshold on freshly prepared specimens (usually mortar) that are exposed to cycles of wetting and drying with a chloride solution to activate corrosion in the reinforcement [1] [19] Also, samples exposed to an electric field between an electrode close to the reinforcement and a stable counter electrode [10] [13] [18] have been used to accelerate the transport of chlorides. Migration tests (e.g. Rapid chloride permeability, Nordtest Build 492 [20]) have also been developed to obtain chloride permeability into concrete after a short period of time. A combination of these methods influenced: the experimental design of the specimens and the exposure methods used in phases I and II (described in chapter 3) to accelerate chloride ion transport used in this investigation. These methods are found to be very effective to achieve the C_T on the rebars in a short period of time when comparing with the natural chloride transport process. In the developed approach; no or only minor disturbance of the passive film at the alloy surface occurred during the curing period and phase I. The implemented accelerated chloride transport can be done in a few months rather than several years. [10] [11] [18]. It is important to point it out that the time to

corrosion initiation is not just a function of the applied method, but also the type of concrete, concrete cover and alloy composition [10] [11] [18]. The accelerated methods have been validated in comparison of traditional non accelerated methods; this mean that the data collected and results are reliable. [10] [11]

2.5 Migration Ions Transport

Migration is the transport of ions in this case in concrete under an electric field through the pore system of the concrete filled with water. Figure 4 shows a schematic illustration of the migration test for a reinforced concrete specimen. It is very important that the concrete is saturated to ensure the migration of the ions. In the migration process, the ions are not able to move by the shortest route like in bulk solution, but they have to find their way along the water-filled tortuous capillary pore system of the concrete [11]. Therefore, the pore volume, pore solution composition, pore geometry, interconnectivity and distribution of the concrete are the factors that governed the velocity of migration.

Electrical current flow from ion migration in concrete is important for electrochemical rehabilitation techniques like chloride removal and for our case to accelerate chloride transport so that C_T can be reached in a short period of time.

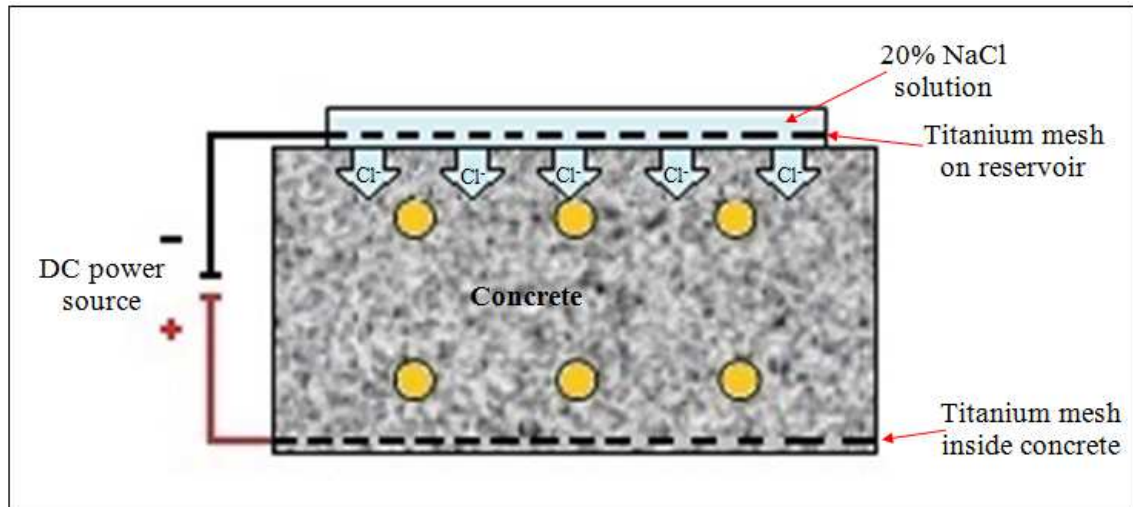


Figure 4 schematic representation of the migration test

One important factor when the chloride migration test is used is that the applied electrical field (and the resulting current) do not alter the microstructure of the concrete, such that during the migration test the chloride transport properties in concrete remain constant. However, during the applied current field not only the ions of chloride are moving but also other ions present in the pore of the solution concrete [11]. The electric field has to be well applied and a reasonable magnitude to prevent/minimize changes, in particular the pH of the concrete pore solution. The electric field can potentially polarize the embedded reinforcement due to ionic current flowing thru the concrete.

3 APPROACH

3.1 Specimens and Materials

Reinforced concrete specimens were prepared at the state materials office (SMO) of Florida Department of Transportation (FDOT). The selected geometry simulates a bridge deck (simulated deck slab with 30cm wide, 30cm long and 15cm high as shown in **Figure 5**. The specimens were made in two batches with the same procedure and mixture composition: 658 cementitious content (lb./yd³), #89 limestone gravel as coarse aggregate, standard Florida's river sand, 10% fly ash as cementitious replacement and 0.42 water/cementitious (w/cm) ratio (see Table 5 for details).

Table 5 Mix design

Raw Material	Material Source / Mine	1 yd ³ Unadjusted Batch Wt. (lb)	Remarks
Cement	Cemex	592.2	
Fly Ash	FL Rock - Class F	65.8	10.00% Cement Replacement
Standard Sand	GA-397	1214.64	-0.57 lb water surplus
#89 Limerock	87-090	1601.58	10.59 lb water surplus
Water	Local	274	
Air Entrainment	Grace Darex AEA	2.02 oz	0.31 oz/cwt
			Typical Range: 0.5-3 oz/cwt
Admixture	Grace WRDA 60	39.50 oz	6.00 oz/cwt
			Range: 3-6 oz/cwt
Admixture	Grace ADVA Cast 600	4.55 oz	0.69 oz/cwt
			Typical Range: 3-6 oz/cwt
Entrained Air		0.079828	4.00 vol % air

The first batch is named batch-1 and the second batch is named batch-2. Six specimens per batch were casted, which consisted of five specimens with 6 rebars and one blank specimen (i.e. with no rebar).

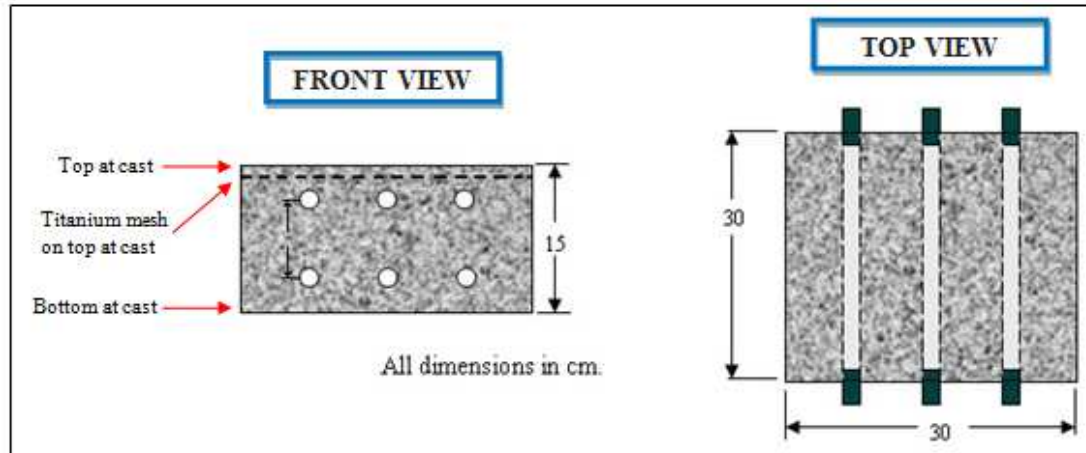


Figure 5 Specimen at cast

Each specimen with reinforcement was fabricated with six embedded bars, three of which are located in a top layer (one inch concrete cover) and the other three are located in a bottom layer (see Figure 5 for dimensions and schematic of the specimen). Stainless steel UNS32101 rebars were embedded in batch-1 samples and UNS32304 rebars were embedded in batch-2 samples (see Table 6 for the composition of the alloys). The rebars on the top layer (were facing the bottom during casting) are 2.5 cm below from the concrete top surface (concrete cover). Each rebar is approximately 1.65 cm in diameter (#5) and approx. 35 cm long. It can be observed from Figure 6 and Figure 7 that the rebars project out approximately 2.5 cm from the concrete block on both sides. The rebar section outside of the concrete block was wrapped at both ends with a plastic heat

shrink tubing (and about 2 cm on both ends of each embedded rebar). An activated titanium mesh was placed on the top side of the concrete (embedded into the concrete by a few mm) when the specimens were casted (see Figure 6 dotted line on front view, depth not to scale). No chlorides were added to the concrete at casting.

Table 6 Reinforcement chemical composition

Name	C	Mn	P	S	Si	Cr	Ni	Mo	Cu	N	Fe
UNS S32304SS	0.03	1.16	0.03	0.002	0.45	22.33	4.16	0.25	0.30	0.11	Bal.
UNS S32101SS	0.04	4.7	0.02	0.001	0.80	22.47	1.68	0.24	0.38	0.117	Bal.

Specimens were casted at the state materials office of FDOT, and 24 hours later the molds were removed. Then specimens were placed in a high moisture environment (fog curing room) for about 45 days at SMO-FDOT. The specimens were then transported to Florida Atlantic University (FAU) laboratories at SeaTech. The specimens were exposed for 15 days to laboratory humidity and temperature (65-70% RH and 22°C). While at SeaTech, the samples were inverted (i.e. bottom at cast is now top of the specimen). During these 15 days, a reservoir was made of acrylic, and was attached with a marine contact adhesive and sealant (See Figure 7) on the top face of the specimen. Each rebar was drilled and tapped on one end to accommodate stainless steel machine screws that were then used as electrical contacts (See Figure 7). Stainless steel screws were installed and adjusted with two washers, a nut and butterfly nut on one side of each rebar to ensure good electrical connection. These connections were used during the electrochemical measurements (see Figure 8 for potential measurements set-up).

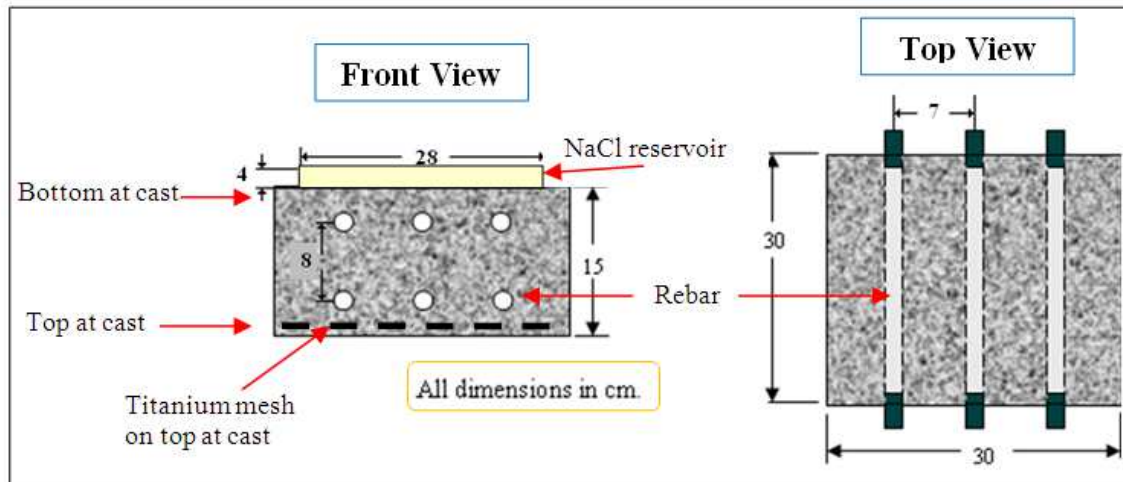


Figure 6 Sample schematic, dimensions and specifications

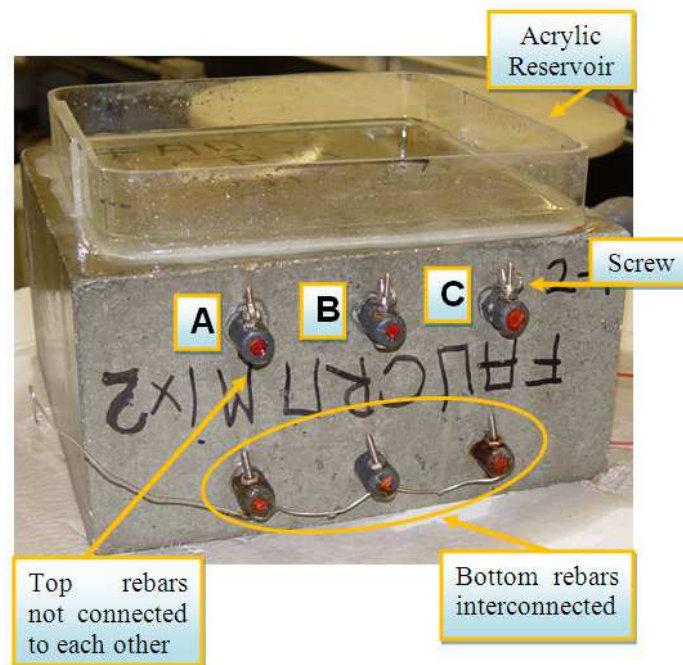


Figure 7 Picture of the specimen

3.2 Chloride Transport Methods

A methodology was implemented to accelerate the chloride transport and it is divided into two phases: Phase I (wet and dry cycles) and Phase II (application of electric field).

3.3 Method during Phase I

Phase I took place when the specimens reached 60 days of age (45 day fog room + 15 laboratory room temperature) During these initial 60 days the passive layer likely formed naturally on the rebar surface and continued to grow. During Phase I, the specimens were exposed in an elevated temperature room (37.8 °C) for 120 days. The elevated temperature room has a system of three heaters; each one is connected to a digital temperature controller to make sure the room is always at the desired temperature; it also has two fans to circulate the air around the room. Specimens were exposed to dry and wet cycles by alternating three days dry and four days wet. The solution was 20% sodium chloride (percentage by mass) and was added to the reservoir during the wet exposure days. This method allows the chloride to be transported through concrete faster due to the higher temperature (hence higher diffusivity) but similar to what is typically done in the laboratory under room temperature. Also, it is likely that the passive layer continue to form, as the chlorides might have not reached the rebar surface within the 120 days of exposure or a low chloride concentration might be present at the rebar depth. In the wet part of the cycle, the NaCl solution is transported through the pores of the concrete to the rebars by diffusion and capillary suction. During phase I, open circuit potential (OCP) measurements were taken twice per week for each rebar on the top row

named A, B, C and for the three bottom interconnected-rebars. The readings were made with a high impedance voltmeter and a saturated calomel electrode (Figure 8). Linear polarization was performed only once during this period on selected specimens and on selected rebars.

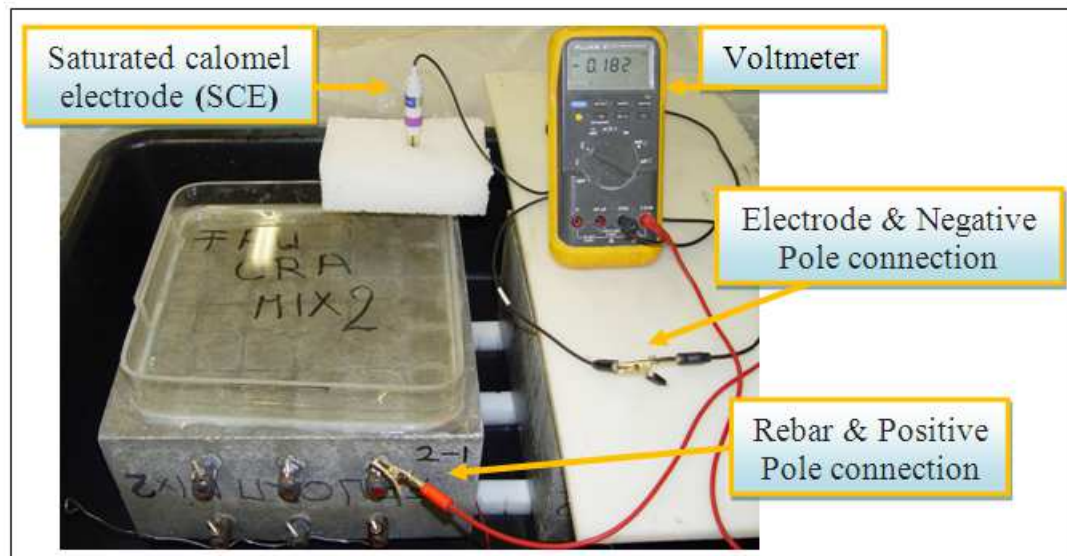


Figure 8 OCP measurement components

3.4 Phase II Electric Field Method

During phase II, the specimens were placed back in the laboratory temperature (22°C), in a high humidity chamber (see Figure 9). The high humidity chamber was made of a prismatic plastic container of 62cm width, 90cm length and 20cm height. The bottom 2 cm of each chamber was filled with fresh water. Then, three white plastic (HDPE) square pieces of about 4 cm height, 4 cm width and 70 cm length were placed on the bottom surface to support the samples and also to prevent the water at the bottom from directly wetting the specimens. Two specimens were accommodated for every chamber. Once transferred from the elevated temperature room, the side faces of the

specimens were sprayed with water every day for 7 days to increase the moisture content of the concrete. This wetting continued during phase II as required (usually twice per week). It is very important that the specimens are as saturated as possible prior the application of the electric field method in order to have an efficient chloride to transport via migration [15].

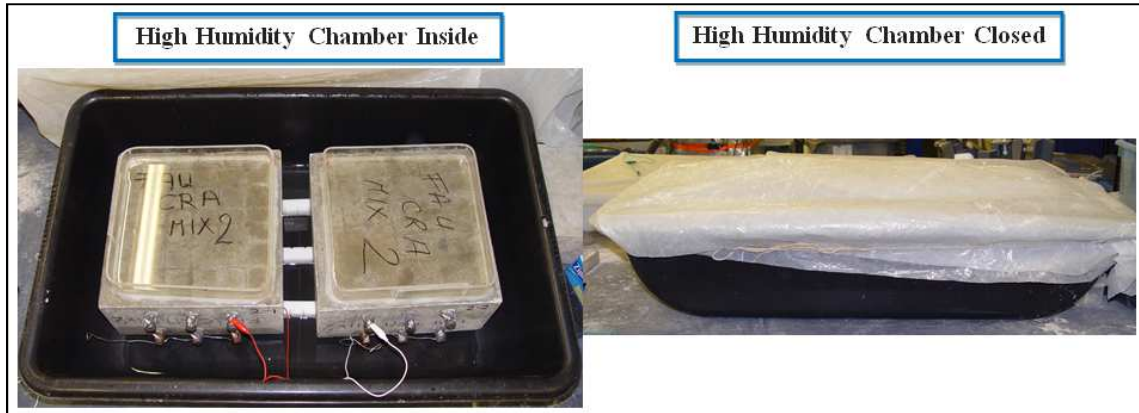


Figure 9 High humidity chamber

A second activated titanium mesh was placed on the solution reservoir. The 20% sodium chloride solution remained in the reservoir all the time and was periodically changed (every three to four weeks). An electric field was then applied periodically to accelerate the chloride transport via migration. A 20 V potential difference was applied between the two Ti MMO meshes and was provided by a power supply (initial and later test used 15 V, see appendix (A)). The positive pole was connected to the bottom mesh, which was already embedded into the concrete, and the negative pole was connected to the top mesh placed on the solution reservoir (see Figure 10). With this set-up the electric field accelerate the chloride transport down through the concrete by migration. The voltage applied to the specimens with the electric field was removed periodically to

monitor the off potential evolution and to identify when corrosion might have initiated. Table 12 in appendix (A) displays the applied voltage schedule showing the days when the electric field was applied for each specimen.

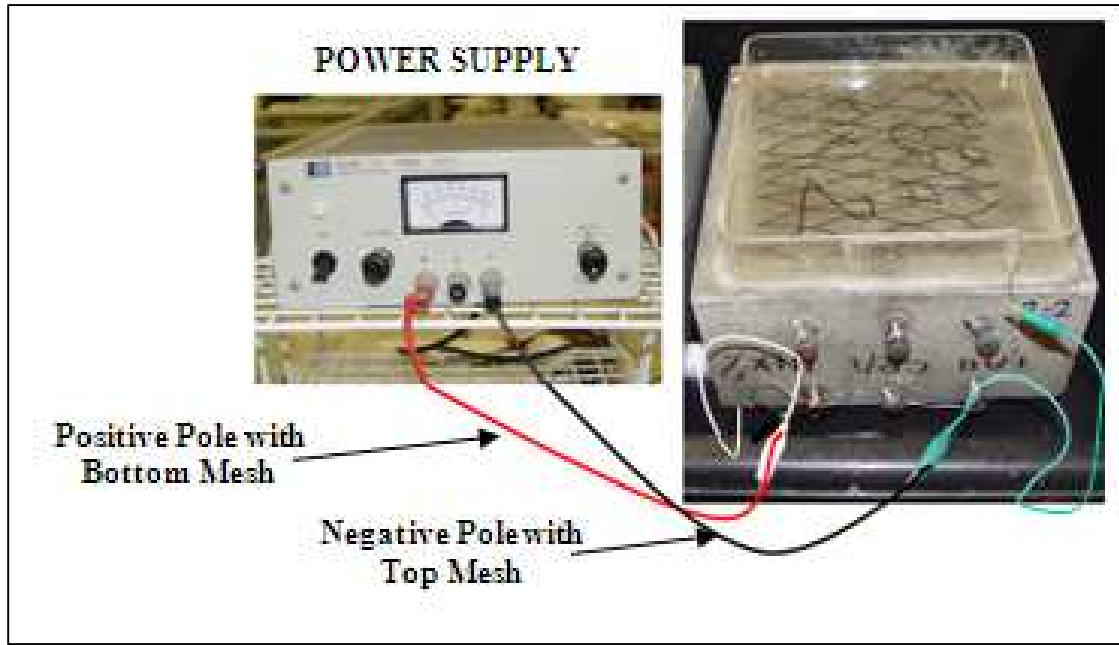


Figure 10 Electric field set up

Batch 1 samples were transported to the high humidity chamber on day 120 of Phase I and Batch 2 samples were transported one week later. The electric field was applied first on batch 1 samples with 15 Volts, but after that week the potential difference was set up to 20 Volts between the two Ti MMO meshes for all samples in batch 1 and batch 2. This voltage adjustment was made to accelerate the chloride transport. A numerical model was implemented and the computed potential difference between the top surface and the top of a rebar with 2.5 cm concrete cover is 2.48 V when applying 15V and 3.25 V when applying 20 V between the two Ti MMO meshes. These two values were obtained by assuming that the rebar were conductive, if the rebars are assumed to be insulators (due to

passive layer) the potential difference at the rebar surface are lower: 1.78 V (15V) and 2.38 V (20V). The actual potential difference between the reservoir and the rebar top (2.5 cm concrete cover) likely is somewhere in between. While the electric field was removed, LPR and EIS were measured on rebars: A, B, C and Bottom-interconnected (the latter, only after day 24 and on selected specimens). These measurements were made one day or more after electric field removal. OCP was measured a few seconds, one hour, 24 hours and every other day if the specimen was left disconnected. After the specimens were left disconnected for more than 20 days the potential measurements were performed once a week.

3.5 Linear Polarization Resistance (LPR) and Electrochemical Impedance Spectroscopy (EIS)

The solution resistance R_s was measured via EIS. The magnitude measured at a frequency of approx. 60 Hz was assumed to be the R_s of the system.

The linear polarization value measured is labeled on the axis as “ R_{p_meas} ”. The R_{p_meas} contains the solution resistance of the system. The linear polarization test was performed from 15 mV below OCP to OCP at a scan rate of 0.1 mV/sec.

The LPR values shown in the results section are the R_{p_meas} minus R_s . An area of 1 cm was assumed during the test, but the actual area under the ponding section is $\sim 42 \text{ cm}^2$ for each rebar. For the bottom 3 interconnected-rebars as they are interconnected the measured area is 126 cm^2 . Performed measurements were divided in two different sub-stages on each sample; one to five days of electric field disconnection was the time to

allow the rebars to depolarize similar to what is done on a depolarization test; sub-stage two was after five days of electric field disconnection and assumes that rebar potentials have stabilized.

3.6 Autopsy of Terminated Specimen

Two specimen(s) for each batch (Batch-1-1, Batch-1-2, Batch-2-1 and Batch 2-2) that became active were designated for autopsy. These specimens were sectioned, the rebars of both layers exposed and evaluated according to the following procedure:

1. Testing/exposure was terminated, the solution in the reservoir removed, and the acrylic reservoir removed,
2. Four (or two) cores were obtained from in between the rebars on the empty space where no rebars are on the way. Each core is drilled from the top surface all through the bottom surface of the specimen as shown in Figure 11. The obtained cores were 3 cm in diameter.
3. Two of the cores (one per each side) were sliced for chloride profiles. Six slices were obtained with a wet saw. Each slice was marked every 0.635 cm (actual slice is thinner due to thickness of the blade). Then each slice was pulverized to perform chloride analysis.

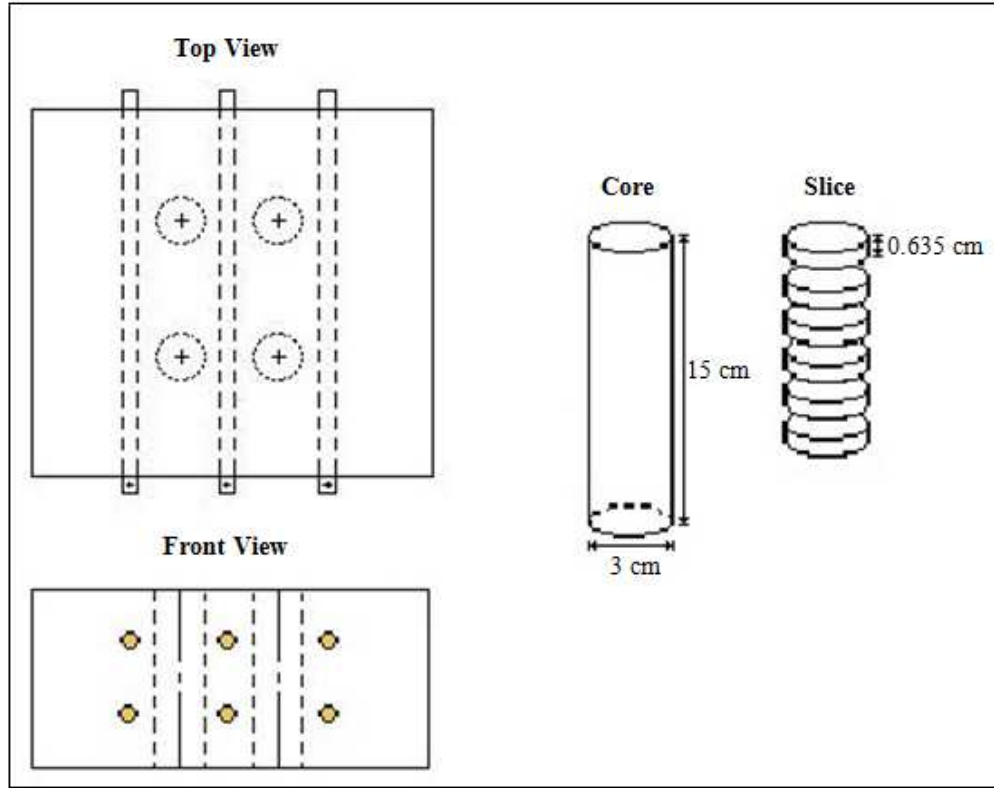


Figure 11 Cores cuts and dimensions

4. Two saw cuts were then made on each specimen. Each cut was made perpendicular to the top surface and parallel to the rebar length. The cut was made at equi-space between the center rebar and each of the two outer bars (see Figure 12 (a)).
5. For each of the three resultant concrete sections, additional secondary saw cuts were made on each of the new exposed cut faces and on the side faces. The cuts were made parallel to the top surface such that the top and bottom rebars could be exposed. The cut was made to a depth approximately 10 mm from each rebar. This procedure was performed at both levels of these rebars (see Figure 12 (b)).
6. Each specimen section was split open by placing a chisel in one of the secondary saw cuts from step 5 and tapping gently with a hammer until fracture occurred. This

exposed both the rebar and its trace, which were then examined for corrosion products and photographed.

7. The rebars surface condition (with corrosion products if already corroding) was captured in pictures as seen just after opening them. Then, a plastic brush was used to remove as much of the corrosion products from these rebars. After this partial cleaning, close up pictures were taken with a stereo microscopy. This was done to appreciate in more detail the corrosion extent. Finally, the corrosion product was removed from each rebar segment per ASTM G-01. This was achieved by repeatedly conducting a procedure of immersion in cleaning solution (93.5 wt% HCl + 0.7 wt% Sb₂O₃ + 4.7 wt% SnCl₂) and then brushed to remove any remaining corrosion products (multiple times if needed until the rebar weight stopped changing). After this additional clean-up, additional close up pictures were taken with a stereo microscope to document and appreciate in more detailed the penetration of the corrosion products (once these have been removed) into the rebar (i.e. to identify how much rebar section was lost).
8. The concrete section above the rebar trace of the top-row rebars was milled to obtain the chloride concentration above the rebar trace. (Portions with corrosion products if present were avoided)

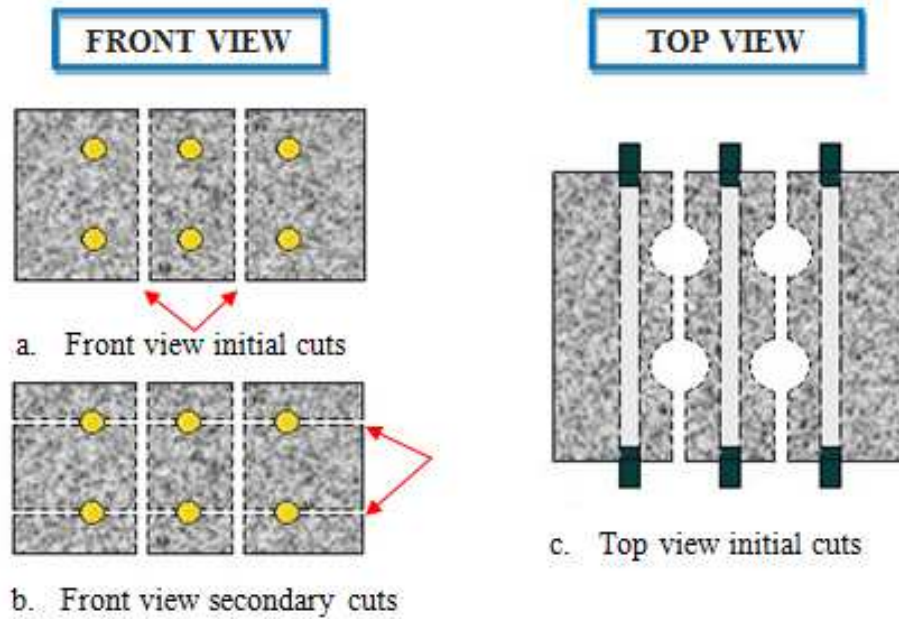


Figure 12 Schematic illustration of the concrete sectioning for specimens as listed in dissection steps 4 and 5 above

3.7 Chloride Analysis

To analyze the chloride concentration at the rebar trace and at different depths titrations were performed. The method used measures the total amount of chlorides and followed a slightly modified that follow FDOT method 5-516 (FM 5-516) [21]. The details of the method can be seen in Appendix (B). Firstly, a blank sample must be prepared to ensure that the procedure will provide a valid concentration. The results and analysis will be presented in the next Chapter.

4 RESULTS/DISCUSSION

4.1 Phase I

The plots on Figure 13 show typical potential evolution vs. time for samples batch 1-5 and batch 2-1. The potential evolution during phase I for the other samples from batch I and II are listed in appendix (A) Figure 39 and Figure 40. Initially the measured potential of the rebars embedded in batch 1 specimens ranged between ~ -50 and ~ -200 mVsce. The potential of rebars embedded in specimens of batch 2 ranged from ~ -100 to ~ -240 mVsce. The potential values of UNS32304 (batch 2) rebars are more negative than the potential values of UNS32101 (batch 1) rebars. Over the first 80 days the potential values of all rebars tend to shift slightly more positive values. Towards the end of phase I (last two sets of measurements) some of the rebar potentials dropped slightly (by \sim approx. 25 mV). The observed potential values suggest that corrosion did not take place on neither of the CRA rebars during phase I. The average of the last five potential measurements in phase I for UNS32101 rebars was -121 mVsce while the average of the last five measurements potential value observed for UNS32304 rebars was -179 mVsce.

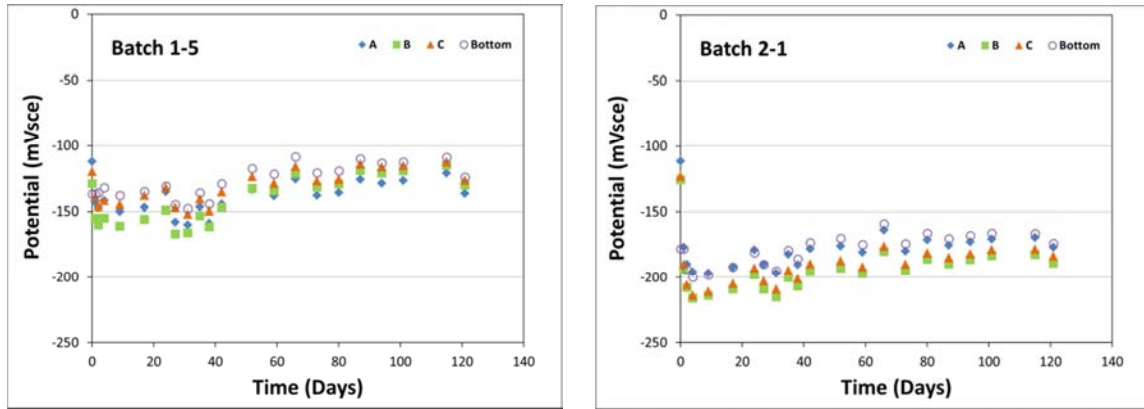


Figure 13 Batch 1 & batch 2 potential measurements over time for Phase I

4.2 Phase II

The number of days is counted with respect to day one of phase II in sections 4.2 and 4.3 (i.e. for batch-1 specimens day 1 is 12/14/2012, and for batch-2 specimens day 1 is 12/20/2012).

4.2.1 Potentials Measurements upon Electric Field Removal

Figure 15 shows plots of the potential evolution vs. time measured during phase II on rebars of batch 1-1 and batch 1-2 (S32101) specimens measured after the electric field has been removed. All potential values shown were measured with the electric field removed (after one or more days). Here the filled symbols correspond to measurements taken between one and five days after the electric field has been disconnected; empty symbols correspond to measurements taken after more than five days of the system being disconnected. Figure 14 shows a graphic explanation of this arrangement. This methodology allows to observe the recovery (i.e. depolarization) and stabilization of the rebar potential after each electric field application.

As indicated above Figure 15 shows the potential evolution of the reinforcement during phase II measured on specimen batch 1-1. The initial measured potential values ranged from ~ -96 mVsce to ~ -126 mVsce before applying any electric field. After spraying water on the samples in the high humidity chamber and the initial electric field application for one week, the potential values of the rebars became slightly more positive (compared to the initial values). Then, upon subsequent application of additional electric field periods, the measured potential values dropped considerably. By day 61, four days after removing the electric field, the rebar OCP values ranged from ~ -277 mVsce (Rebar A) to ~ -357 mVsce (Rebars B and C); then by days 98 (after 38 day of electric field being disconnected), the OCP values of rebars A and B had shifted to more positive OCP values and remained stable at ~ -83 mVsce and ~ -136 mVsce respectively; but, rebar C only recovered slightly and the potential remained at ~ -320 mVsce. Finally, after additional periods of electric field applications, on day 166 four days after removing electric field the rebar OCP values ranged from ~ -440 mVsce to ~ -484 mVsce. The potential of the top three rebars ranged between ~ -341 mVsce and ~ -572 mVsce by day 188 (~ 46 days after this last disconnection), suggesting that corrosion might have initiated. Batch-1-1 specimen was terminated on day 189.

Figure 15 also shows the rebar potential evolution measured on specimen batch 1-2. The plot for Batch-1-2 shows that initially the potential values ranged from ~ -82 mVsce to ~ -100 mVsce. The last set of potential values measured during phase I (elevated temperature room) ranged from ~ -115 mVsce to ~ -125 mVsce. Thus, the potential values measured at the beginning of phase II are somewhat nobler; this difference can be explained by the lower temperature in the lab during phase II than

phase I. After spraying water on the samples in the high humidity chamber and the initial electric field application for one week, the potential value of rebar B (located top middle row) dropped significantly to a potential of -244 mVsce. The other rebars remained at potential values of ~ -72 mVsce. Then, after application and removal of additional electric field application; the potential of all rebars ranged drops from ~ -100 mVsce to ~ -300 mVsce. No electric field was applied from day 50 for 45 days (i.e. up to day 95). During this period of time, rebar A and C recovered to potential values of ~ -81 mVsce to ~ -135 mVsce respectively (i.e. noble potential values); but, rebar B only recovered slightly and then remained at about ~ -310 mVsce potential value. Then, the electric field was applied for additional period of time to try to initiate corrosion on the other two rebars on the top row. By day 140; all three rebars show potential values more negative than ~ -300 mVsce and remained stable at this potential value over the next few days. Rebar C eventually recovered to a potential value of ~ -231 mVsce by day 157. This suggests that corrosion might have initiated at rebars A and B by day 152 of phase II. Batch-1-2 specimen was terminated on day 158.

The potential evolution of the rebar in the other three specimens batch-1-3, 1-4, and 1-5 have similar behavior than that described above for Batch-1-1 and Batch-1-2 specimens. After several applications of the electric field (i.e. chloride have been transported to the rebar surface) the potential values measured on the top row rebars dropped significantly. By day 188, rebar potential values below ~ -300 mVsce were observed on: two rebars of Batch-1-3 specimen, three rebars on Batch-1-4, and two rebars on Batch-1-5 (all rebars on the top layer). Figure 41 in Appendix (A) contains the potential evolution vs. time measured during phase II for all specimens on batch 1.

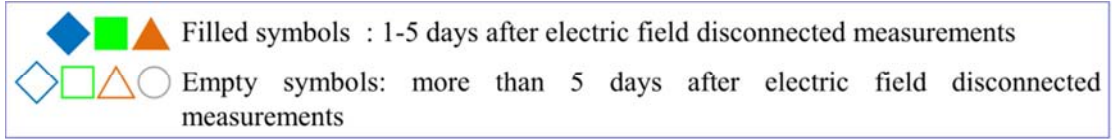


Figure 14 Plots symbols clarification

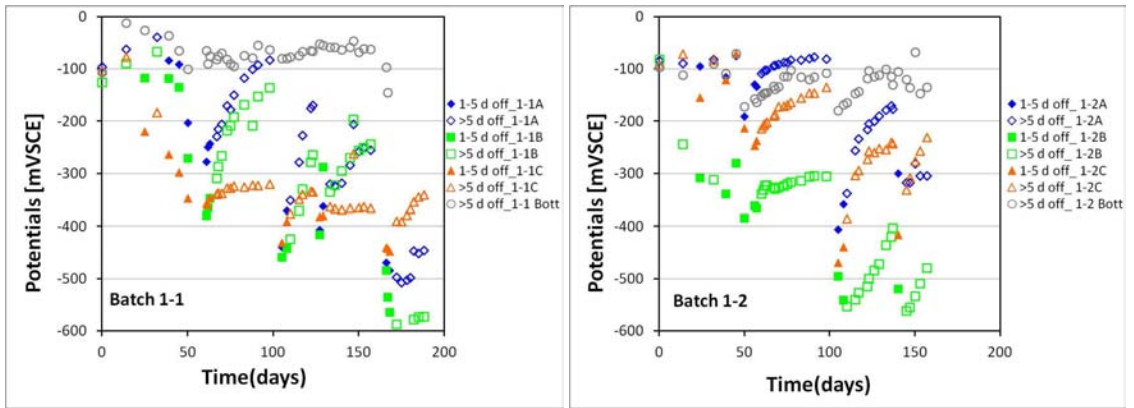


Figure 15 Batch 1 samples OCP measurements over time for Phase II

Figure 16 shows the rebars potential evolution measured on batch-2-1 and batch-2-2 specimens during phase II. All potential values shown were measured after the electric field was removed for one day or more days (see Figure 14 for explanation of the symbols).

Figure 16 shows that the initial potential values measured on the rebars of batch-2-1 specimen ranged from ~ -160 mV_{sce} to ~ -192 mV_{sce}. Upon applying electric field for several periods (see appendix (A)), the measured potential values dropped considerably. On day 61 the potential values ranged from ~ -252 mV_{sce} to ~ -399 mV_{sce} four days after the electric field had been disconnected. After 38 days of no electric field application (i.e. by day 100) the potential values of the rebars shifted to more positive values and then remained stable at potential values that ranged from ~ -163 mV_{sce} to ~ -249 mV_{sce}. After additional periods of electric field were applied the rebar potential

values ranged from ~ -440 mVsce to ~ -484 mVsce by day 162. By day 183, after the electric field was disconnected for 21 days the potential value of rebar A was ~ -203 mVsce and rebars B and C potential values were ~ -301 mVsce and ~ -305 mVsce, respectively, suggesting that corrosion might have initiated on rebars B and C.

Figure 16 also shows the rebar potential evolution measured on specimen batch-2-2. The plot for rebars of Batch-2-2 specimen shows that the initial potential measured values ranged from ~ -150 mVsce to ~ -170 mVsce. However, the last set of potential values measured during phase I (elevated temperature room) in this specimen ranged from ~ -180 mVsce to ~ -185 mVsce. Hence, the potential values measured at the beginning of phase II are somewhat nobler; this difference could be explained by the lower temperature in the lab during phase II than phase I. After specimen batch 2-2 spent a few days on the high humidity chamber the rebar potential values tended to shift to slightly more positive values, then, after additional electric field application; the potential of all rebars dropped and ranged from ~ -400 mVsce to ~ -350 mVsce. . No electric field was applied after day 50 for 45 days (i.e. up to day 95). During this period rebar A and C recovered to potential values of ~ -160 mVsce to ~ -170 mVsce respectively (i.e. noble potential values); but, rebar B only recovered slightly and then remained at ~ -277 mVsce potential value. Then, the electric field was applied for additional period of time to try to initiate the corrosion on the other two rebars on the top row. By day 135; all rebars show potential values that were more negative than ~ -300 mVsce. Then, after 17 day (i.e. by day 152) of the electric field being disconnected, the rebar potential of C recovered to a nobler potential value of ~ -202 mVsce. The potential for rebars A and B stayed below ~ -300 mVsce. This suggests that corrosion might have initiated at rebars A

and B by day 152 of phase II. Batch-2-2 specimen was terminated on day 154.

The potential evolution of the rebar in the other three specimens batch-2-3, 2-4, and 2-5 have similar behavior than that described above for Batch-2-1 and Batch-2-2 specimens. After several applications of the electric field (i.e. chloride have been transported to the rebar surface) the OCP values dropped significantly. By day 188 rebar potential values below ~ -300 mV_{SCE} were observed on: two rebars of Batch-2-3 specimen, one rebars on Batch-2-4specimen, and no rebars on Batch-2-5 specimen. Figure 42 in Appendix (A) contains the potential evolution vs. time measured during phase II for all batch 2 specimens.

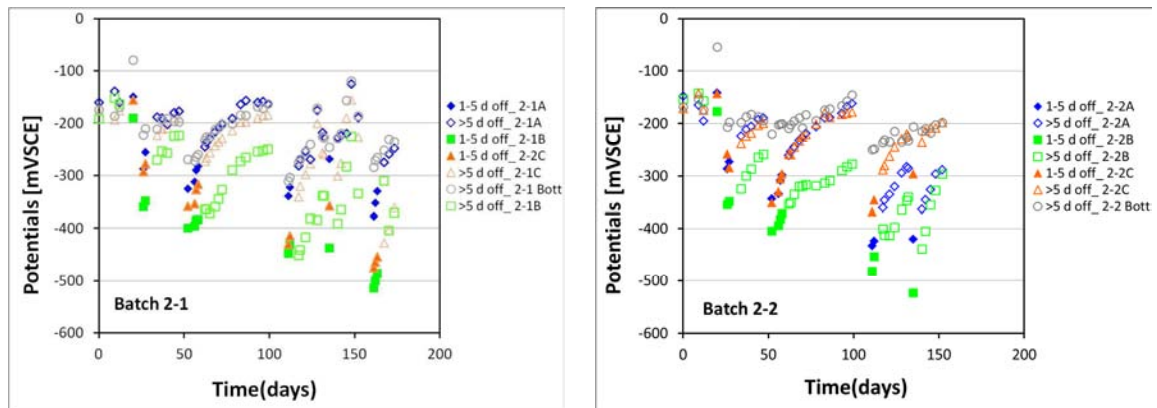


Figure 16 Batch 2 samples OCP measurements over time for Phase II

4.2.2 Solution Resistance -Electrochemical Impedance Spectroscopy (EIS) Measurements

The electrochemical impedance spectroscopy measurement (EIS) was performed to measure the solution resistance (R_s) for the same electrode configuration than that used when measuring LPR. Figure 22 shows the evolution of the solution resistance (R_s)

- i.e. the modulus of the impedance obtained at ~60 Hz - values as a function of time measured for rebars on Batch-1-1 and Batch-1-2 specimens.

Figure 17 shows that the initial value of R_s ranged from 0.47 k Ω to 0.51 k Ω for rebars in Batch-1-1 specimen. Then, over the first 150 days the value of R_s did not change much and fluctuated little around the initial range of measured values. However, at day 168 the values of R_s dropped significantly; for rebar A the R_s value was 0.34 k Ω (from 0.48 k Ω), and for rebars B and C the values were about 0.25 k Ω (from 0.44 k Ω). This drop in R_s might be indicative that by day 168 a crack might have formed on batch-1-1 specimen. This was verified by Figure 21 where it was shown that there was no crack on the specimen during the inspection performed on day 168; but, a crack was first observed during the inspection carried out on day 177.

Figure 17 also shows the evolution of R_s over time for rebars on Batch-1-2 specimen. The rebars in this specimen had initial R_s values that ranged between 0.46 k Ω and 0.56 k Ω ; then on day 63 it showed a sudden drop in the measured R_s values to values that ranged from 0.27 k Ω to 0.46 k Ω . This sample was the first one in which corrosion initiated from Batch-1 based on the potential evolution described in the previous section. This specimen was terminated and upon autopsy the three rebars showed corrosion to various degrees (See section 4.3). However, cracks were observed only above one of the rebar at the time of the autopsy. It is believed that this sample was the first one where a crack took place according to the R_s values vs. time and autopsy results for specimen batch-1-2.

The R_s evolution for the rebars of the other specimens (1-3, 1-4, and 1-5) is included in Figure 43 in Appendix (A). Rebars on specimen 1-3 showed an abrupt drop

on the R_s values measured; this drop was observed by day 168; however there was no crack evidence for this specimen during the inspection performed on day 188. Sample 1-4 showed a drop in R_s values on day 108; after this day the values of the R_s continue to drop, but only slightly. Rebars on specimen 1-5, showed an abrupt R_s drop on measured values by day 168.

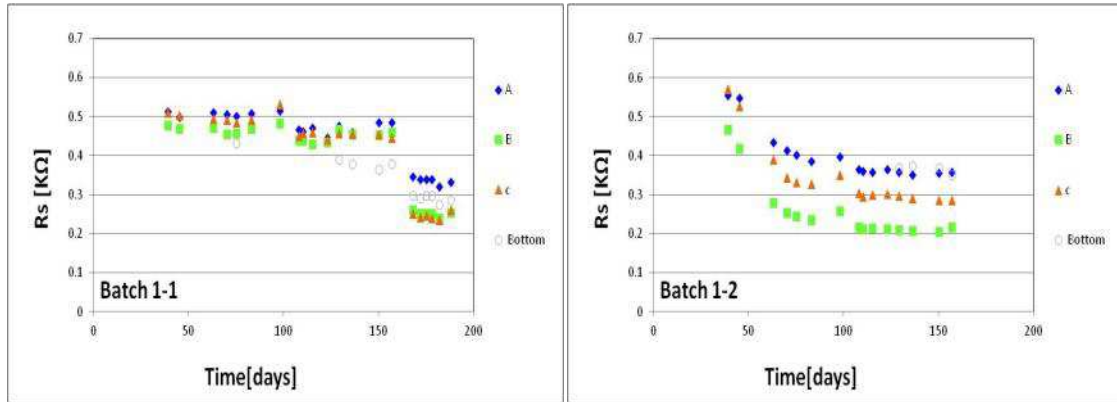


Figure 17 solution resistance plot over time for samples batch 1-1 and 1-2

Figure 18 shows R_s evolution over time for rebars in Batch-2-1 specimen; the initial values of R_s ranged from 0.50 kΩ to 0.57 kΩ. Then, over time the value of R_s fluctuated and dropped slightly to values that ranged from 0.45 kΩ to 0.53 kΩ by day 111. Then, the R_s values remained stable until day 188: at this point the R_s values ranged from 0.43 kΩ to 0.54 kΩ.

Figure 18 shows the evolution of R_s over time on rebars in Batch-2-2 specimen. The initial R_s values measured on rebars of specimen ranged from 0.53 kΩ to 0.64 kΩ; then on day 111 a modest drop in the R_s values was recorded. The R_s values dropped to values that ranged from 0.42 kΩ to 0.55 kΩ. This sample was the first one from Batch 2 to initiate corrosion and have a large crack at the time of the autopsy (this sample was

terminated). It is believed that this sample was the first to show a crack according to the R_s , potential and linear polarization values and autopsy results for batch-2 specimens.

The R_s evolution of other samples (2-3, 2-4, and 2-5) can be seen in Figure 44 in Appendix (A). The R_s values of those samples showed a small drop over time. Also these specimens show either a small crack (2-4 and 2-5) or not crack (2-3) on day 188.

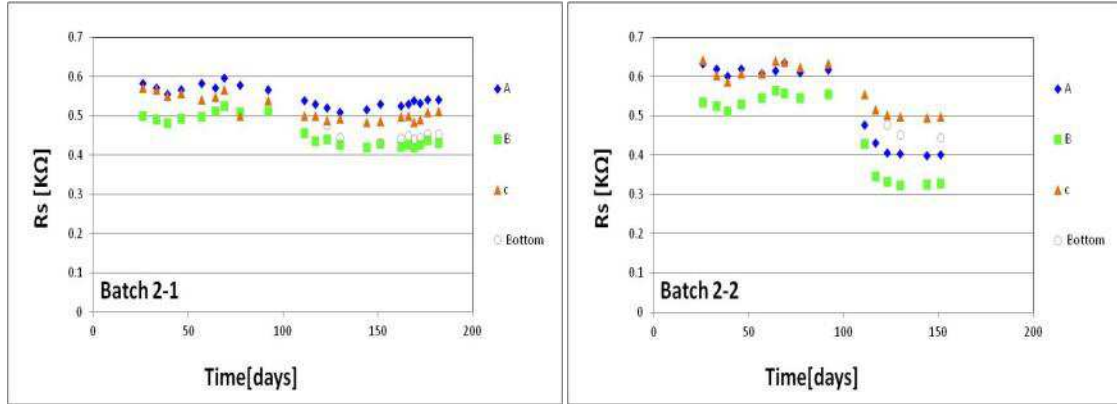


Figure 18 Solution resistance plot over time for samples batch 2-1 and 2-2

4.2.3 Linear Polarization Resistance (LPR) and Electrochemical Impedance Spectroscopy (EIS) Measurements

Figure 19 shows the LPR evolution measured on the specimens of batch 1-1 and 1-2 during phase II. The LPR value shown has the solution resistance subtracted but the shown values are not corrected for area. The initial LPR measurement values were performed on day 39 for batch 1-1 and on day 24 for batch 1-2 (Days counted from the beginning of phase II and three days after disconnection of the electric field application).

Figure 19 shows the initial values of LPR measured on rebars of batch 1-1 specimen. The LPR ranged between 3.7 KΩ and 10.4 KΩ by day 39, after three days of the electric field being disconnected. Then, after additional electric field application the measured LPR values dropped considerably. By day 108, the LPR values ranged from 0.8

K Ω to 1.1 K Ω - three days after disconnecting the electric field. On day 157, i.e., after 28 days of disconnection of the electric field the LPR values increased to values that ranged from 3.5 K Ω to 4.6 K Ω . Upon additional electric field application, the LPR values dropped considerably. On day 168 the LPR values of rebars were very small, ranging from 0.2 K Ω to 0.7 K Ω - one day after the last electric field application. Then, after 20 days (i.e., by day 188) of the electric field being disconnected, the LPR values slightly increased and became stable at a range of LPR values between 0.4 K Ω and 1.5 K Ω . This suggests that by then corrosion or electrochemical reactions are taking place at a high rate. The lower potential values and smaller LPR values are believed to be due to the presence of chlorides at the rebar's surface exceeding the critical concentration, which is likely at a concentration high enough to initiate corrosion. The application of the electric field polarizes the rebars (due to the ionic current); this polarization might have caused corrosion to initiate at a lower chloride concentration than would be observed under natural exposure. The smaller LRP values measured during the propagation (once corrosion has initiated) are also influenced by the residual effects of the additional electric field applications and any remaining ionic current present (i.e., stray current on those where corrosion had initiated), this likely caused a faster rate of corrosion which in turn produced corrosion products at a higher rate than if corrosion had initiated naturally.

Figure 19 shows that the initial values of LPR measured on rebars of batch 1-2 specimen, for rebars A and C had LPR values of 7.9 K Ω and 9.9 K Ω respectively, and rebar B was 1.2 K Ω by day 24, and three days after disconnecting the electric field. These initial LPR values were taken after several periods of electric field application. Then, after additional electric field applications occurred, the LPR values drop considerably. On

day 57 the LPR values ranged from 4.9 K Ω to 6.6 K Ω for rebars A and C respectively, and the LPR value for rebar B was 0.7 K Ω . These tests were performed one day after disconnecting the electric field. On day 98, i.e., 42 days after disconnecting the electric field, the LPR values measured on rebars A and C shifted back up (7.7 K Ω to 9.9 K Ω respectively), and the LPR value for rebar B was 2.4 K Ω . Upon additional electric field application, the LPR values dropped considerably. By day 110 the LPR values measured on all rebars were very small, ranging from 0.2 K Ω to 0.9 K Ω . These tests were done 5 days after removing the electric field. Afterwards, the LPR values of rebars A and C slightly increased and became stable at 2.1 K Ω and 4.6 K Ω respectively by day 188 (i.e., 46 days after last disconnection). The LPR value measured on rebar B remained at ~0.3 K Ω . The negative potential (<-300mVsce) and LPR < 4 k Ω observed on rebar B after prolonged electric field disconnection, might suggest that corrosion had initiated on rebar B.

The LPR evolution of other samples (batch 1-3, 1-4, and 1-5), also have similar behavior as described for batch 1-1 and 1-2 specimens. After several applications of the electric field, the LPR values dropped. By day 188, the LPR values measured on rebars B and C were below 4 k Ω by day 188 on specimens 1-3 and 1-4. For specimen 1-5, the LPR value measured on rebar B was also below 4 k Ω by day 188. Figure 45 in Appendix (A) contains the LPR evolution measured during phase II for batch 1 specimens.

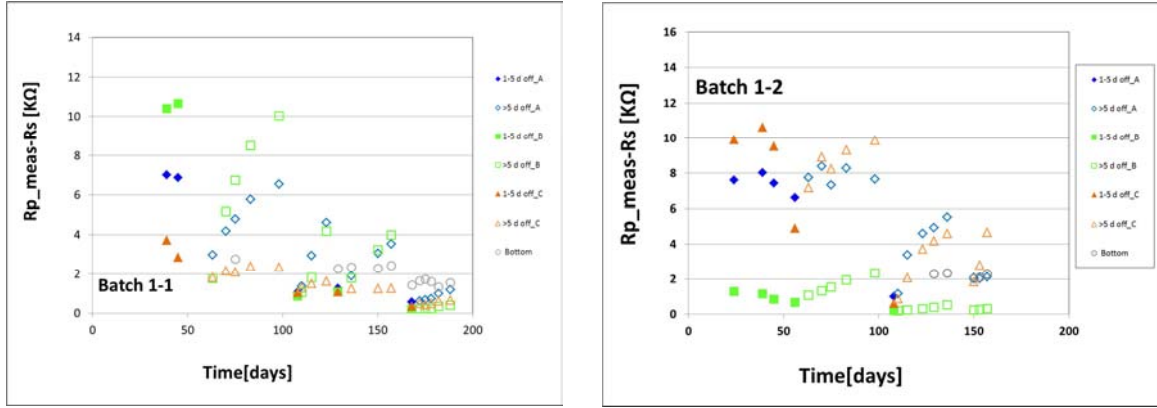


Figure 19 $R_{p_meas}-R_s$ over time for Phase II plots of samples Batch 1-1 and 1-2

Figure 20 shows the LPR evolution measured during phase II on the rebars of batch-2-1 and batch-2-2 specimens. The LPR values shown have the R_s value subtracted from the measured value but the shown values are not corrected for area. The initial LPR measurement values were carried out 26 days after the initiations of phase II and three days after disconnecting the electric field application.

Figure 20 shows that initial LPR values measured on rebar of sample batch 2-1 ranged between 4 KΩ and 14.1 KΩ by day 24 (3 days after the electric field has been disconnected). Then after some additional periods of electric field application the LPR value measured on the rebar dropped considerably. On day 57 the LPR values ranged from 2.4 KΩ to 9.5 KΩ. These measurements were performed one day after the electric field has been disconnected. Subsequently, the measured LPR values increased and ranged from 15 KΩ to 26 KΩ by day 92, after the electric field had been off for 35 days. Upon additional electric field application(s) the measured values of the LPRs dropped considerably. On this specimen day 165 was the last day when the electric field was applied. The measured LPR values were smaller (i.e. below 5 KΩ) three days after electric field had been disconnected (day 168). Then the values of rebars B and C

slightly recovered and became stable at 4.5 K Ω and 6.7 K Ω by day 188 (46 days after the last disconnection). For rebar A the LPR value recovered considerably to a value of 13 k Ω by day 188. Rebars B and C showed a negative potential ($<-300\text{mV}_{\text{sce}}$) on day 188, and a LPR below 7 k Ω . This set of values might suggest that corrosion might have initiated on these two rebars.

Figure 20 also shows that the initial values of LPR measured on rebars of sample batch 2-2 ranged between 4 K Ω and 14 K Ω by day 24 (i.e., three days after electric field had been disconnected). Then after additional periods of electric field application the LPR values measured dropped. On day 57 the LPR values ranged from 2.5 K Ω to 11.1 K Ω for measurements performed three days after electric field had been disconnected. The electric field remained off for the following 35 days. The LPR values measured for rebars A and C increased considerably to a value 30.0 K Ω , while the LPR value of rebar B only recovered slightly and became stable at 7.1 K Ω by day 92. Upon additional electric field application the measured LPR values dropped considerably. The measured LPR values were small and ranged from 0.9 K Ω to 6.5 K Ω , on tests performed two days after the electric field had been disconnected. Then the LPR values of rebar A slightly increased and became stable at value 7.0 K Ω . The LPR value of rebar B remained stable at 2.5 K Ω by day 151 (41 days after last disconnection). However, the LPR of rebar C increased to a value of ~ 24 K Ω . The negative potential ($<-300\text{mV}_{\text{sce}}$) and LPR < 7 k Ω observed after prolonged electric field disconnection might suggest that corrosion had initiated on rebars A and B.

The LPR evolution of the rebars on the other specimens (batch 2-3, 2-4, and 2-5) also shows similar behavior as described above. The LPR values measured on rebars in

sample 2-3 were below 5 k Ω on day 188. However, the LPR values of rebars B and C in sample 2-4 were below 5 k Ω on day 188. The LPR values of all rebars in sample 2-5 were above 9 k Ω on day 188. Figure 46 in Appendix (A) contains the LPR evolution measured during phase II for specimens of batch 2.

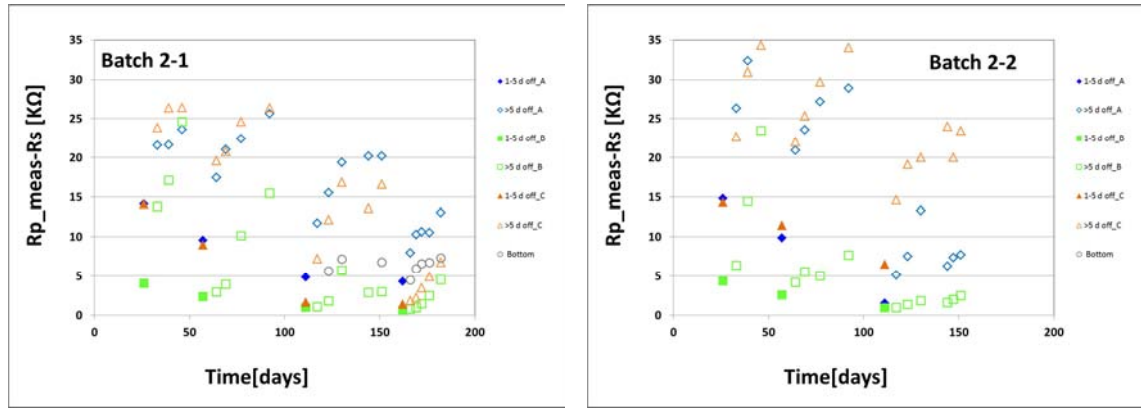


Figure 20 Batch 2 samples Rp_meas-Rs over time for Phase II

4.2.4 Observed Surface Cracks

Several days to several weeks after corrosion had initiated on one or more rebars, the top concrete surface (i.e., reservoir face) of some specimens of both batch-1 and batch-2 started to show cracks. The propagation of the crack(s) was recorded and mapped in drawings. Each drawing was made in an engineering paper with 1.00:3.75 scale. The reported lengths are based on measurements made on the specimen and crack(s).

Figure 21 shows the propagation of the crack(s) on the top surface of specimen batch1-1 at the indicated dates. The red line(s) in the drawings represents the new crack which was identified on the day of the inspection and the black line represents the crack recorded on the previous inspection. No cracks were observed on day 168 on specimen batch-1-1. Then, at the next inspection on day 177, there was a crack as shown in Figure

21 by the red line. This was a very thin crack less than 0.01 centimeter (cm). By day 185; the crack had propagated to other directions and the previously recorded crack became wider than before, but still less than 0.01 cm wide. The new crack branches can be seen by the red line. Finally, by day 186 the crack did not change in length with respect to the previous inspection.

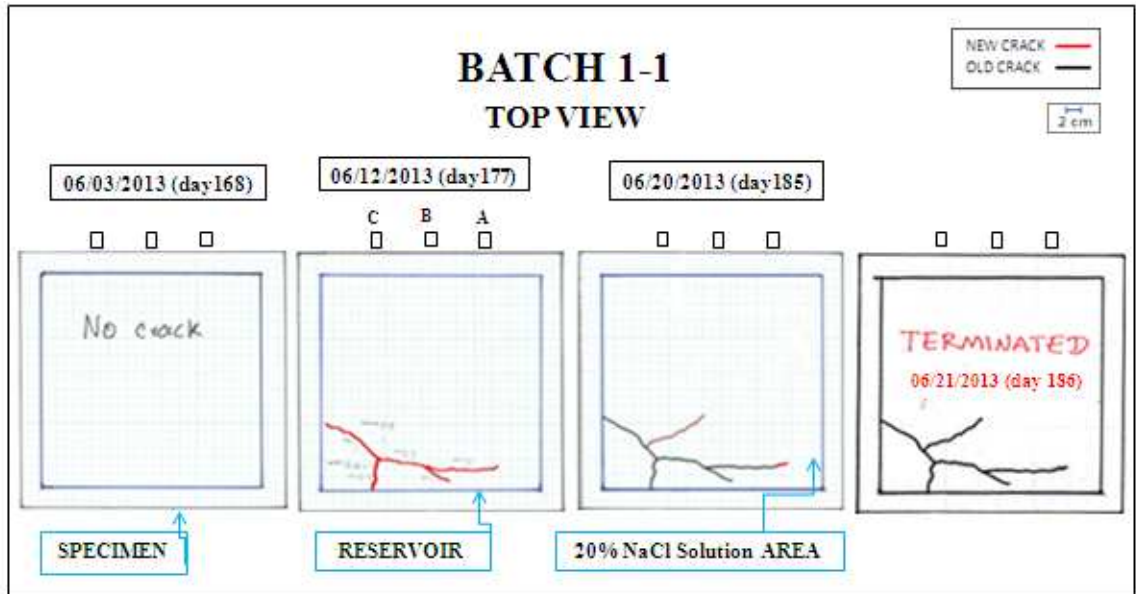


Figure 21 Diagram of the crack evolution over time for specimen batch 1-1

Figure 22 shows lateral pictures for specimen batch 1-1 after performing the secondary saw-cuts. As shown in the figure, a crack was observed that was about 11 cm long and was observed on each of the three shown cuts corresponding to each top three rebars. It is not clear if the corrosion products from more than one rebar contributed to these observed cracks. According with the visual observation after autopsy (see section 4.3.1); it is possible that the lateral crack might have initiated from the corrosion products of rebar B or rebar C. The crack was observed on both sides of the transversal faces (i.e.

the crack was all across segment that contains rebar B) and extended to the other segments that contain rebars A and C.

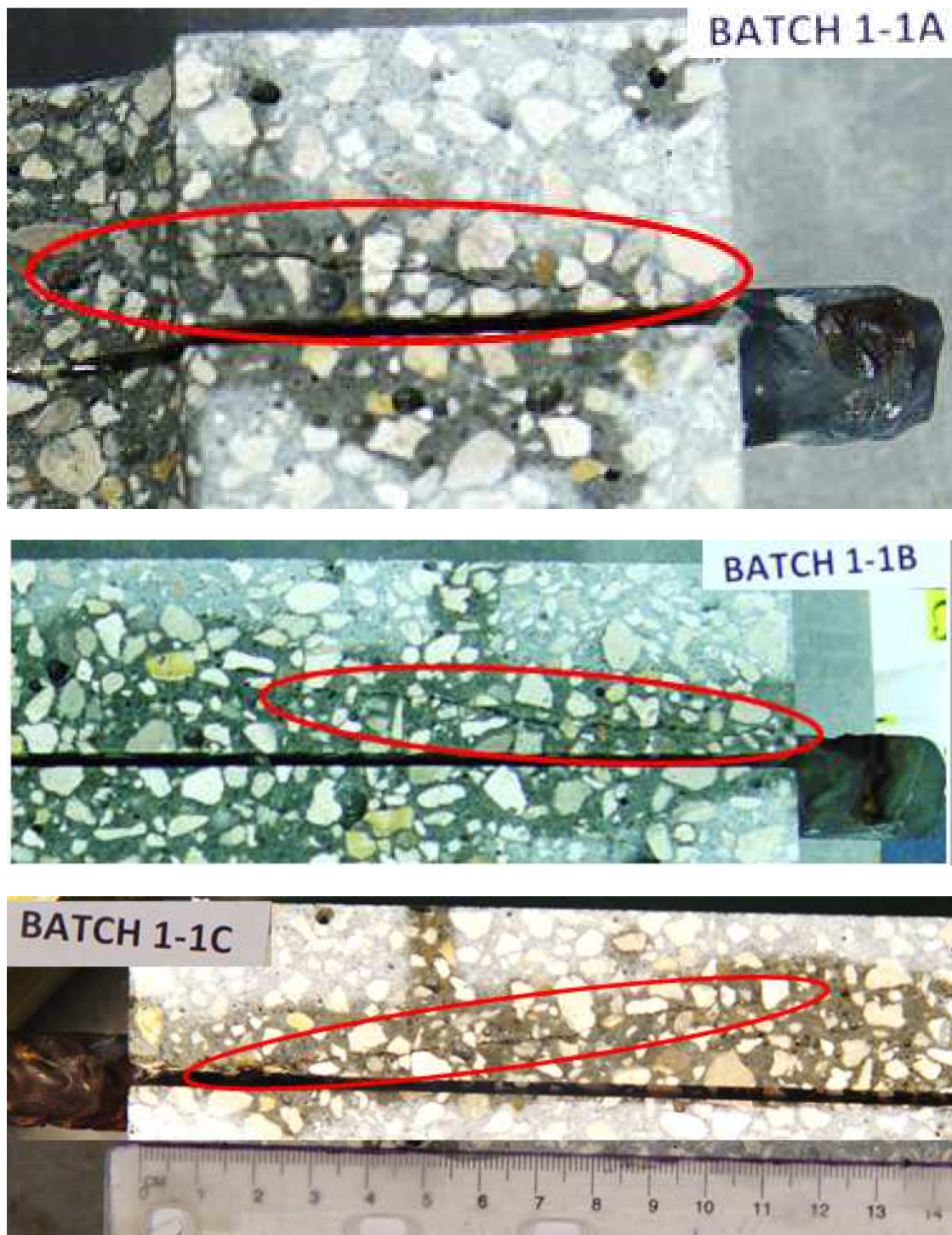


Figure 22 Lateral cracks pictures for specimen Batch 1-1

Figure 23 shows the propagation of the crack(s) on the top surface of specimen batch 2-1 at the indicated dates. The red line indicates the new crack length which was identified in the day of the inspection and the black line indicates the crack(s) length recorded on the previous inspection. For this sample by day 168 there were two cracks on both ends above rebar B (center rebar on top). Each crack length was about 4 centimeters (cm) long and less than 0.01 cm width. Then, during the next inspection on day 177 the cracks length did not change. Finally, by day 186 the cracks length still remained the same.

When comparing the crack evolution observed on batch 1-1 (Figure 21) and batch 2-1 (Figure 23) specimens, it is relevant to mention that the crack observed on specimen batch 1-1 grew up significantly from day 162 to day 179. On the other hand, the recorded cracks on batch 2-1 specimen did not change during all inspections. This, crack evolution suggest that when the rebars on batch-1 (S32101) specimens corrode, the corrosion rate is faster than the corrosion rate observed on corroding rebars (S32304) from batch-2 specimens.

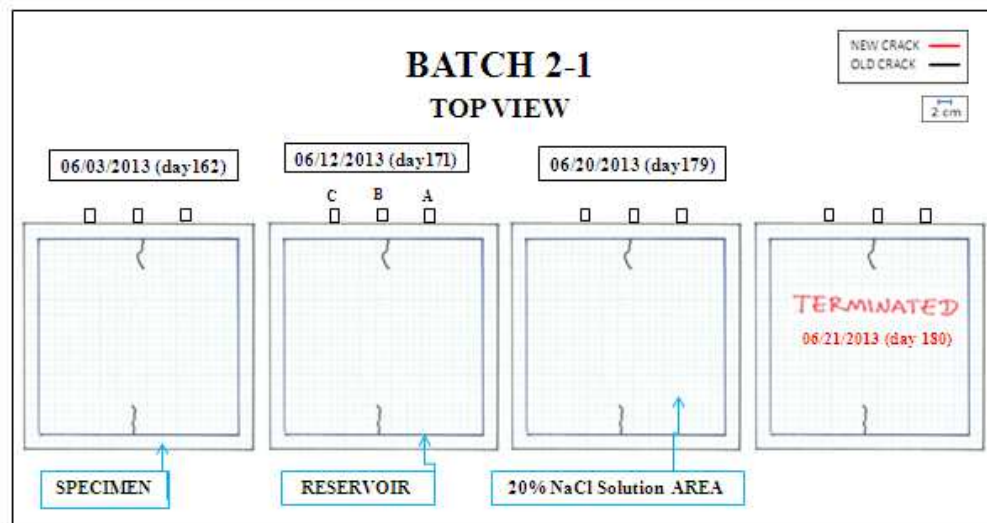


Figure 23 Diagram of the crack evolution over time for specimen batch 2-1

Figure 24 shows a picture of the top view of Batch-1-2 specimen. The picture also contains a highlighted view of the observed cracks (red lines drawn for emphasis). This specimen has a crack on each side of the middle rebar. It is speculated that corrosion initiated on rebar B first and due to the additional electric field applied to attempt to initiate corrosion on rebars A and C, this caused corrosion to proceed at a high rate (due to stray current) which eventually lead to a crack(s) to be visible on the top surface of the sample.

All the other specimens of batch-1 (1-3, 1-4, 1-5) have visible crack(s) when inspected on day 162. During the inspection performed on day 200 all of the visible cracks observed on day 162 have grown over time. Figure 47 in Appendix (A), shows how the crack maps evolved with time for every batch-1 specimens (except for batch-1-2 specimen which was terminated on day 158).

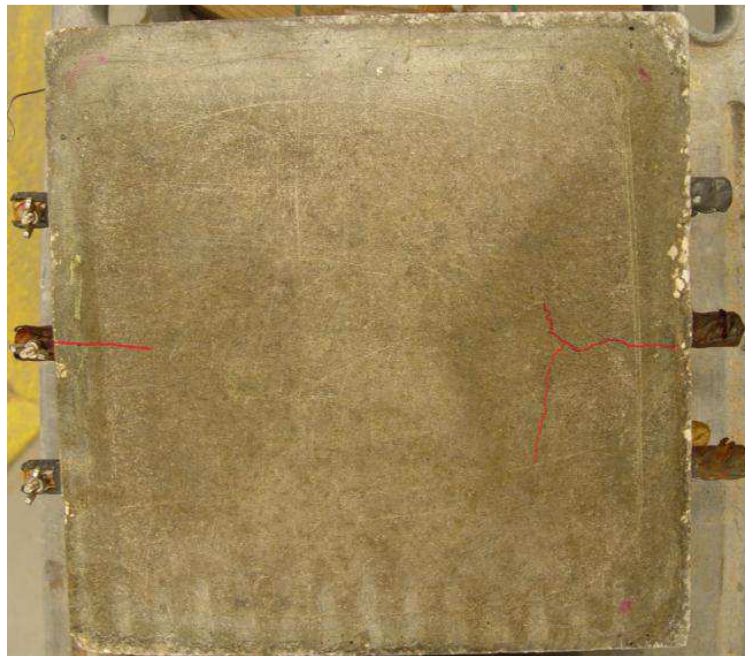


Figure 24 final crack picture of specimen batch 1-2

Figure 25 shows a picture of the top view of Batch-2-2 specimen taken on day 152. The picture also contains a highlighted view of the observed cracks (red lines). The specimen has a crack on one side above the center rebar B. This crack extends parallel to the rebar approximately 7 cm long; about 3 cm of the specimen edge two crack branches expand perpendicularly to the left and to the right (each one approximately 6 cm long). Similar to what was described above for Batch-1-2 specimen, it is speculated that corrosion initiated on rebar B first and due to the additional electric field applied to attempt to initiate corrosion on rebars A and C, this accelerated corrosion on rebar B (due to stray current) which eventually lead to a crack to be visible on the top surface of the sample.

As indicated above, specimen Batch-2-1 showed one crack on each side (approximately 4 cm long each one) above and along rebar B (center rebar). These cracks were visible during the inspection performed on day 162; during subsequent inspections (up to day 185) the cracks lengths remained the same. Specimen Batch-2-3 showed no cracks during the initial inspection (day 162) nor after the inspection done on day 186. Sample 2-4 showed one crack on rebar B, approximately 7 cm long on the inspection done on day 162; after inspection done on day 185 the crack remained the same length. Sample 2-5 showed no cracking at the initial inspection (day 162); but during the final inspection on day 185, it showed a crack approximately 5 cm long. Figure 47 in Appendix (A) shows the results of the crack propagation for every specimen per inspection day for batch-2 (except for specimen Batch-2-2).



Figure 25 final crack picture of specimen batch 2-2

4.3 Specimens Terminated and Dissected

Four specimens, two per each batch 1 and batch 2, were selected to be terminated and autopsy for internal visual examination of the corrosion propagation that took place on the corroding reinforcing bars.

4.3.1 Specimen 1-1 Termination and Dissection

Specimen batch 1-1 was selected for autopsy because the measured values of OCP and LPR suggested that corrosion had initiated. Figure 28 shows pictures of the rebars and rebar trace taken within a few minutes after opening this specimen. These pictures capture the corrosion extent.

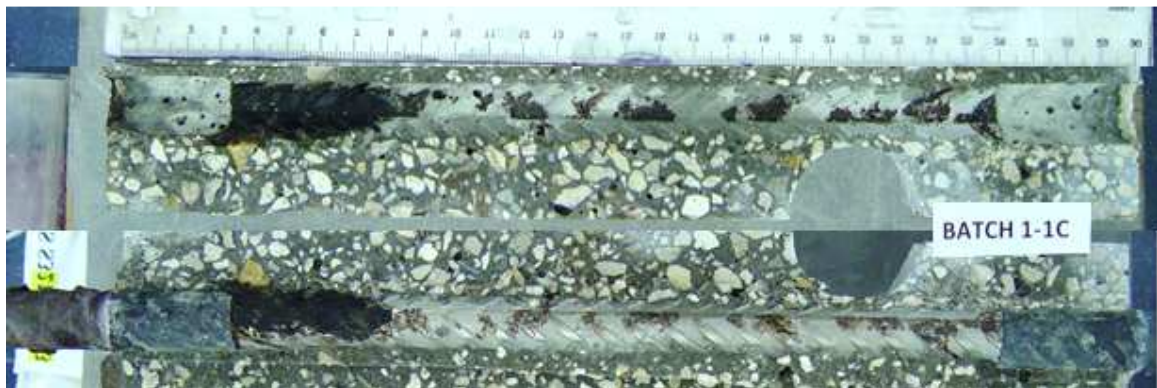
Figure 26 (a) shows a top view of rebar A. The picture shows the corrosion products observed upon exposure of the top surface of this rebar. The corrosion products have a dark brown and black color. Spots of corrosion products are observed almost all along the rebar; but, it has three large spots: on the left (largest of the three), on the middle, and on the right. Rebar B corrosion extent is shown in Figure 26 (b). The corrosion products have a dark brown and black color. The corrosion on this rebar extends from the left side all the way to the middle of the rebar and covers all the top surface about (11 cm long and 1 cm width). This rebar is the one that has most corrosion products and likely the rebar that caused the crack observed on the surface. Corrosion products observed on Rebar C are shown in Figure 26 (c). The corrosion products have a dark brown and black color. The corrosion is almost all along the rebar, but except for a large corrosion spot on the left, the other corrosion sites consisted of smaller spots than those observed for Rebars A and B. The biggest corrosion spot is on the left side of the rebar (about 5 cm long and 1 cm width). The back side of each rebars A, B, and C showed no corrosion. The condition of the three bottom rebars is shown in Figure 48 in the appendix. No corrosion products were observed on these rebars. It is suggested that the chloride concentration above the bottom rebars did not exceed C_T ; so, corrosion did not initiate at this depth (concrete cover about 10.5 cm).



(a) Autopsy and visual examination picture of specimen batch 1-1 rebar A



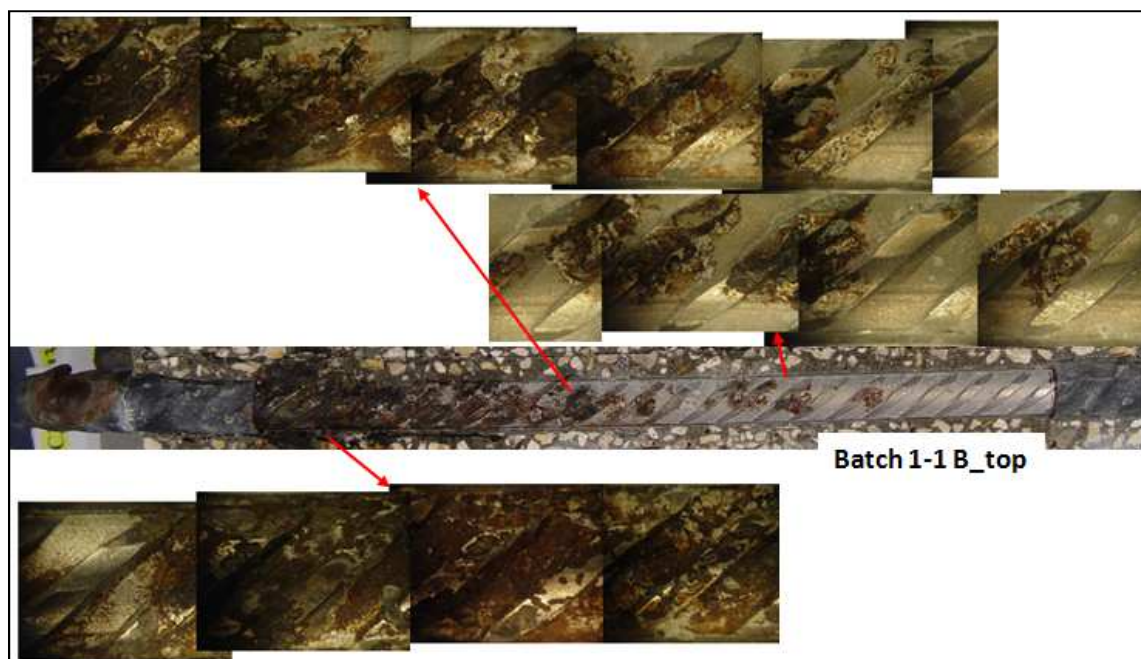
(b) Autopsy and visual examination picture of specimen batch 1-1 rebar B



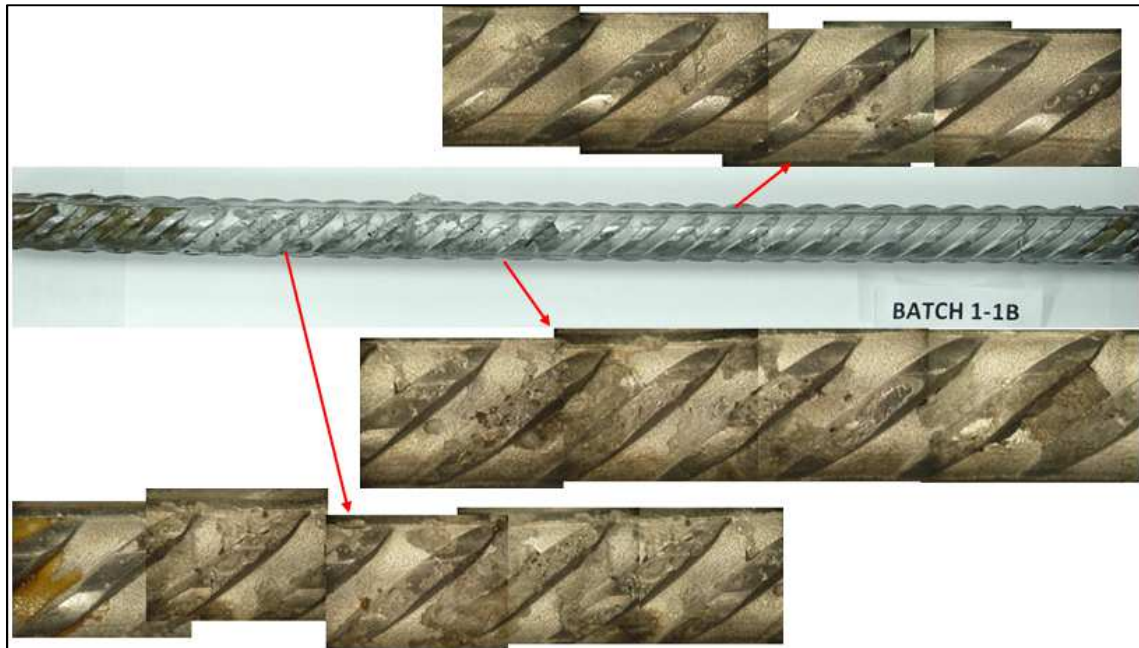
(c) Autopsy and visual examination picture of specimen batch 1-1 rebar C

Figure 26 Autopsy and visual examination of batch 1-1

The corrosion products on the rebars were partially cleaned with a plastic brush and then cleaned as per ASTM G-01. Figure 27 shows the surface of rebar B (batch 1-1 specimen) after brushing and after acid cleaning. The top part of the picture shows the corrosion on the surface of the rebar; but, without the excess of corrosion products. After cleaning, pitting corrosion on the rebar surface was observed of various size and depths (Figure 27 bottom). Here we can see the craters where the pitting corrosion took place. Figure 49 and Figure 50 in the appendix (A) shows close-up pictures after cleaning for rebars A and C respectively of batch 1-1 sample; similar form of corrosion was observed for these rebars, but to a lesser extent.



(a) Picture of Batch 1-1B after cleaning with a plastic brush



(b) Picture of Batch 1-1B after cleaning as per ASTM G-01

Figure 27 Close-up picture of sample batch 1-1B rebar before and after cleaning

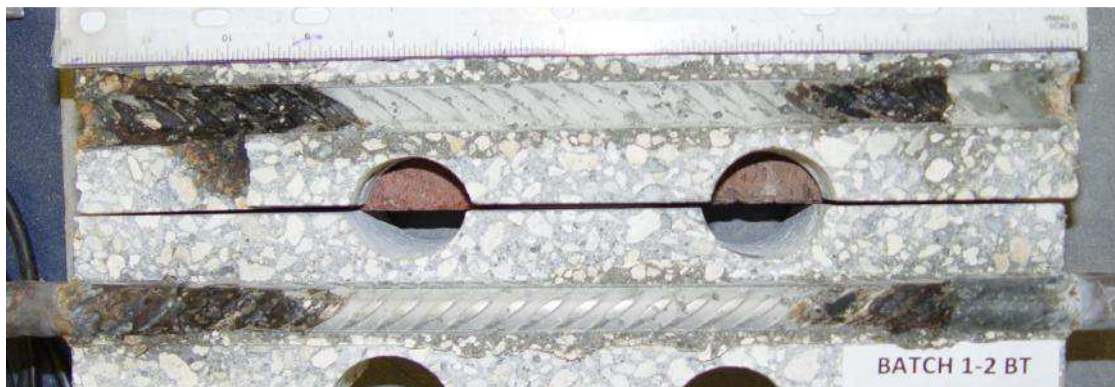
4.3.2 Specimen 1-2 Termination and Dissection

Specimen batch 1-2 was selected for autopsy because the measured values of OCP and LPR suggested that corrosion had initiated. Figure 28 shows pictures of the rebars taken within a few minutes after opening the sample. These pictures capture the extent of corrosion Figure 28 (a) shows a top view of rebar A. The picture shows corrosion products on two sites of this rebar. The color of the corrosion products is black on both side; the dimensions are: right side (5 cm long and 1.2 cm width) and the other site (4 cm long and 1.2 cm width). Rebar B corrosion extent is shown in Figure 28 (b). The rebar have two corrosion sites, left side is (7 cm long and 1.2 cm width) and the other is (5 cm long and 1 cm width). The corrosion product on this rebar is completely black color. Rebar C corrosion extent is shown in Figure 28 (c). Rebar C has two corrosion

sites. The corrosion spot on the right side of therebar is (4.5 cm long and 1.1 cm width), and the other is (2 cm long and 0.8 cm width). No corrosion spots were observed upon inspection on the back side of each rebar (not shown).The condition of middle bottom rebar is shown in Figure 28 (d). For this rebar, located at depth of 10.5 cm corrosion did not take place. The condition of all bottom rebars is shown in Figure 51. No corrosion products were observed on these rebars. It is suggested that the chloride concentration above the bottom rebars did not exceed C_T ; so, corrosion did not initiate at this depth (concrete cover about 10.5 cm).



(a) Autopsy and visual examination picture of specimen batch 1-2 rebar A



(b) Autopsy and visual examination picture of specimen batch 1-2 rebar B



(c) Autopsy and visual examination picture of specimen batch 1-2 rebar C



(d) Autopsy and visual examination of specimen batch 1-2 middle bottom rebar

Figure 28 Autopsy and visual examination of batch 1-2

The surface of the rebars with corrosion product was cleaned with a plastic brush and then cleaned as per ASTM G-01. Figure 29 shows the surface of batch 1-2 B rebar after brushing and after acid cleaning. Figure 29 shows in color pictures the corrosion on the surface of the rebar after brushing it. After acid cleaning, pitting corrosion on the rebar surface can be seen as shown in Figure 29 by the collage of pictures in gray scale. Here we can see the craters where the pitting corrosion took place. Figure 52 shows close-up picture for batch 1-2 specimen rebars A and C after cleaning; similar form of corrosion was observed for these rebars, but to a lesser extent.

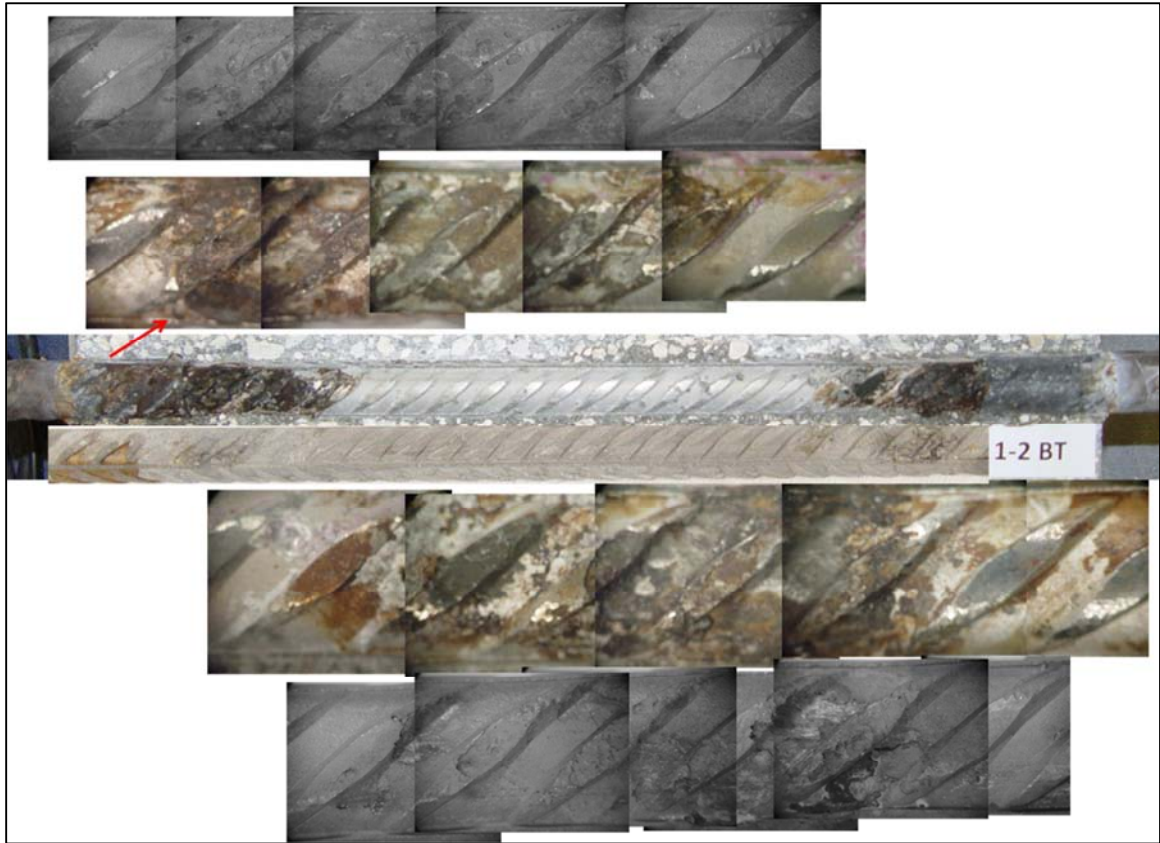


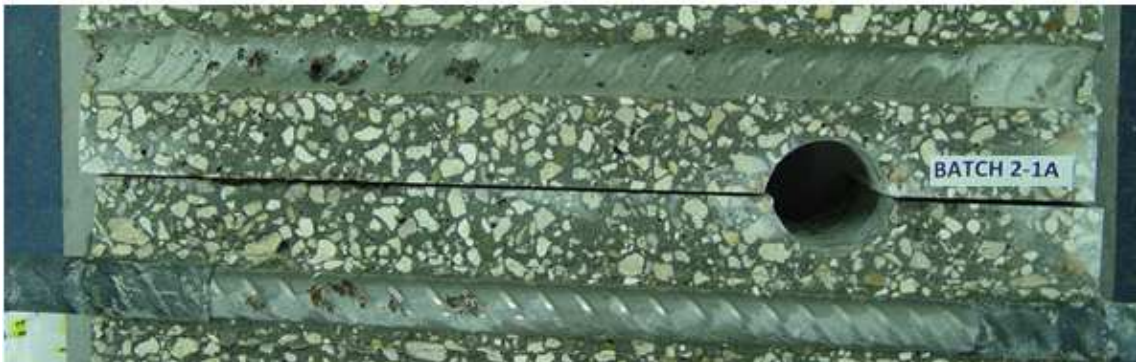
Figure 29 Close-up picture of sample batch 1-2B rebar before and after cleaning

4.3.3 Specimen 2-1 Termination and Dissection

Specimen batch 2-1 was selected for autopsy because the measured values of OCP and LPR suggested that corrosion had initiated. Figure 30 shows pictures of the rebars taken within a few minutes after opening the sample. These pictures capture the extent of corrosion.

Figure 30 (a) shows a top view of rebar A. The picture shows the corrosion products observed upon exposure of the top surface of this rebar. The corrosion products have a dark brown and black color. Rebar A has a few small corrosion spots on the left

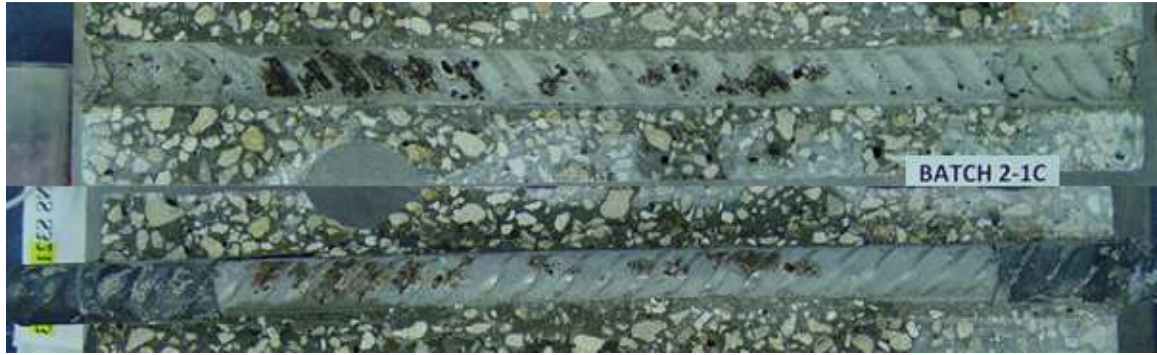
side of the rebar. Rebar B corrosion extent is shown in Figure 30 (b). The corrosion products have a dark brown and black color. This rebar have corrosion products in both sides but the right side is the largest (about 4 cm long and 1 cm width). Rebar C corrosion propagation is shown in Figure 30 (c). The corrosion products have a dark brown and black color. The corrosion spots are found almost all along the rebar length. The biggest corrosion spot is on the left side of the rebar (about 6 cm long and 1 cm width). The condition of the three bottom rebars are shown in Figure 53 in the appendix. No corrosion products were observed on these rebars. It is suggested that the chloride concentration above the bottom rebars did not exceed C_T ; so, corrosion did not initiate at this depth (about 10.5 cm).



(a) Autopsy and visual examination picture of specimen batch 2-1 rebar A



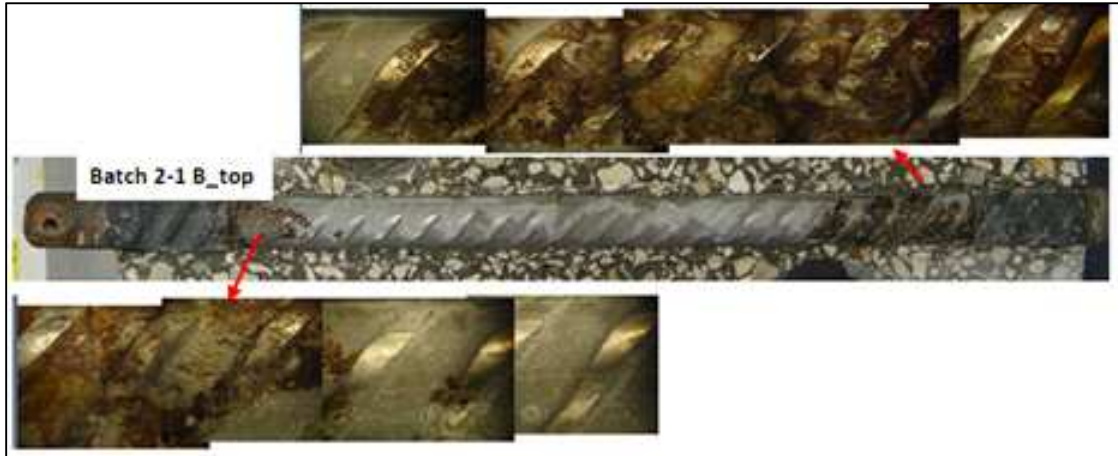
(b) Autopsy and visual examination picture of specimen batch 2-1 rebar B



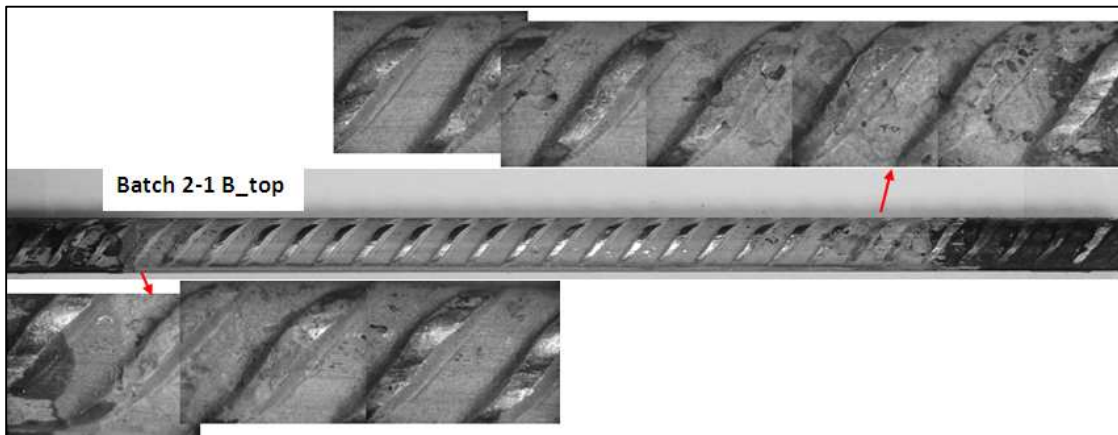
(c) Autopsy and visual examination picture of specimen batch 2-1 rebar C

Figure 30 Autopsy and visual examination of batch 2-1

The rebars surface with corrosion product was cleaned with a plastic brush and then cleaned as per ASTM G-01. Figure 31 shows the surface of batch 2-1B rebar after brushing and after acid cleaning. Figure 31 (a) (top part of the figure) shows corrosion on the surface of the rebar after brushing it. After acid cleaning, pitting corrosion on the rebar surface can be seen as shown in Figure 31 (b) (the bottom part of this figure). Here we can see the craters where the pitting corrosion took place. Figure 54 shows close-up pictures for batch 2-1 sample rebars A and C after cleaning; similar form of corrosion was observed for these rebars. However, the corrosion was less than that observed on rebar 2-1B



(a) Picture of Batch 2-1B after cleaning with a plastic brush



(b) Picture of Batch 2-1B after cleaning as per ASTM G-01

Figure 31 Close-up picture of sample batch 2-1B rebar before and after cleaning

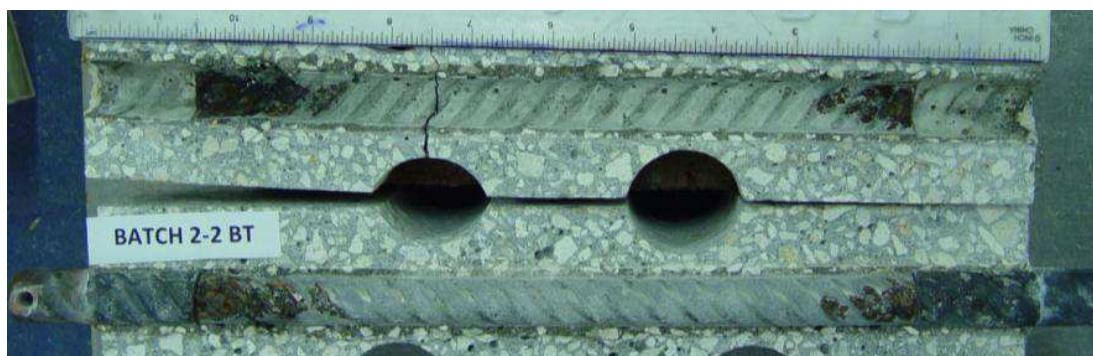
4.3.4 Specimen 2-2 Termination and Dissection

Specimen batch 2-2 was selected for an autopsy because to the measured values of OCP and LPR values indicated that corrosion had initiated. Figure 32 shows pictures of the rebars taken within a few minutes after opening. This specimen was opened one day after the secondary cuts were made. These pictures capture the extent of corrosion on each rebar. Figure 32 (a) shows a top view of rebar A. Corrosion took place on one site

on this rebar. The corrosion products were black, about 5 cm long and it was located about 2 cm from the shrink wrap. Corrosion extent on rebar B is shown in Figure 32 (b) and it was the largest of the three top rebars. The corrosion on this rebar had a black color. Rebar C corrosion is shown in Figure 32 (c). Rebar C had corrosion only in one side but is away from the plastic heat shrink tubing. The corrosion site was very small and appears to have just initiated. The condition of bottom rebars is shown in Figure 55 in the appendix. No corrosion products were observed on these rebars. It is suggested that the chloride concentration above the bottom rebars did not exceed C_T ; so, corrosion did not initiate at this depth (about 10.5 cm).



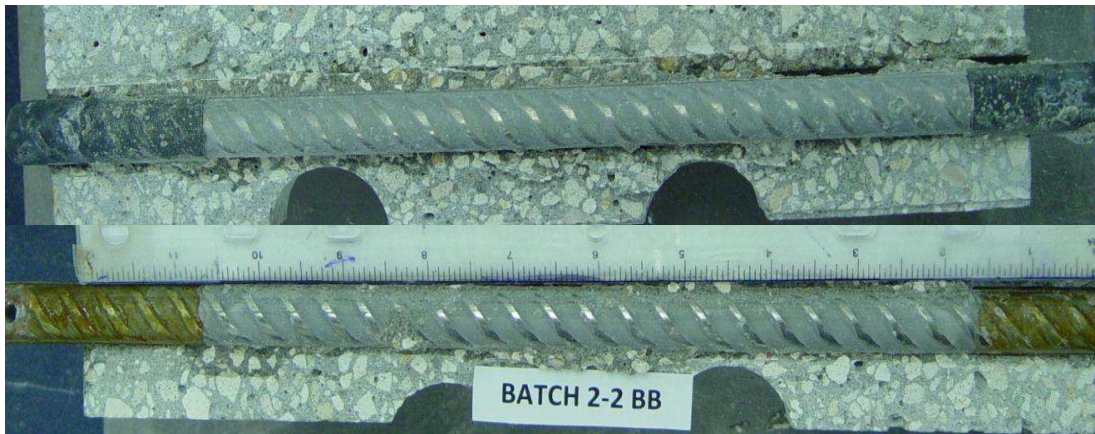
(a) Autopsy and visual examination picture of specimen batch 2-2 rebar A



(b) Autopsy and visual examination picture of specimen batch 2-2 rebar B



(c) Autopsy and visual examination picture of specimen batch 2-2 rebar C



(d) Autopsy and visual examination picture of specimen batch 1-2 middle bottom rebar

Figure 32 Specimen batch 2-2 termination rebar and autopsy picture

The rebars were cleaned with a plastic brush and then following ASTM G-01. Figure 33 shows the surface of rebar B embedded in batch 2-2 specimen, after brushing and after acid cleaning. The top part of the picture shows pitting corrosion on the surface of the rebar with significant amount on corrosion products for both sides. . We can see this by the pits with crater shape where pitting corrosion took place. Figure 34 shows the rebar A before and after cleaning. For rebar A, a similar form of corrosion than on rebar

B was observed, but the pits were not as deep.

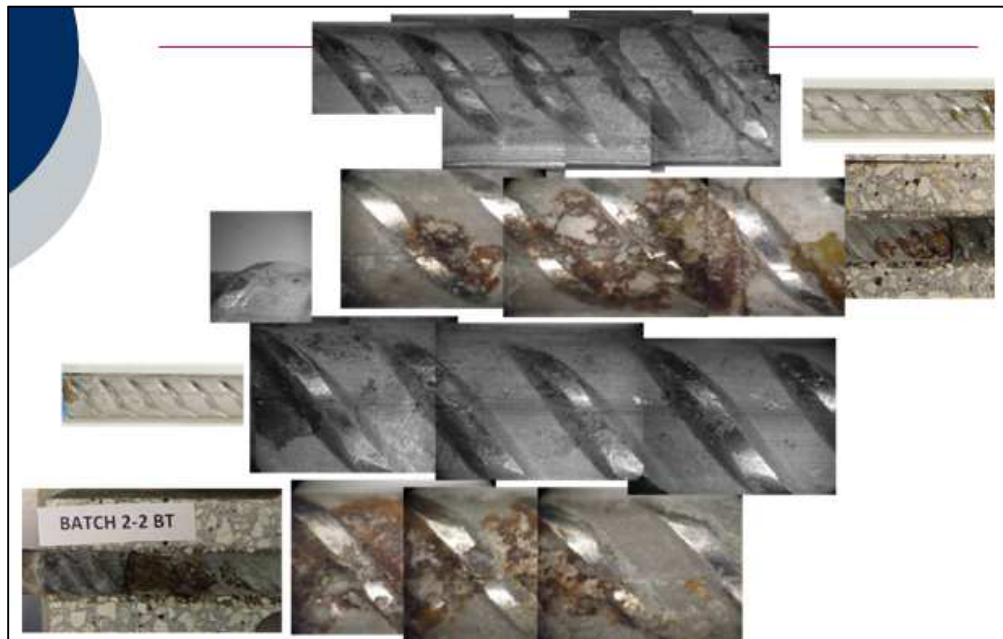


Figure 33 Close-up picture of sample batch 2-2 B before and after cleaning

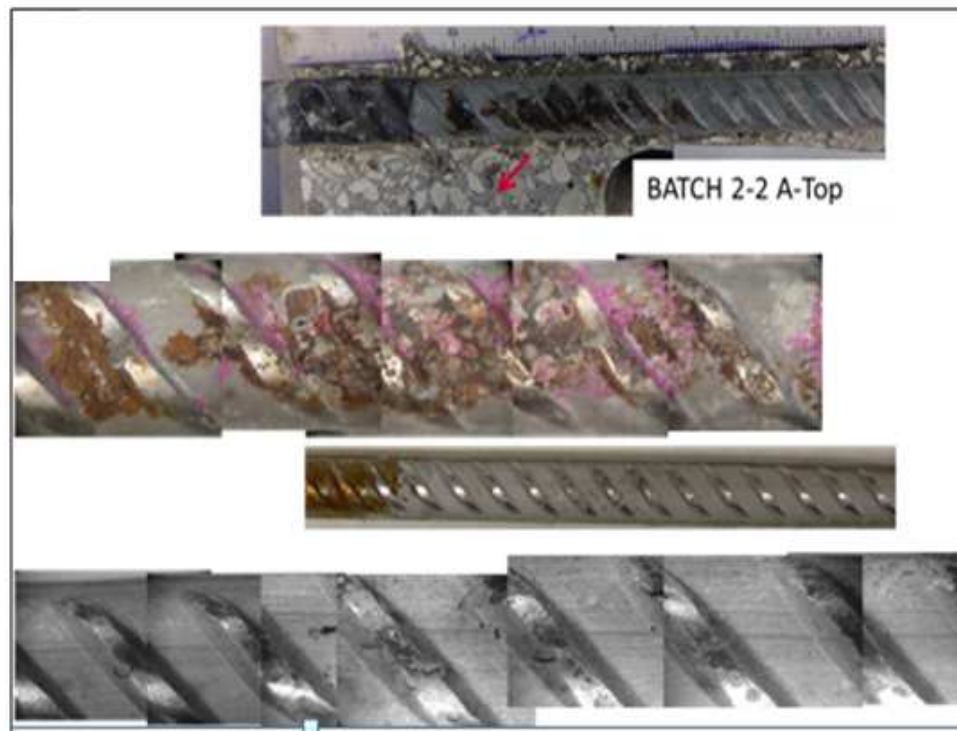


Figure 34 Close-up picture of sample batch 2-2 A before and after cleaning

4.4 Chloride Analysis

Figure 35 shows the chloride profile and the chloride at the rebar trace for batch 1-1 specimen. As expected the chloride content of the cores decreases as a function of depth. The chloride content at the rebar trace for rebar A and C was higher compared to the concentration measured on the slice at the same depth (2.5); but the chloride concentration measure at the trace of rebar B was slightly lower. This can be caused by the fact that the concrete powder collected on this rebar trace was less than for the other two rebar traces. It is important to point out that the transport of the chloride is not quite uniform and depends on the pore structure and tortuosity. Also a certain amount of chlorides might have been consumed at the corrosion sites due to the autocatalytic nature of pitting corrosion.

Figure 35 shows on the plot on the right side the chloride profile and the chloride at the rebar trace for batch 2-1 specimen. As expected the chloride content of the cores is decreasing as a function of depth. The chloride content measured at the trace of rebar A and C was higher compared (as suggested by previous research [22]) to the concentration measured from the core at the same depth (2.5cm). The chloride concentration measured at the trace of rebar A was slightly lower. This could have been caused by the concrete heterogeneity and also the chloride migration reached higher concentrations at some areas of the concrete than others (due to the meshes shape). It is important to point out that chloride transport also depend on the pore structure and tortuosity.

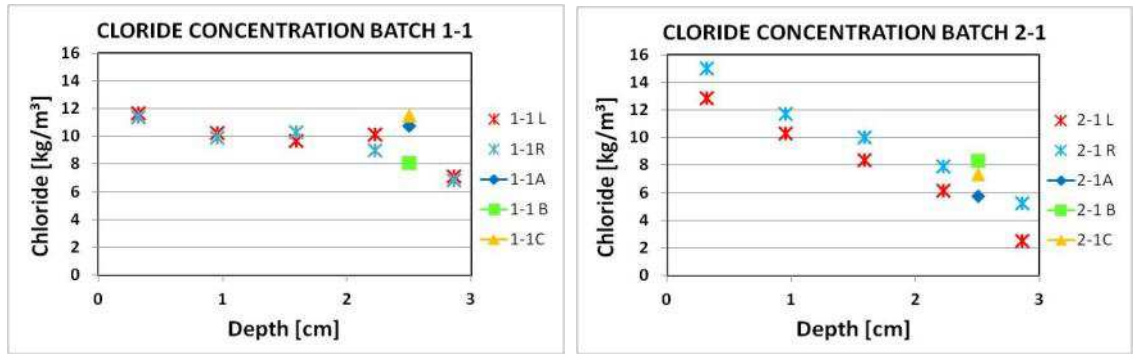


Figure 35 Chloride profile for specimens batch 1-1 and 2-1

4.5 Chloride Threshold of Austenitic and Duplex Stainless Steels

Table 7 and Table 8 shows the chloride concentration obtained from the concrete powder milled at the rebar trace of each rebar on the top row. According to the chloride concentrations in these tables, it is clear that the specimen that were open first (i.e., specimens batch 1-2 and batch 2-2) have lower chloride concentration at the rebar trace than specimens that were open 30 days later. It is important to point out that during those 30 days one additional cycle of electric field potential was applied for 8 days with a potential difference of 15 volts. On Table 8 the chloride average for specimen batch 2-2 was taken from rebars A and B only because rebar C showed only a very small corrosion spot. Each table contains the concentration in kg/m^3 units and in weight percent with respect to the total cementitious amount (WC%). The average WC% on specimen Batch 1-1 was 2.6 percent and for Batch 1-2 it was 1.24 percent. Whereas, for Batch 2-1 specimen WC% was 1.84 percent, and for Batch 2-2 the WC% was 1.22 percent.

Table 7 Chloride concentration at rebar trace (kg/m³) and chloride by weight cementitious percentage (WC%) for Batch 1-1 and Batch 1-2

alloy	Specimen Rebar	kg/m ³	WC %		alloy	Specimen Rebar	kg/m ³	WC %
S32101	1-1 A	10.77	2.76		S32101	1-2 A	4.31	1.10
	1-1 B	8.10	2.08			1-2 B	6.57	1.68
	1-1 C	11.52	2.95			1-2 C	3.69	0.95
	1-1 (average)	10.13	2.60			1-2 (average)	4.86	1.24

Table 8 Chloride concentration at rebar trace (kg/m³) and chloride by weight cementitious percentage (WC%) for Batch 2-1 and Batch 2-2

alloy	Specimen Rebar	kg/m ³	WC %		alloy	Specimen Rebar	kg/m ³	WC %
S32304	2-1 A	5.80	1.49		S32304	2-2 A	4.15	1.06
	2-1 B	8.35	2.14			2-2 B	5.41	1.39
	2-1 C	7.35	1.88			2-2 C*	1.93	0.49
	2-1 (average)	7.17	1.84			2-2 (average)	4.78	1.22

Table 9 shows a comparison of the critical chloride threshold concentration (C_T) corresponding to different steels (including austenitic and duplex) as reported from several authors. In a few instances corrosion did not initiate; for those cases the values shown are lower bound values, i.e., C_T is greater than the value shown. This data is compared with the results of this research and parallel ongoing research being conducted at FAU. It is important to point it out that the results may vary from author to author because the experiments were performed with different specimen geometry (small and large specimens), with different total surface area exposed, and different methods of chloride transport (i.e. dry/wet cycles, electric field application, chlorides cast during mix preparation). However, all rebars were embedded in mortar or concrete specimens. Trejo [17] reports values of C_T by weight cement % that are low compared with the values

reported by the others authors' (see Table 9). This lower C_T values can be caused from the way in which the experiment was performed; small mortar geometry was used for the specimens (7.5 cm X 15 cm cylinder). The experiment used a migration cell to accelerate the chloride transport. An electric field was applied at periodic intervals by setting a potential difference of 20 V between a cathode in a reservoir with Cl^- solution and an anode embedded at the depth of the reinforcement. The electric field applied by Trejo was considerably larger than the one employed in this investigation (See approach section 3). Table 9 also shows the C_T values reported by Castellote [13] for carbon steel. The WC% reported by Castellote is close to 1%: a migration cell approach was used but the anode electrode was not at the rebar depth, and the potential difference was 12V across a mortar specimen 7 cm thick. The rebar was embedded in mortar (7cm X 7 cm). The electric field was applied between the NaCl reservoir and plate bottom (electrical connected, wet sponge, to the sample). Periodic intervals of potential difference were applied. The w/c was 0.37 for the mortars. Table 9 also shows the C_T values reported by Bertolini [23] for 316, 2101 and 2304 stainless steel. C_T values for duplex range from 3 to 5 % by weight of cement.

Table 9 Critical Chloride Threshold Value for different authors and steels by Weight by cement (WC) %

Author	alloy	kg/m ³	WC %	w/c or w/cm	Corroded Y/N	Note
Trejo	carbon steel	0.5	0.1	0.5	Y	mortar geometry
[17]	microcomposite	4.5	0.8	0.5	Y	
	S30400	5.0	1.2	0.5	Y	migration Cl penetration method
	S31600	10.8	1.9	0.4	Y	Counter at rebar depth - XX potential
Castellote [13]	carbon steel		1.1	0.4	Y	mortar geometry, migration cell, 12V
Bertolini	S32101		3 to 5		Y	mortar geometry
[23]	S32304		3 to 5		Y	Cl added to the mix
	S31600		8.0		Y	
Schonning & Randstrom [5]	S30400		>4		N	mortar geometry
	S31600		>4		N	Cl added to the mix
	S32101		>4		N	
	S32304		>4		N	
[F. Presuel, F. Gutierrez, personal communication]	C2 S32304	25.0	3.9	0.5	N	mortar geometry
	C4 S32304	31.1	4.9	0.5	Y	dry/ wet -15% NaCl Solution
	C4 S32101	30.9	4.9	0.6	Y	
	C3 S30400	25.6	4.0	0.5	N	
	C1 S30400	24.1	3.8	0.5	N	
	S03-S32304	32.8	5.2	0.4	Y	
Presuel [24]	S32304	13.9	6.5	0.5	Y	SDS Geometry/ Concrete
	S30400	13.9	6.5	0.5	Y*	Outdoor exposure
	S31600	16.1	7.7	0.5	N	weekly dry/wet 15% NaCl solution
This Investigation	S32101	7.9	1.9	0.4	Y	SDS Geometry / Concrete 10%FA as cementitious
	S32304	6.0	1.5	0.4	Y	dry/wet & migration Cl penetration method

In Bertolini's experiment, the rebars were embedded in mortar (25cm x 15cm x 5cm) and chloride was added by mass of cement upon casting for those that caused corrosion to initiation. Table 9 shows the C_T values reported by Presuel [24]; the C_T values were measured on mortar specimens and also on concrete specimens, for UNS32304 the values is close to 5%. The overall average of C_T values from this investigation, were 1.9 for

UNS32101 (averaging all values from specimen 1-1 and 1-2) and 1.5 for UNS32304 (averaging value from specimen 2-1 and 2-2). These values are larger than those reported by Trejo's but lower than Bertolini's or Presuel's. This observation confirms that the migration approach polarizes the steel due to the ionic current flowing and this appears to lower C_T even if a mature passive layer is present. Specimens tested at an early (28 days to 2 months) age appear to have even lower C_T values (Trejo's [17]). Chlorides casted into the concrete as for specimens tested by Bertolini might have prevented or modified passive layer formation with the concrete pore solution, thus these C_T might need to be considered as lower bound values.

4.6 Localized corrosion penetration causing concrete cover to cracks

Corrosion of the reinforcing steel causes the concrete cover (C) to crack, when the metal loss reaches a critical penetration depth X_{crit} . This value is very important for predictive models of the corrosion propagation stage. In previous investigations [25] it was found that the values of X_{crit} increased when corrosion becomes more localized. This investigation compares X_{crit} values calculated from the results of this investigation (assumptions given below) with models based on empirical equations proposed by [25] and [26].

Table 10 shows the mass loss approximation of the rebars (S32101 and S32304) and the different parameter used to calculate it. This investigation did not have the initial weight of the rebars. In order to obtain the mass loss of the corroded rebars the following procedure was performed:

- After opening the specimens, the corrosion product was removed from each rebar segment as per ASTM G-01. This was achieved by repeatedly conducting a procedure of immersion in cleaning solution (93.5 wt% HCl + 0.7 wt% Sb₂O₃ + 4.7 wt% SnCl₂) and then brushed to remove any remaining corrosion products (multiple times if needed until the rebar weight stopped changing).
- After the clean up the weight on the rebars were measured (see Table 10 for the results).
- Then, the approximate volume of each rebar was calculated based on the rebar length (see Table 10 for the results).
- Since the bottom rebars did not corrode; they were used as reference to find out the density of each rebar type (S32101 and S32304). The average density for each alloy was calculated (see Table 10 for the results). These values assumed cylinder shape for the rebar.
- Then, with each rebar volume and the average density, the apparent initial weight of each rebar was calculated (see Table 10 for the results).
- Finally, the mass loss for each rebar was calculated by subtracting from the apparent initial weight the measured weight after cleaning (see Table 10 for the results).

Table 10 Mass loss approximation and parameters

		final measure d mass g	total length cm	volume cm ³	density g/cm ³	mean density g/cm ³	apparent calculated initial mass g	mass loss g
Bottom Rebars	1-1A	562.2	37.3	79.76	7.05	7.04		
	1-1B	558.8	37.2	79.54	7.03			
	1-1C	542.2	36	76.98	7.04			
	2-1A	556.3	35.7	76.34	7.29	7.28		
	2-1B	555.7	35.8	76.55	7.26			
	2-1C	555.5	35.6	76.12	7.30			
Top Rebars	1-1A	529.4	35.2	75.27			529.82	0.419
	1-1B	559.7	37.2	79.54			559.92	0.222
	1-1C	550.5	36.7	78.47			552.40	1.896
	1-2A	555.8	36.9	78.90			555.41	
	1-2B	549.4	36.6	78.26			550.89	1.491
	1-2C	538.7	35.8	76.55			538.85	0.150
	2-1A	555.2	35.7	76.34			555.84	0.636
	2-1B	553.2	35.6	76.12			554.28	1.079
	2-1C	556.4	35.7	76.34			555.84	
	2-2A	554.9	35.6	76.12			554.28	
	2-2B	553.9	35.6	76.12			554.28	0.379
	2-2C	554.7	35.6	76.12			554.28	

In Table 10 the highlighted cell in yellow are the rebars that likely caused the crack(s) for each specimen. These are the rebars that have the largest mass loss per each specimen. Some rebars mass loss are not shown; as a negative value would be reported because the penetration of the pitting corrosion was small and due also to the simplified approach used to calculate the original mass.

A previous investigation [26] proposed a relationship between X_{crit} and the length of the localize corrosion. When the length is short the amount of X_{crit} is greater compared to the case of more uniform corrosion [25]. Base on experiments from other

investigation [25] where corrosion surface of the corroding segments was approximately approaching uniform states:

$$X_{crit} = 0.0111 \left(\frac{C}{\emptyset} \right) \left(\frac{C}{L} + 1 \right)^2 \quad (1)$$

Where C is the concrete cover depth, \emptyset is the rebar diameter assuming cylinder shape of the rebar, and L is the length of the corroding segment. For our investigation the L value was obtained from measurements on the rebar side where the crack was observed, and from the summation of the different length of each small pitting corrosion spots that were observed to be deep enough to contribute to the crack formation. An illustration of how L value was obtained for specimen 1-1 rebar C (46 mm) is shown in Figure 36. The top picture shows the corrosion spots circled in red and the bottom picture is the same image without the circled spots.

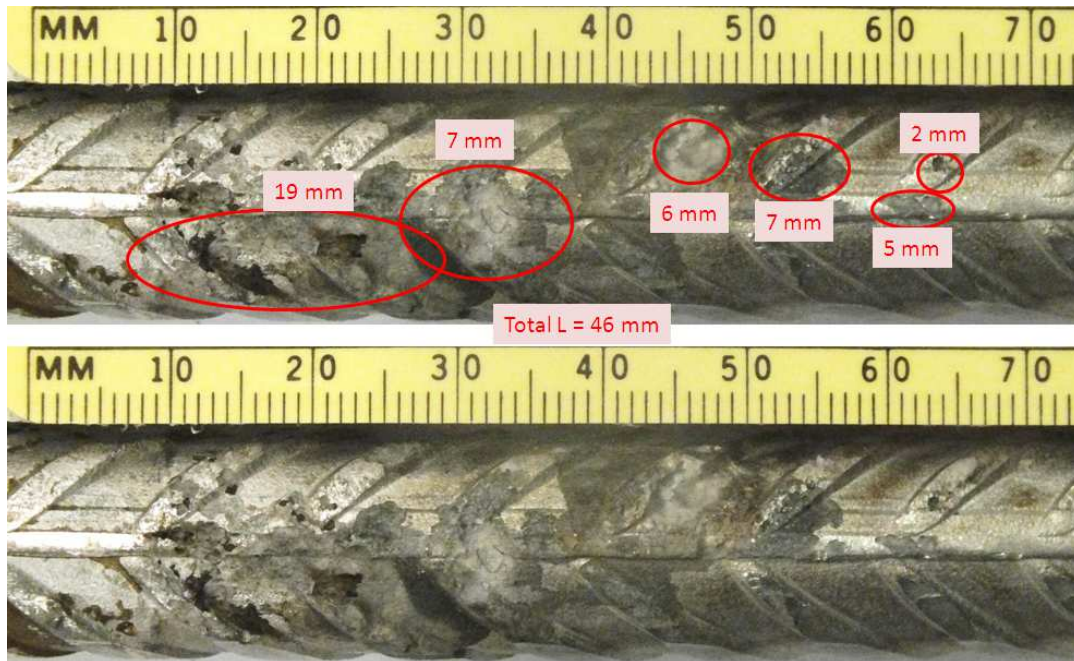


Figure 36 Observed length L and value explanation process for specimen 1-1 rebar C

Figure 37 shows an illustration of the area where the measurement for L was obtained for rebar 2-2 B (17.86 mm). The top picture shows the corrosion spots circled in red and the bottom picture is the same image without the circled spots.

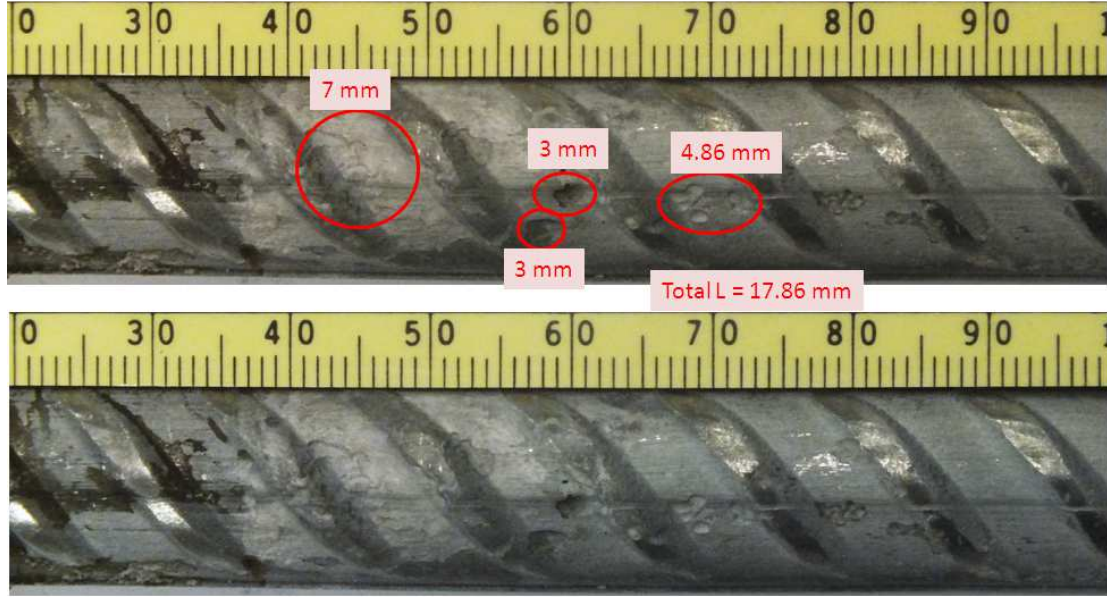


Figure 37 Observed length L and value explanation process for specimen 2-2 rebar B

A more recent investigation [26], proposed equation (1) be modified. Investigation [26] replaced the exponential 2 of the term $\left(\frac{C}{L} + 1\right)$ of equation (1) and replaced it by 1.48 that was obtained by an exponent of 1.48. This new exponent was obtained by a fit to previous reported values [26] and Busba [25] reported their results. Thus:

$$X_{crit} = 0.0111 \left(\frac{C}{\phi}\right) \left(\frac{C}{L} + 1\right)^{1.48} \quad (2)$$

Table 11 shows the predicted X_{crit} values for $\left(\frac{C}{L} + 1\right)$ and (C/ϕ) pairs relevant to our experiment using empirical equations (1) and (2). Table 11 also shows X_{crit} values. Calculated X_{crit} were obtained using the mass loss (ΔW) from Table 10 for those rebars that likely caused the cracks and the following equation [26]:

$$X_{crit} = \frac{\Delta W \times 10^3}{\pi \phi L \rho_{Fe}} \quad (3)$$

Table 11 values for different equations and parameters

	ΔW (g)	ϕ (mm)	$\rho(Fe)$	L (mm) corrode	X_{crit} equ 3	C (mm)	X_{crit} equ 1 n=2	X_{crit} equ 2 n=1.48
1-1C	1.896	16.5	7.86	46	0.1012	23	0.03481	0.02820
1-2B	1.491	16.5	7.86	41	0.0893	23	0.03770	0.02991
2-1B_T	1.079	16.5	7.86	31	0.0854	23	0.04695	0.03518
2-2B	0.379	16.5	7.86	17.86	0.0521	23	0.08098	0.05266

Although the rebars investigated here are CRAs; we assumed the density of iron in equation 3. Figure 38 shows the estimated critical penetration X_{crit} , calculated for the rebars that likely caused the crack(s). Recall, that here L is the summation of the length of the spots affected by corrosion as explained above. Here the continuous lines are calculated from equations (1), (2) and the triangle symbols are the calculated X_{crit} values from this research. The calculated X_{crit} values from this research are larger than those from both models when the C/L ratio is between 1 and 2; but for values of C/L greater

than 2 the X_{crit} is similar to the values suggested by equation (2). The larger X_{crit} values can be caused because in our experiments the corrosion was more localized (corrosion was observed only on one side of the rebar and in most areas it did not cover all the top rebar surface width) whereas the empirical equations assume that corrosion is uniform along L .

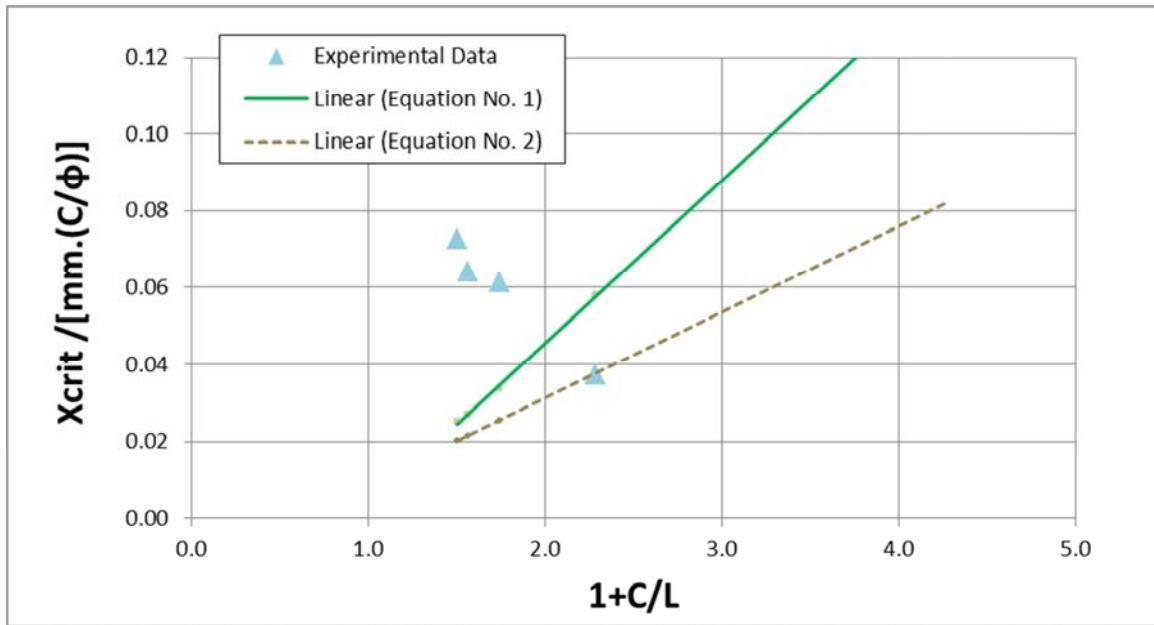


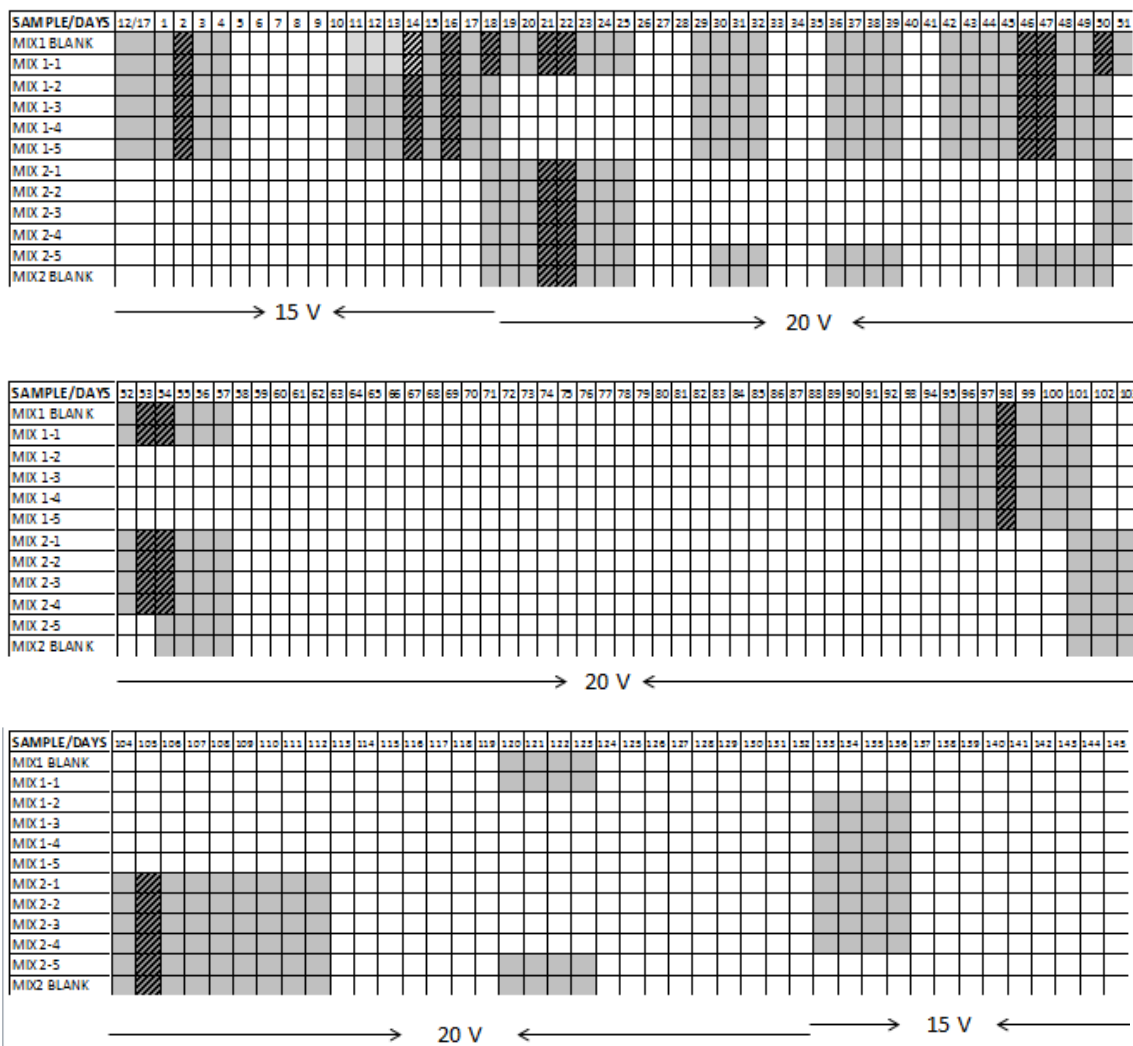
Figure 38 Plot of the X_{crit} values for equations (1), (2) and experimental results as a function of C/L ratio

5 CONCLUSION

- Developed a methodology that allows for corrosion to initiate and propagate on concrete specimens embedded with CRAs and initially chloride free.
- Stray current might have caused an accelerated corrosion rate (due to additional electric field application once corrosion had initiated) on reinforcing bar(s) where corrosion had initiated.
- The results from this investigation suggests that UNS S32304 rebars corrode at a slower rate than UNS S32101 rebars (once corrosion has initiated).
- The average C_T for UNS S32101 rebars was found to be 1.9 % by cementitious weight and for UNS S32304 rebar was found to be 1.5 % by cementitious weight.
- According to the chloride concentrations measured at the rebar trace, corrosion initiated on duplex S32101 rebars on average at 7.9 kg/m^3 , and corrosion initiated on duplex S32101 rebars on average at 6.0 kg/m^3 .
- The results of C_T values from this investigation, of UNS S32101 rebars and UNS S32304, are found to be lower compared to reported C_T values on specimens under non-accelerated chloride transport.

APPENDIX A. FIGURES & TABLES

Table 12 Applied voltage schedule



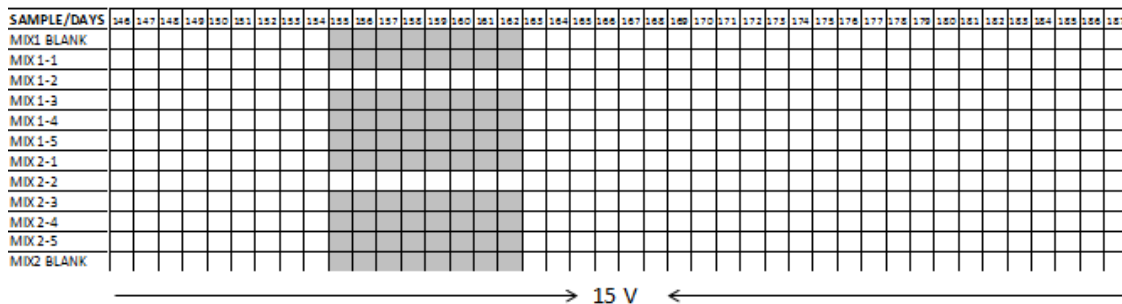


Figure 39 Open Circuit Potential (OCP) Measurements of Phase I – Batch 1 Samples

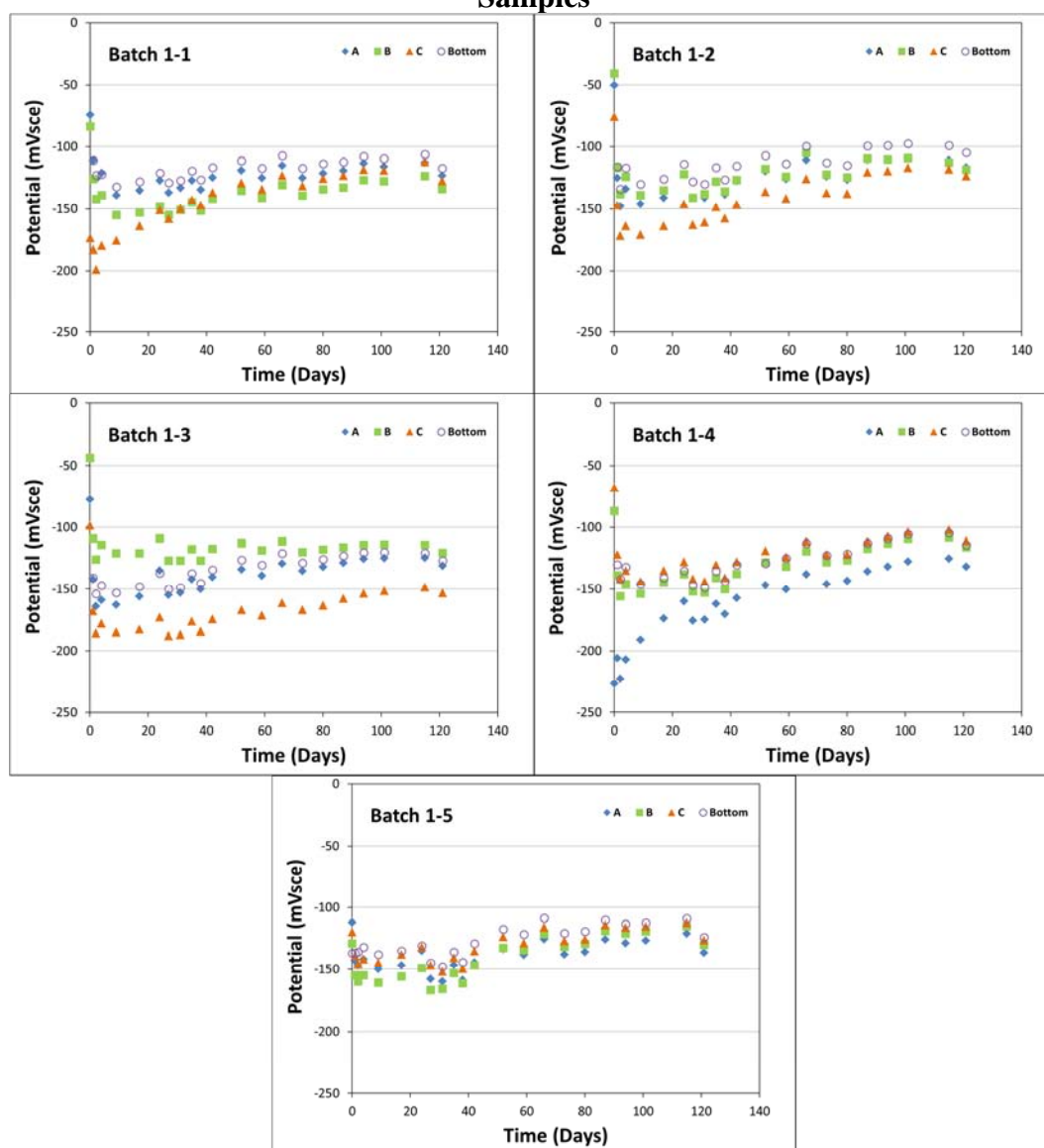


Figure 40 Open Circuit Potential Measurements (OCP) of Phase I – Batch 2 Samples

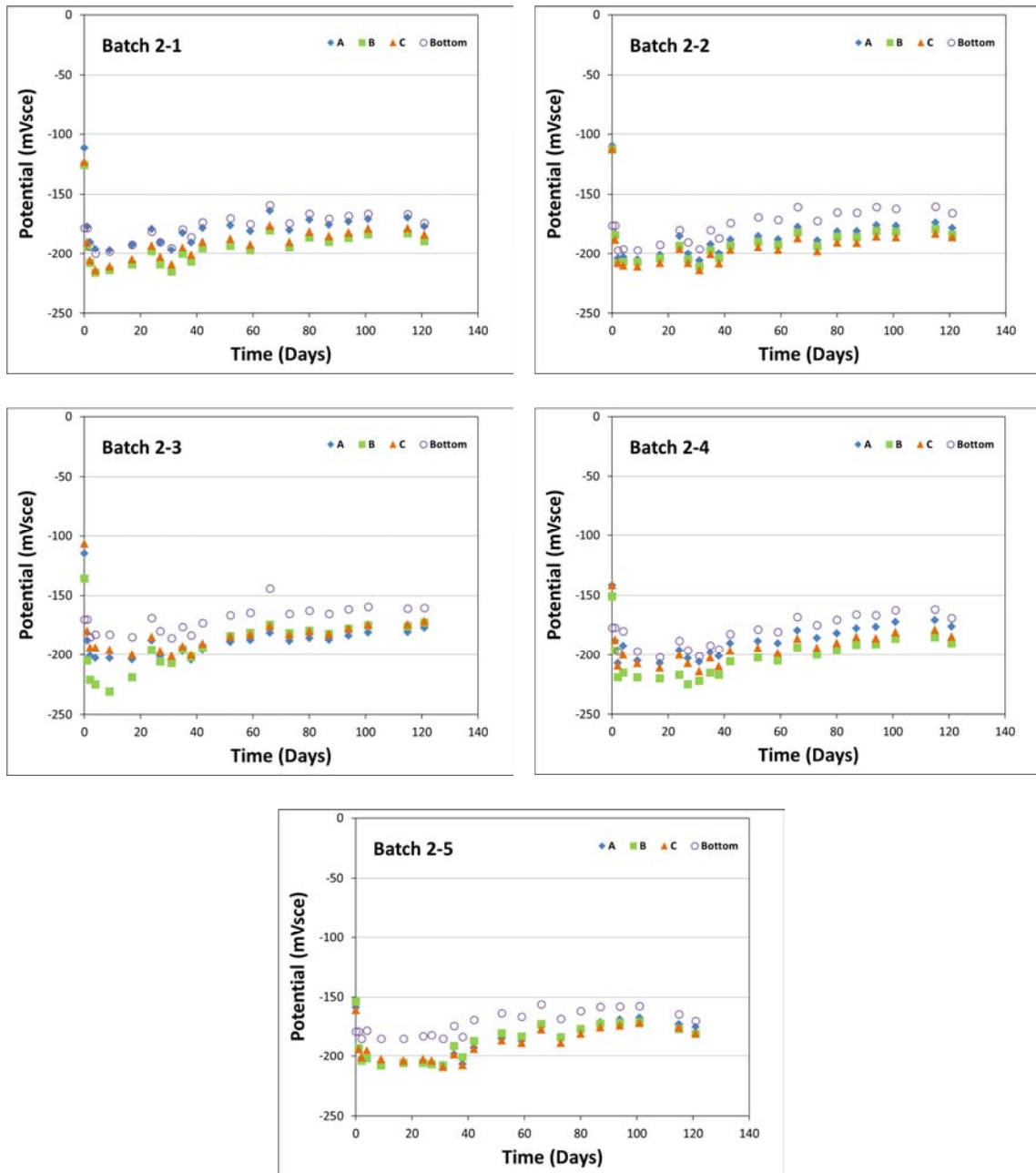


Figure 41 OCP measurements over time for batch 1 samples at Phase II

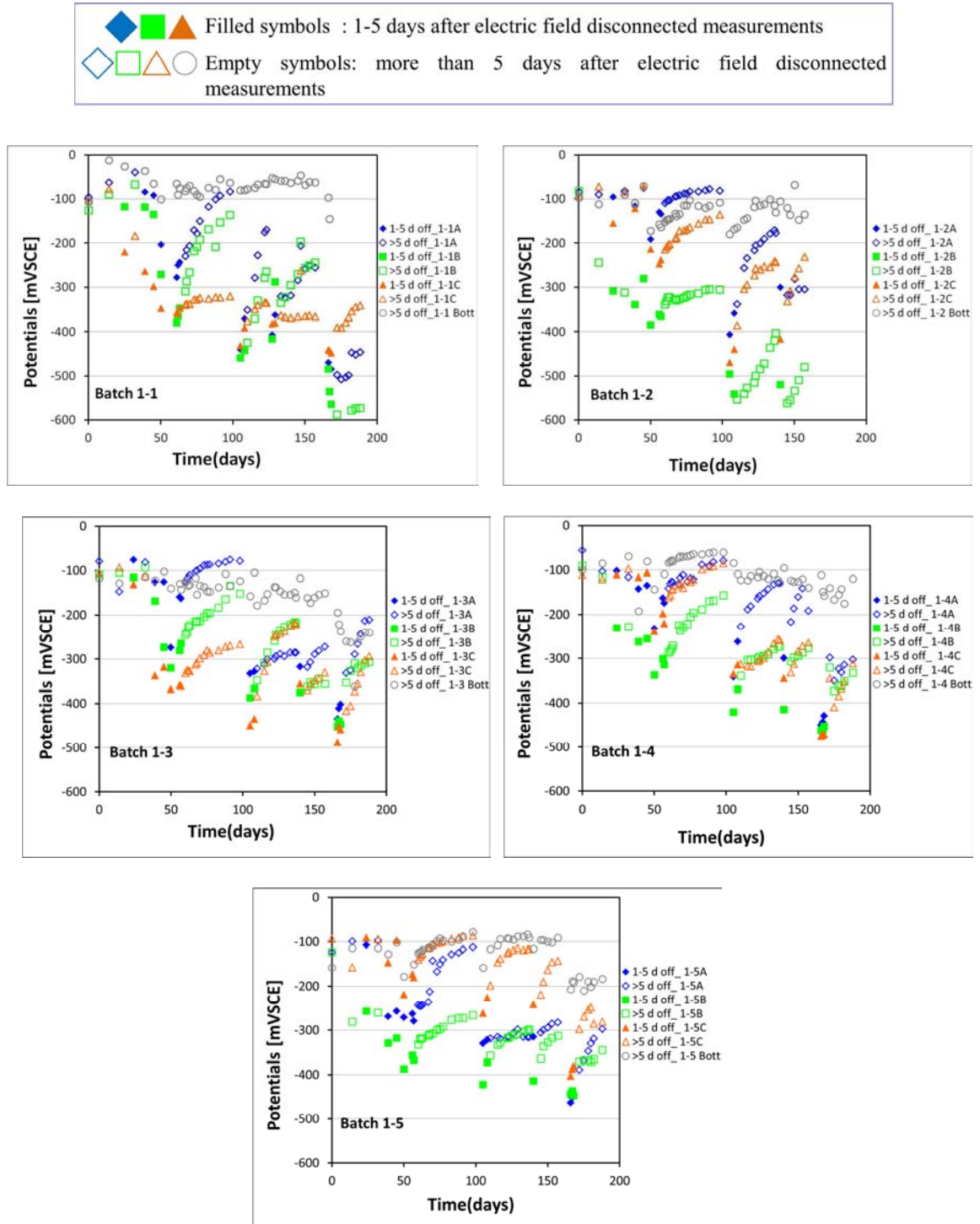


Figure 42 OCP measurements over time for batch 2 samples at Phase II

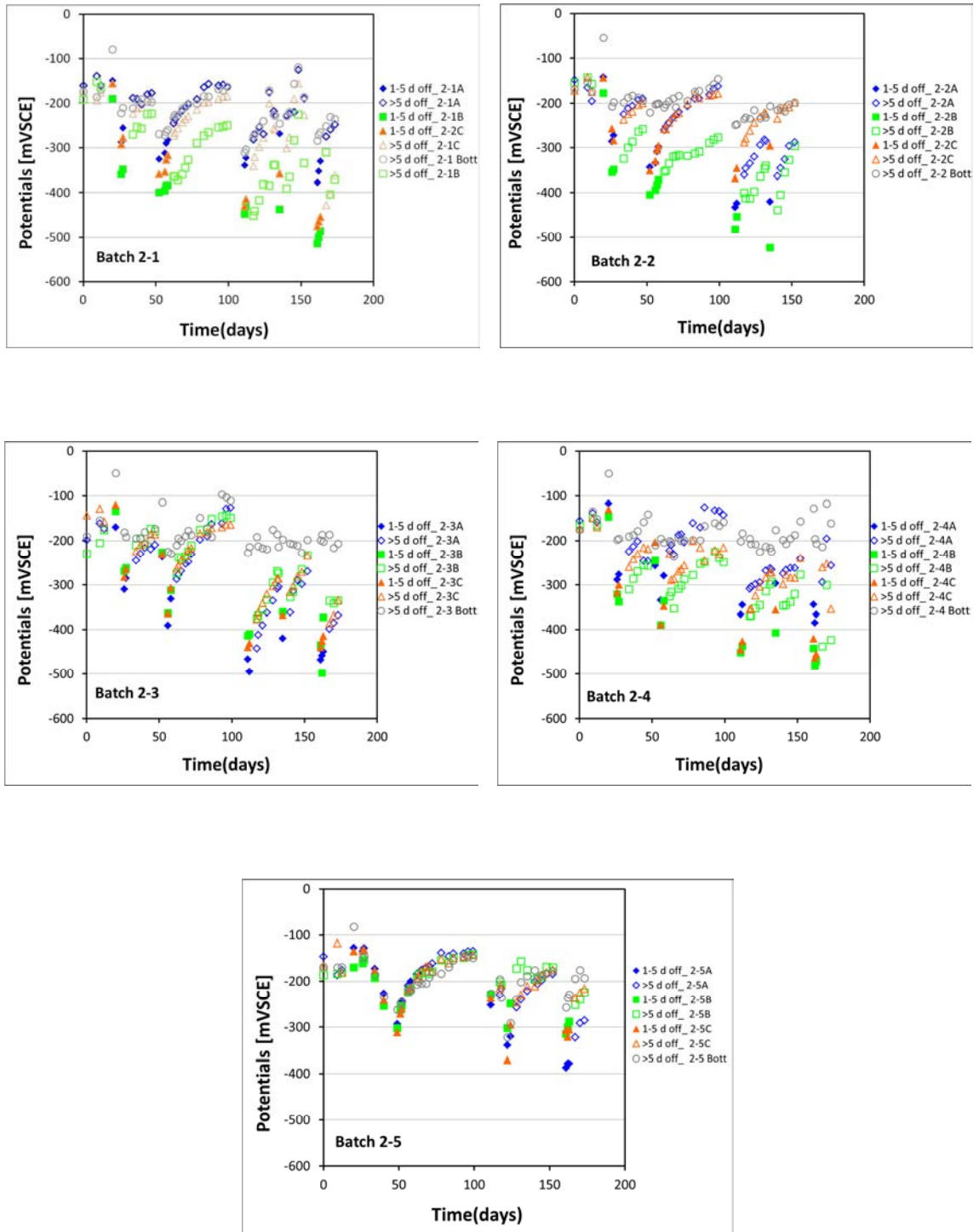


Figure 43 Solution Resistance over time for samples batch 1 phase II

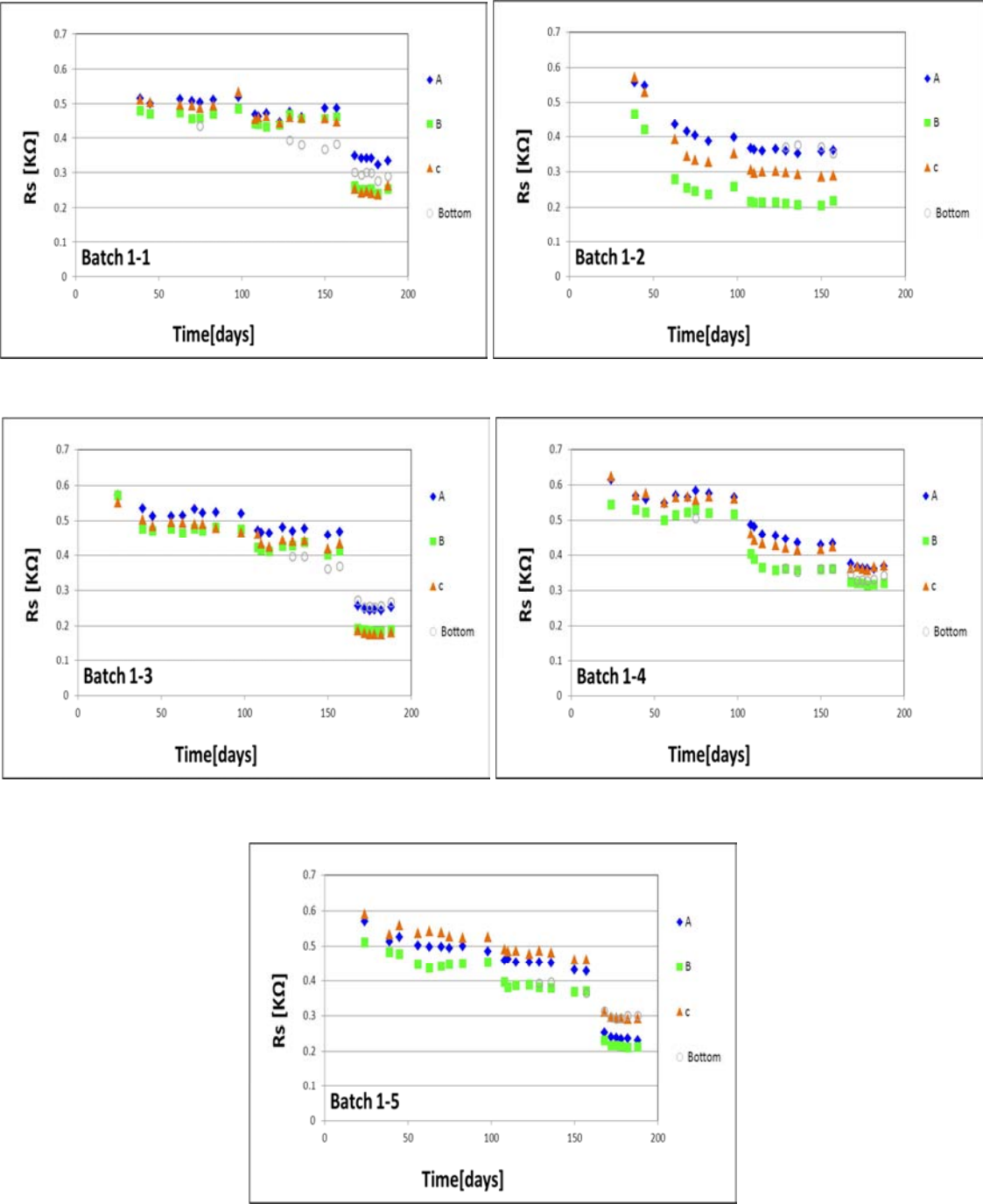


Figure 44 Solution Resistance over time for samples batch 2 phase II

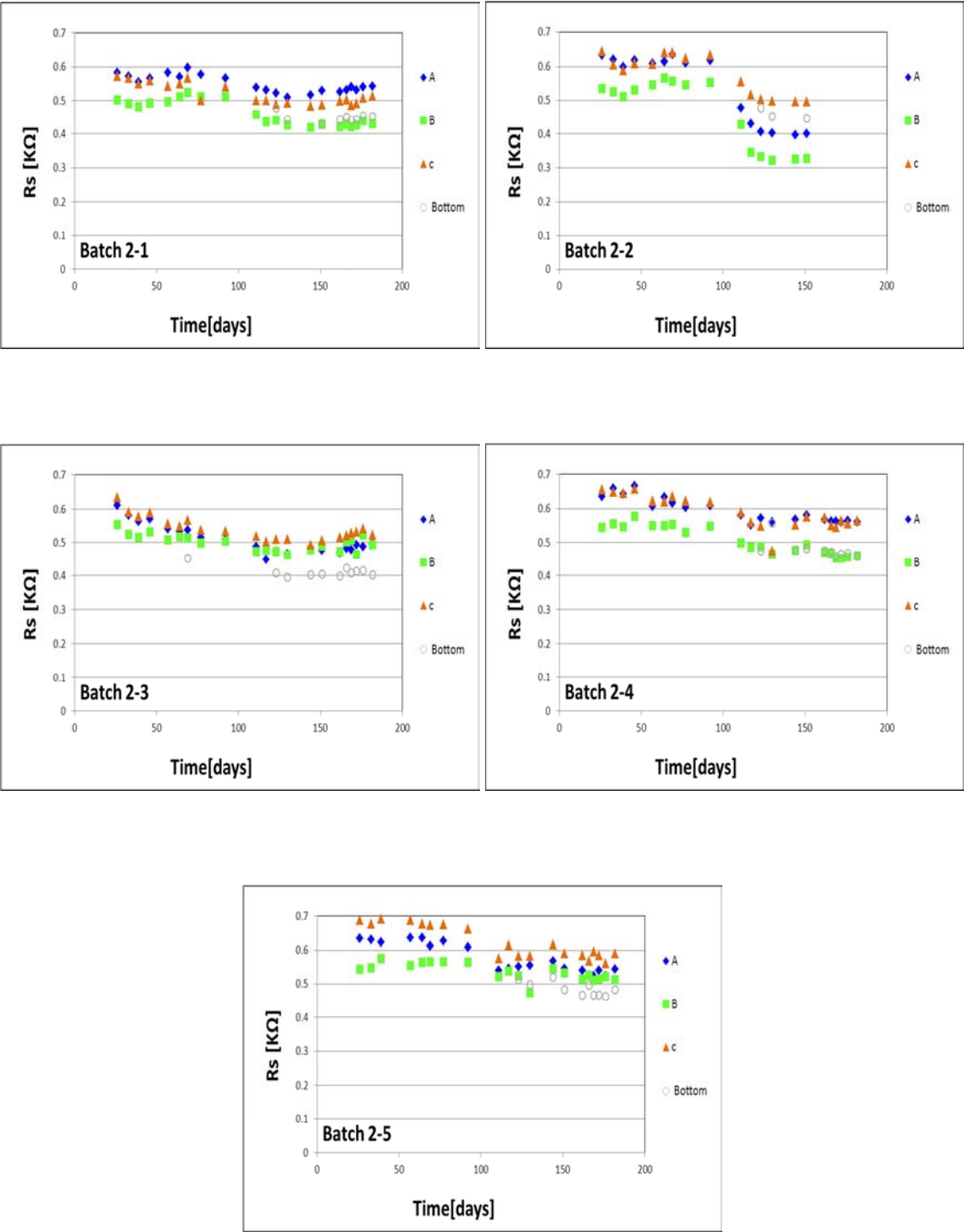


Figure 45 Rp_meas-Rs over time for batch 1 samples at Phase II

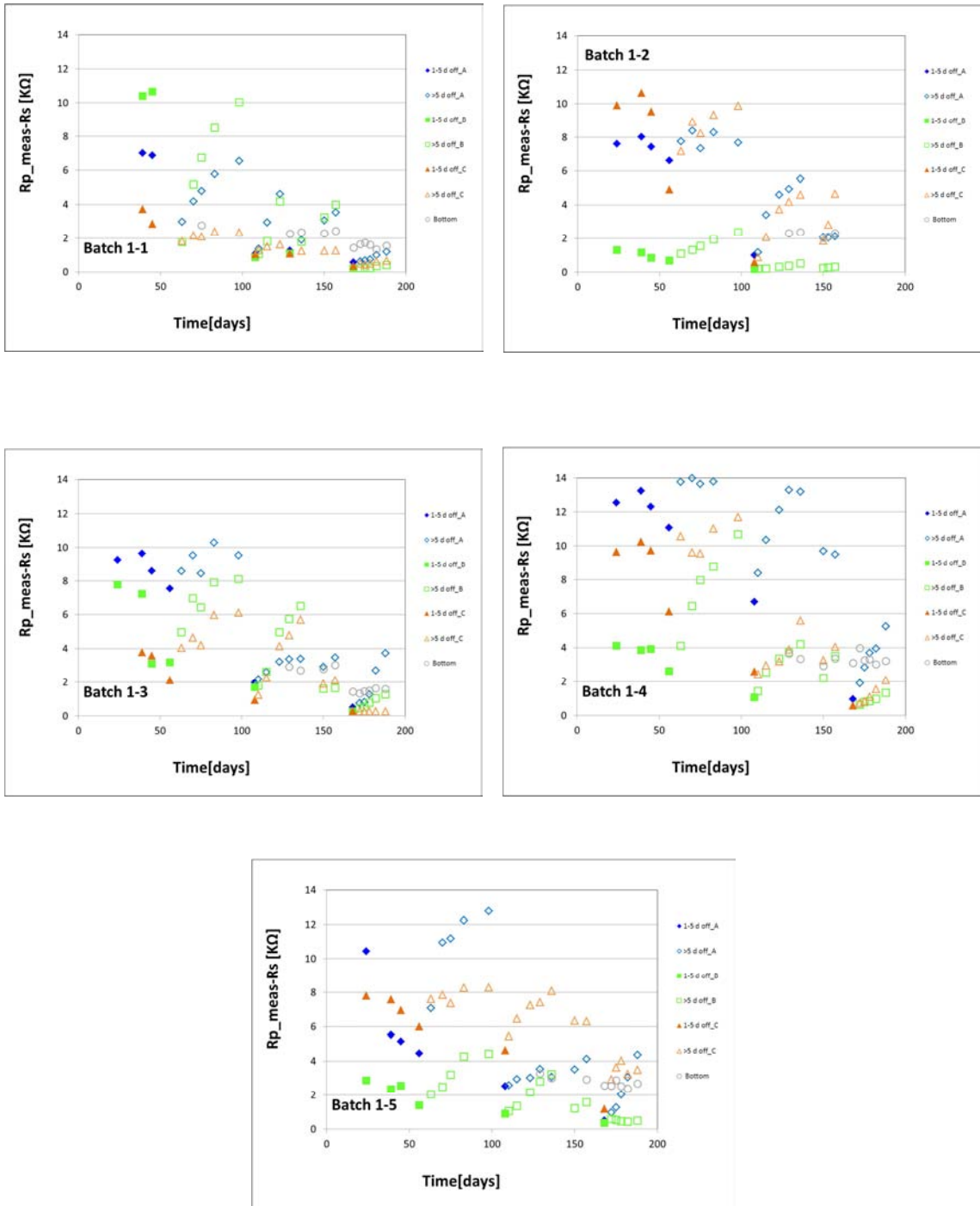


Figure 46 Rp_meas-Rs over time for batch 2 samples at Phase II

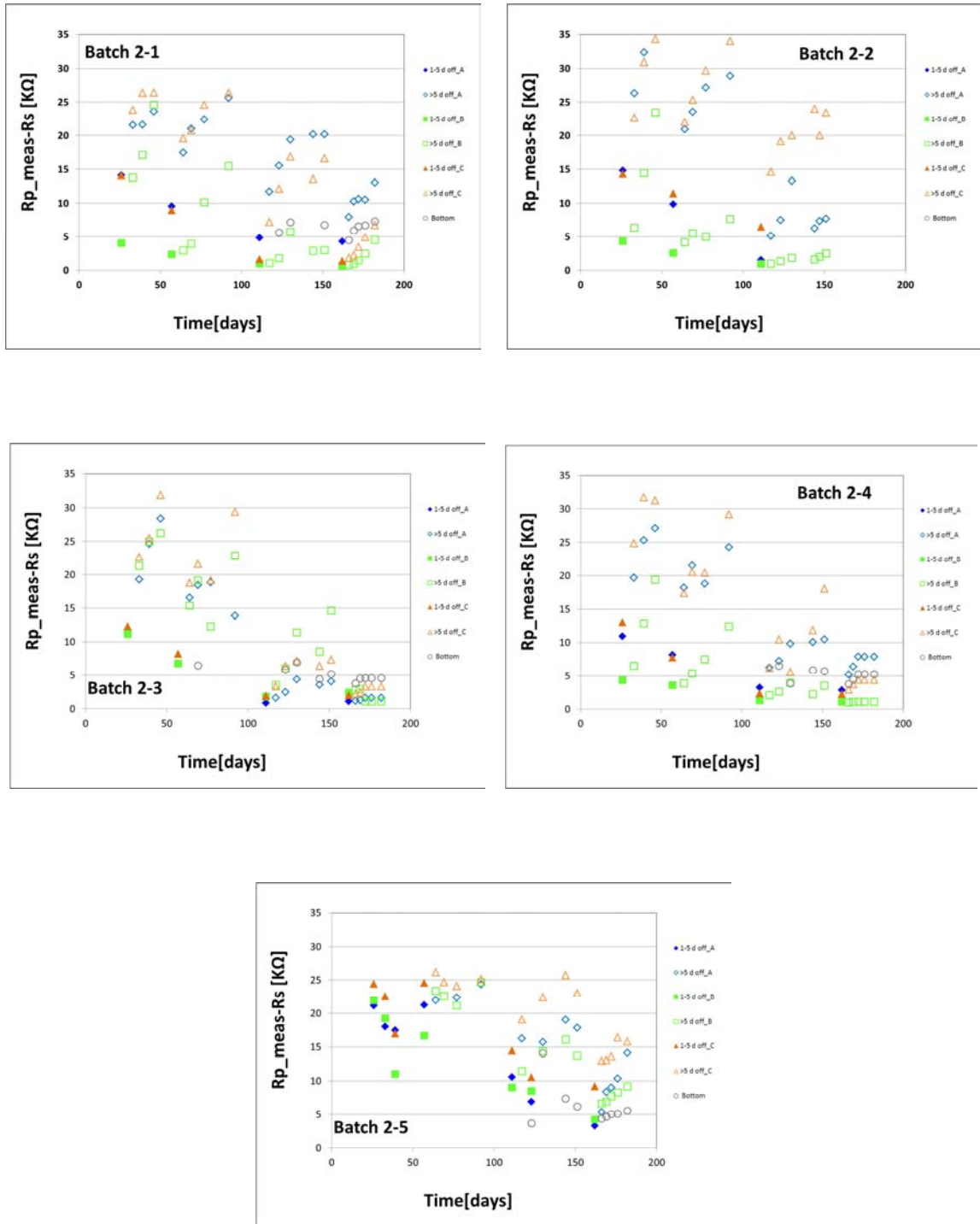
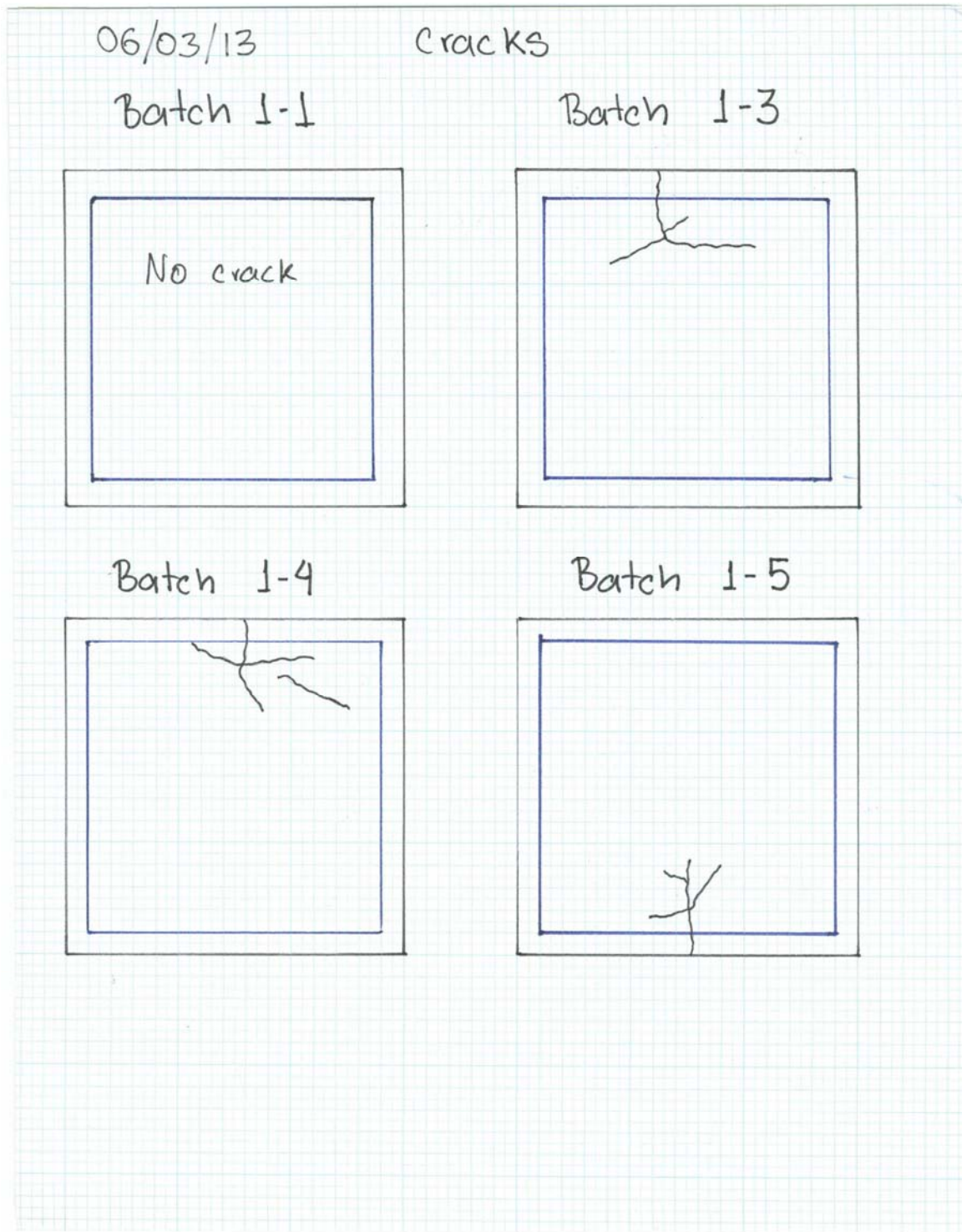


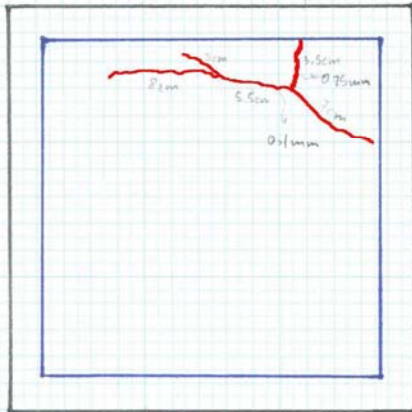
Figure 47 Crack by inspection day for batch 1 and 2



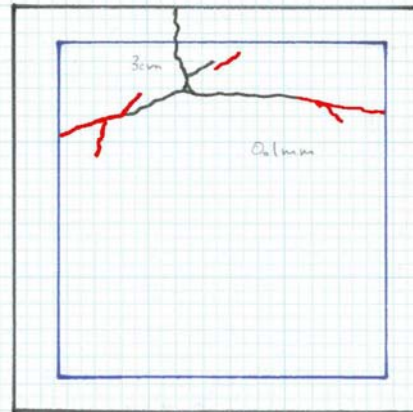
06/12/13

CRACKS

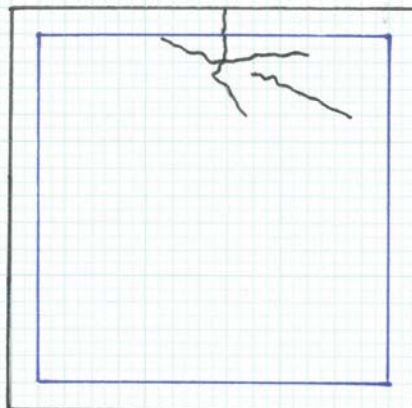
Batch 1-1



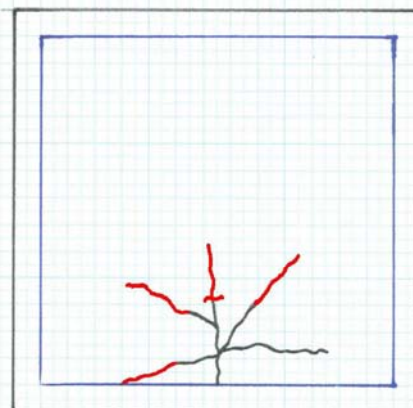
Batch 1-3



Batch 1-4



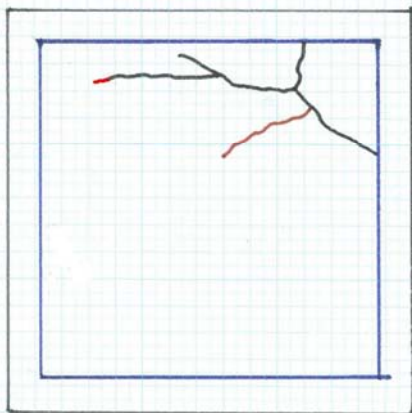
Batch 1-5



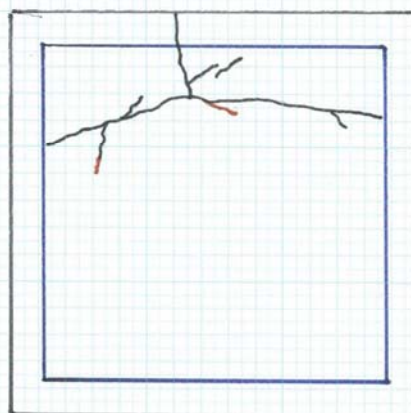
06/20/13

Cracks

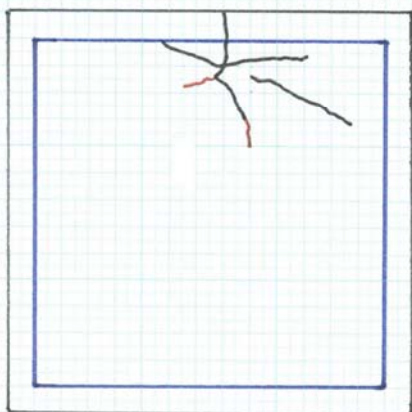
Batch 1-1



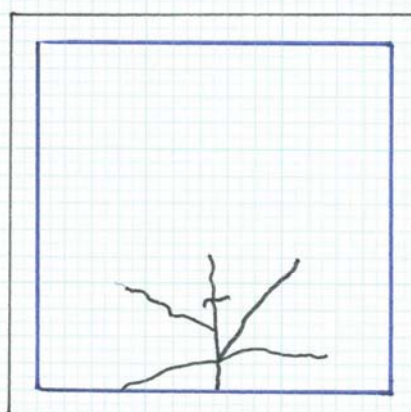
Batch 1-3



Batch 1-4



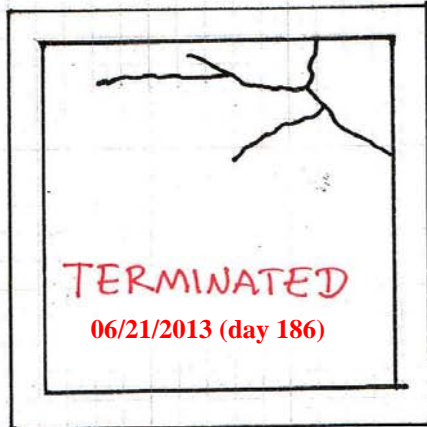
Batch 1-5



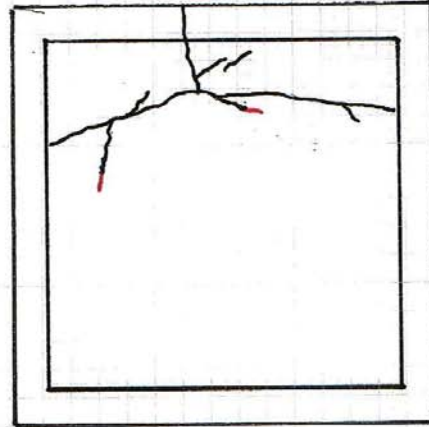
06/28/13

Cracks

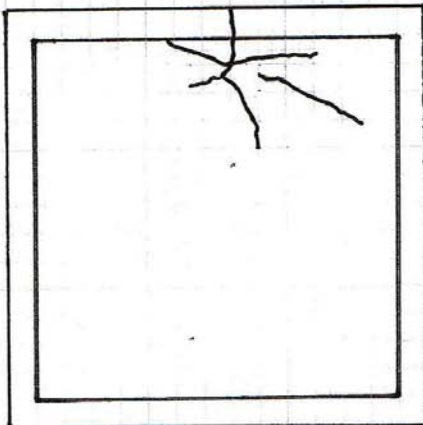
Batch 1-1



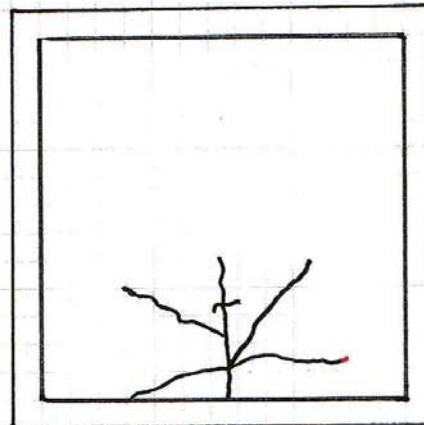
Batch 1-3



Batch 1-4



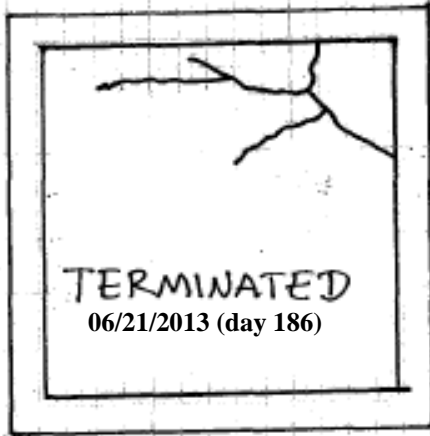
Batch 1-5



07/05/13

Cracks

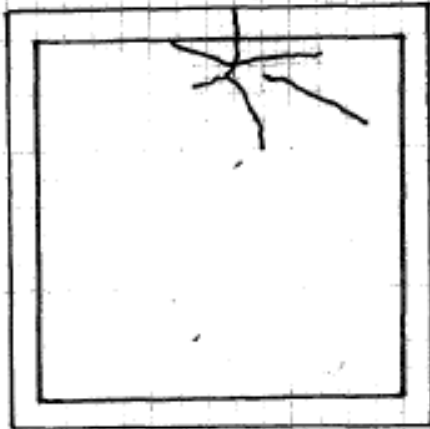
Batch 1-1



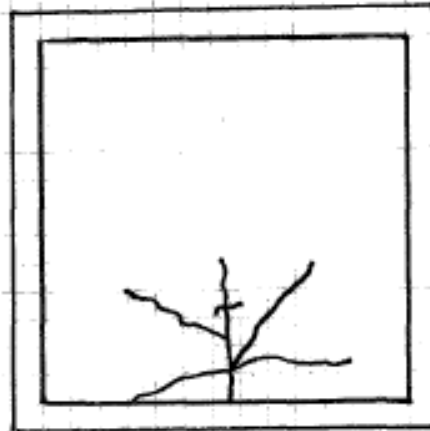
Batch 1-3



Batch 1-4



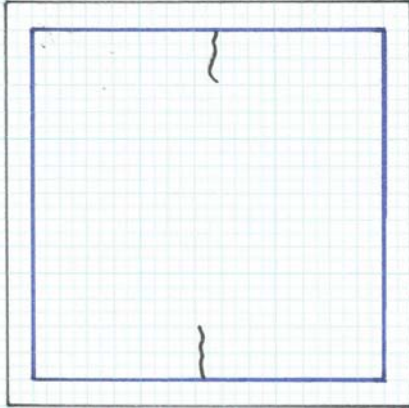
Batch 1-5



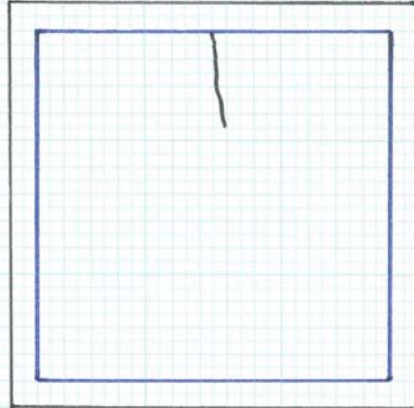
06/03/13

Cracks

Batch 2-1



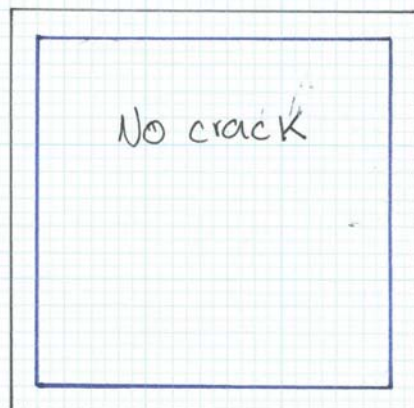
Batch 2-4



Batch 2-5



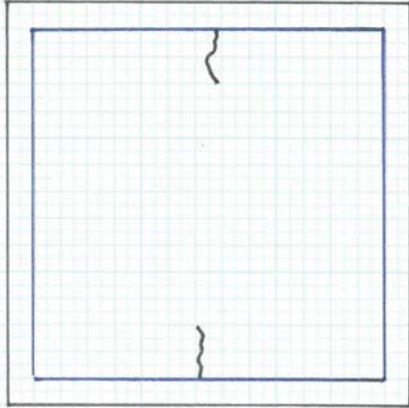
Batch 2-3



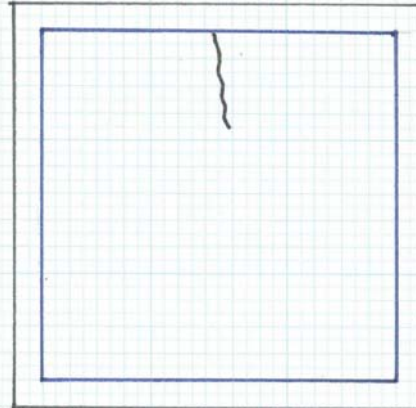
06/12/13

CRACKS

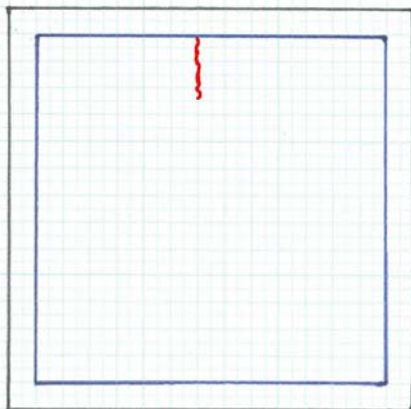
Batch 2-1



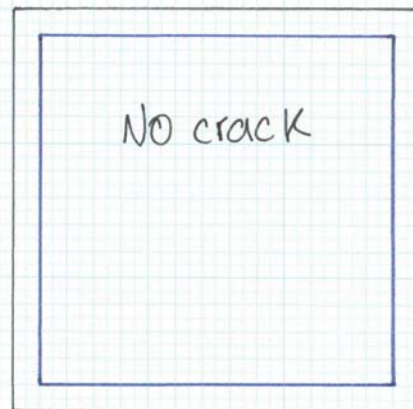
Batch 2-4



Batch 2-5



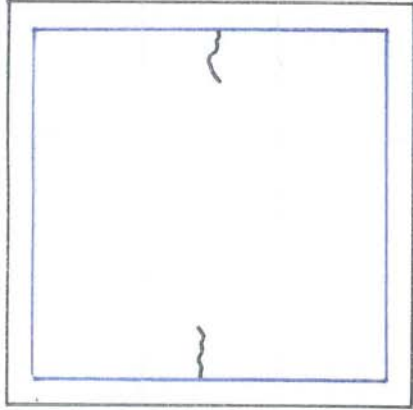
Batch 2-3



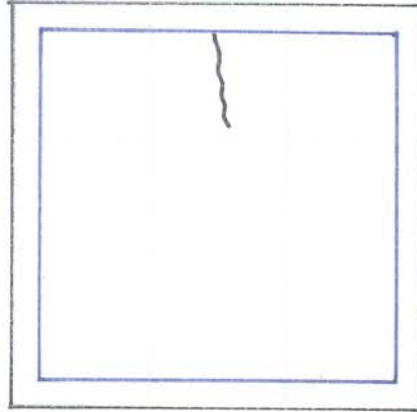
06/20/13

CRACKS

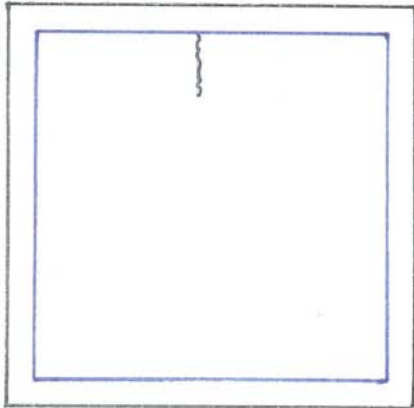
Batch 2-1



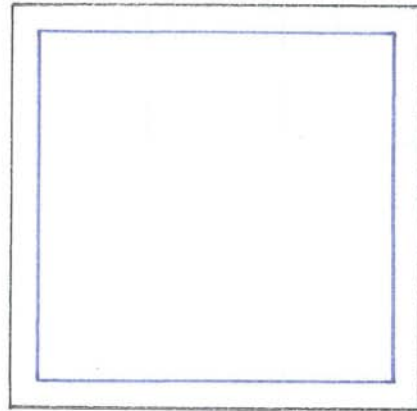
Batch 2-4



Batch 2-5

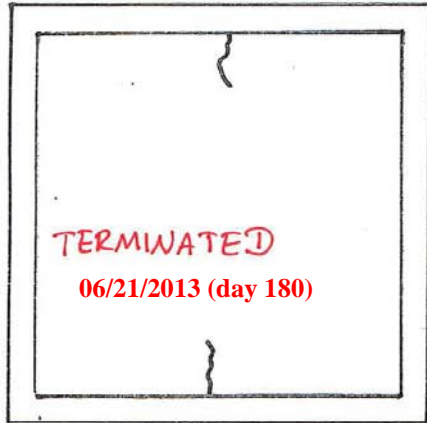


Batch 2-3

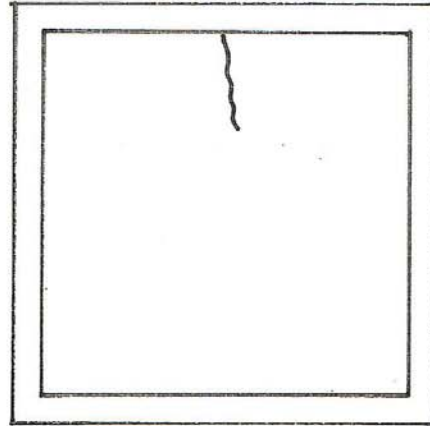


06/28/13

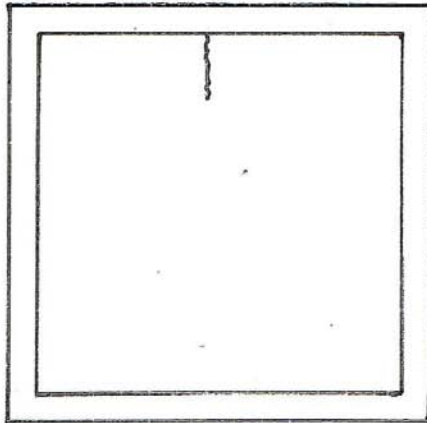
Batch 2-1



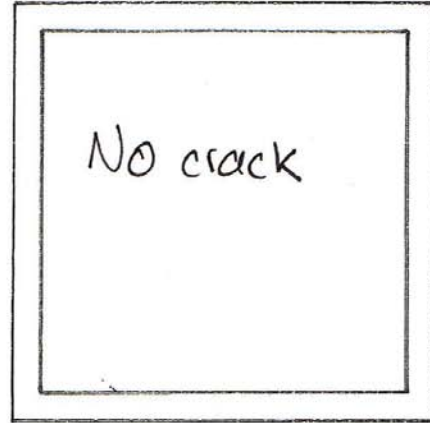
Batch 2-4



Batch 2-5



Batch 2-3

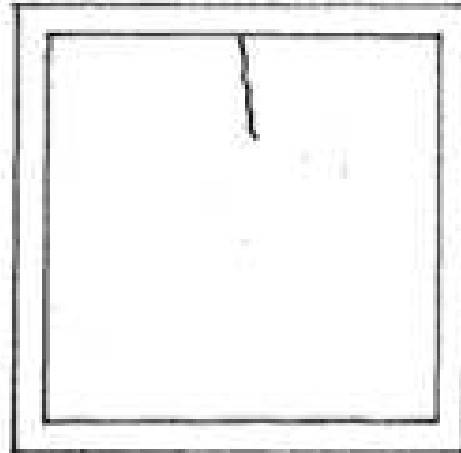


07/05/13

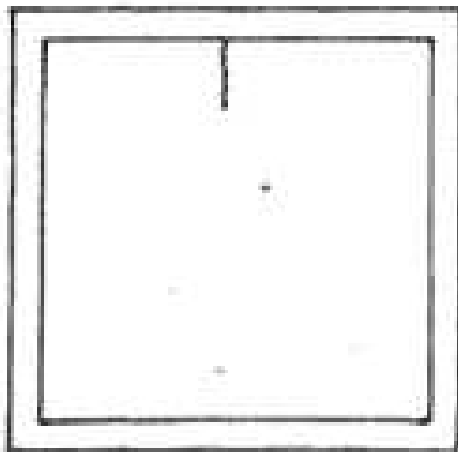
Batch 2-1



Batch 2-4



Batch 2-5



Batch 2-3



Figure 48 Autopsy and visual examination of bottom rebars batch 1-1

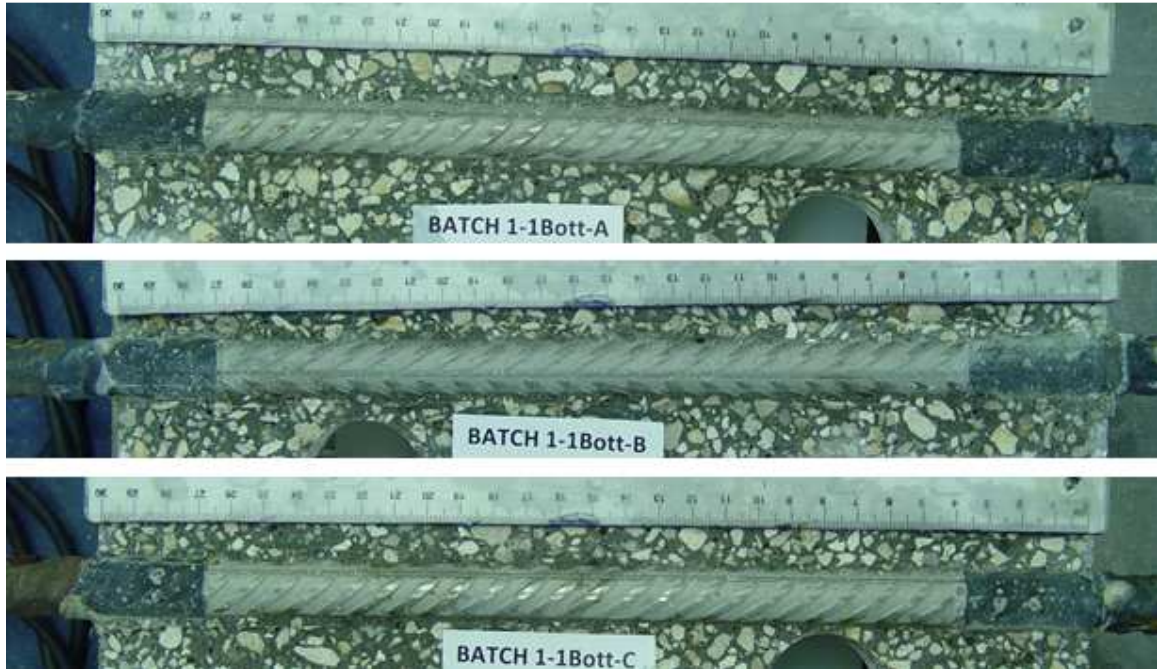
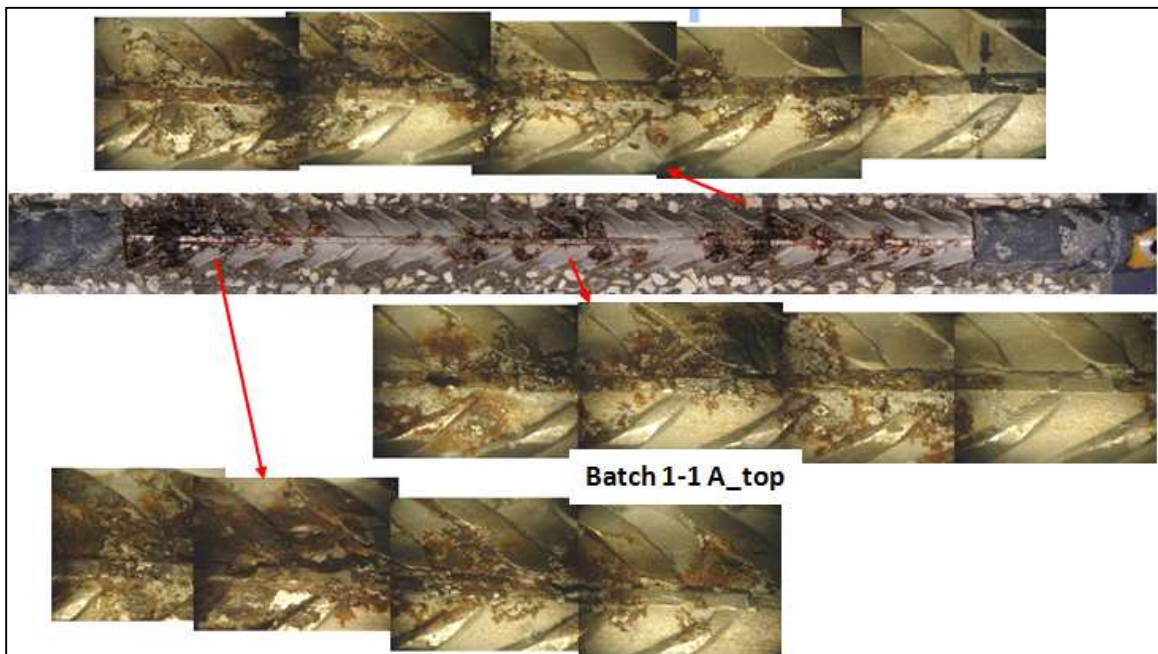


Figure 49 Close-up picture of sample batch 1-1A rebar before and after cleaning



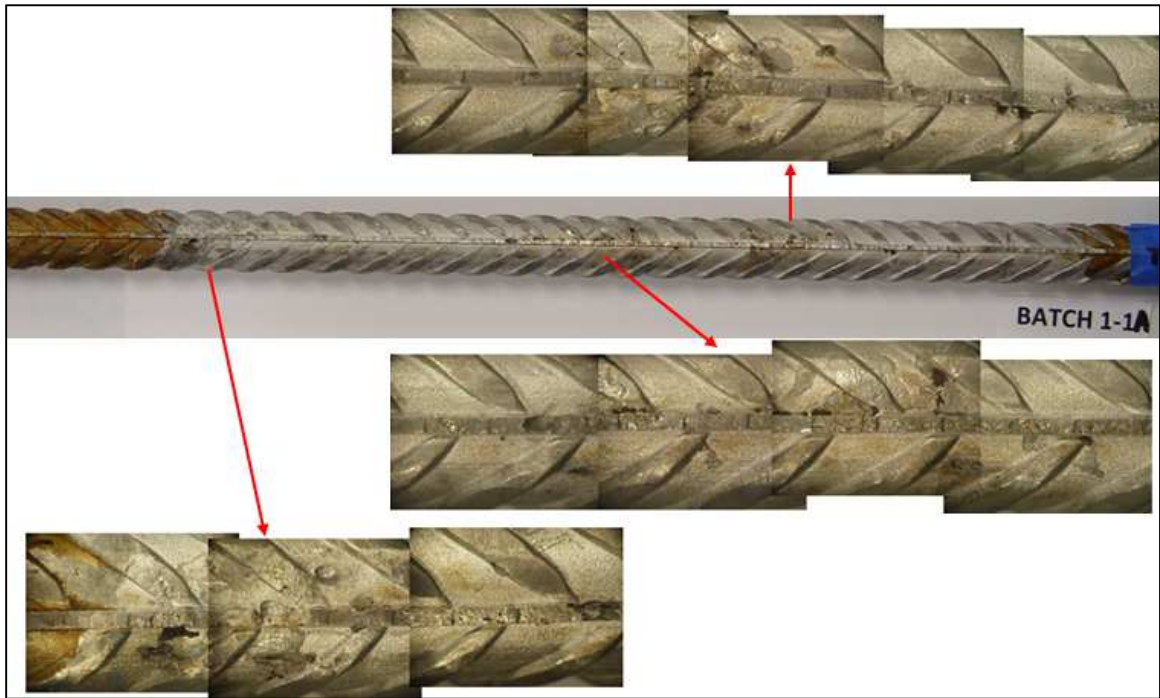
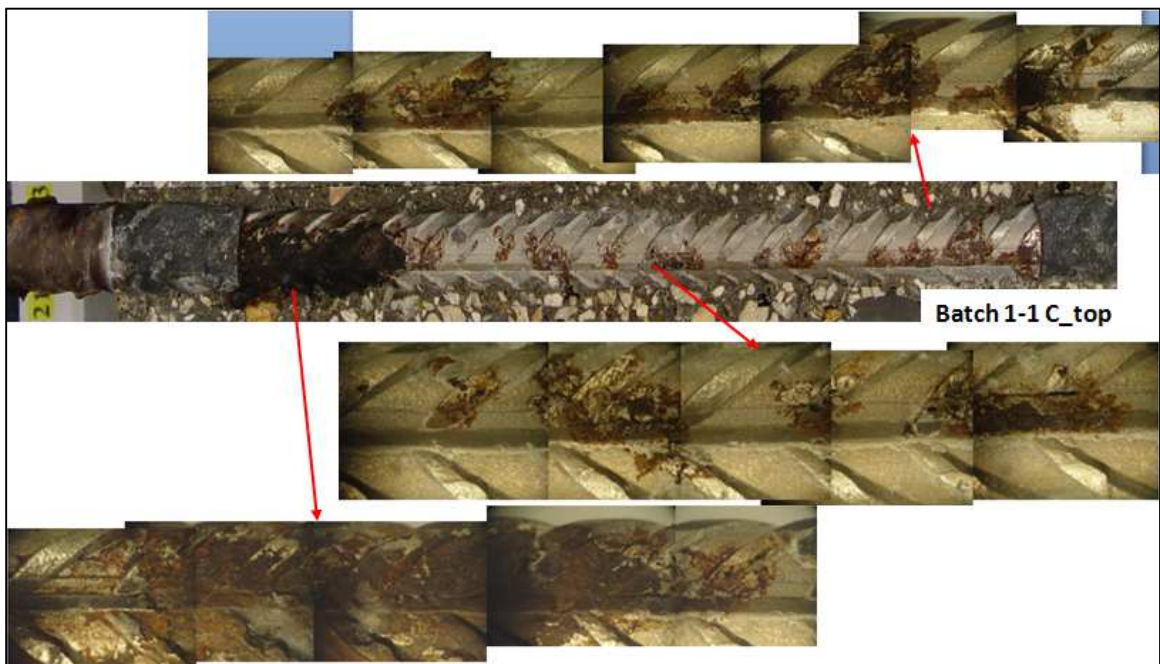


Figure 50 Close-up picture of sample batch 1-1C rebar before and after cleaning



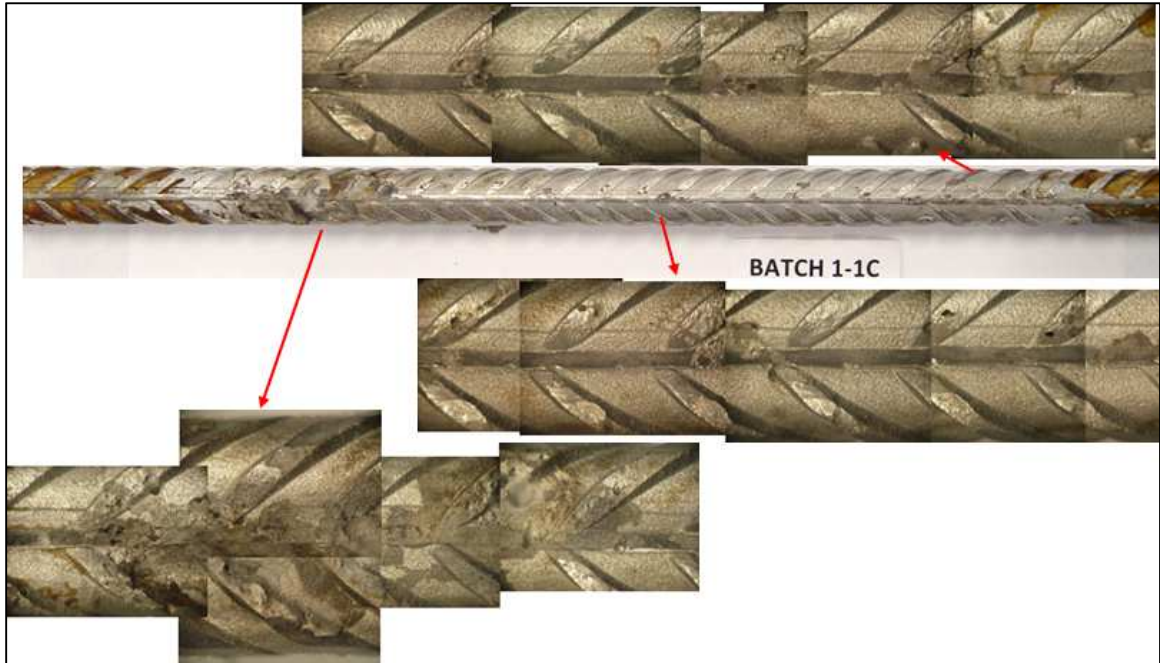


Figure 51 Autopsy and visual examination of bottom rebar batch 1-2

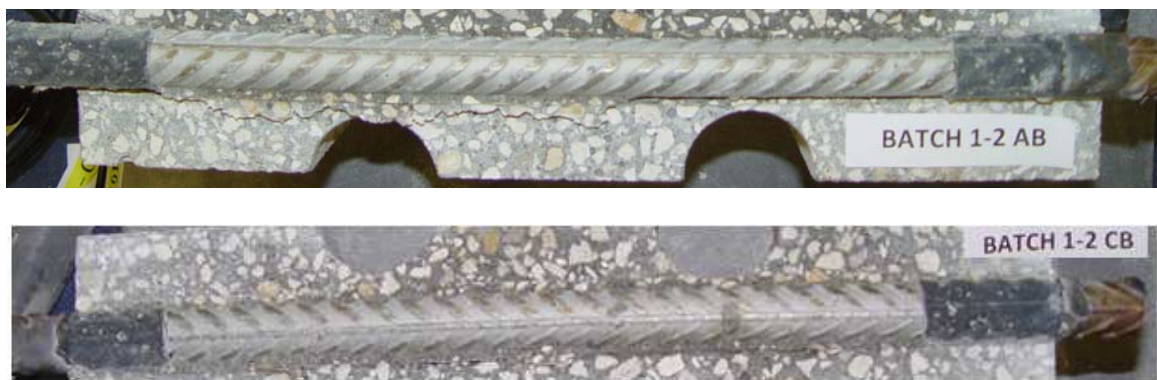


Figure 52 Close-up pictures before and after cleaning for batch 1-2

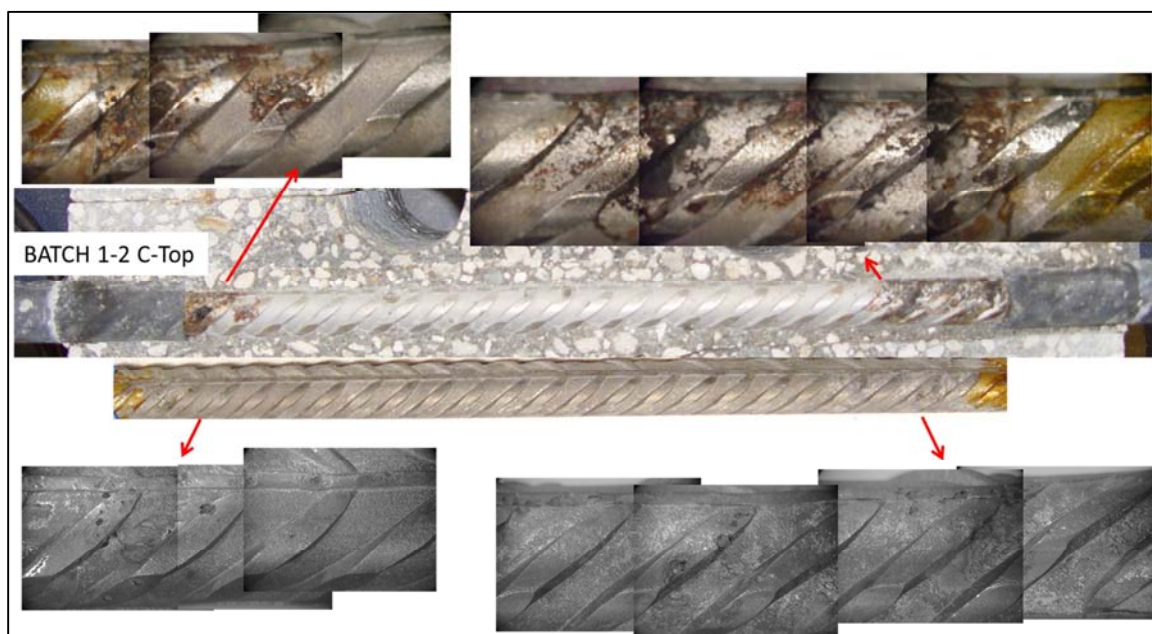
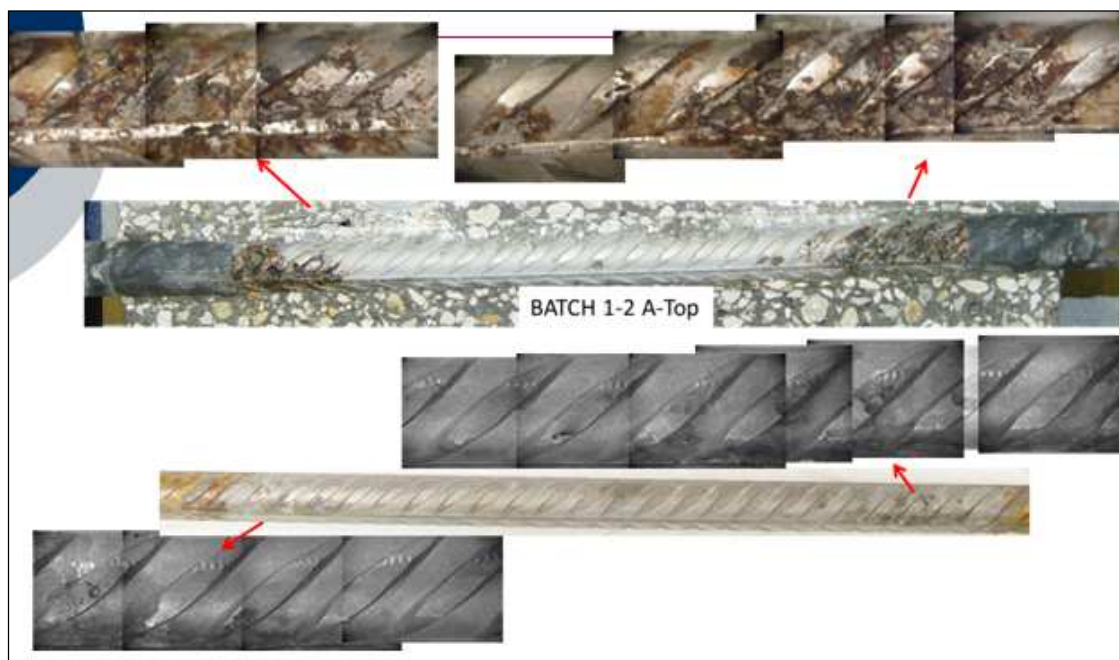


Figure 53 Autopsy and visual examination of bottom rebars batch 2-1

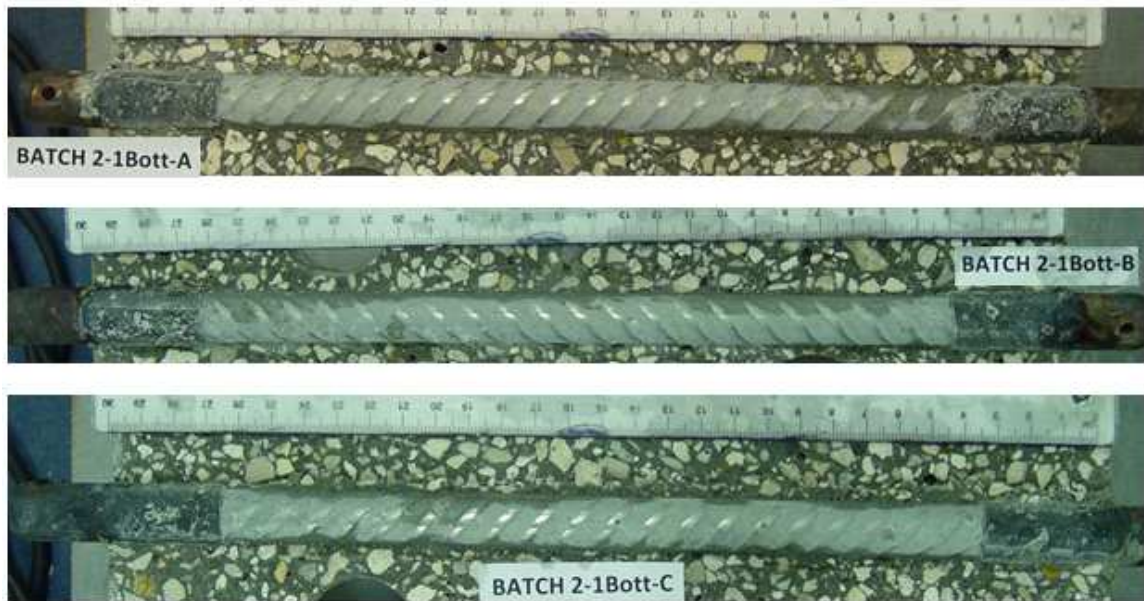
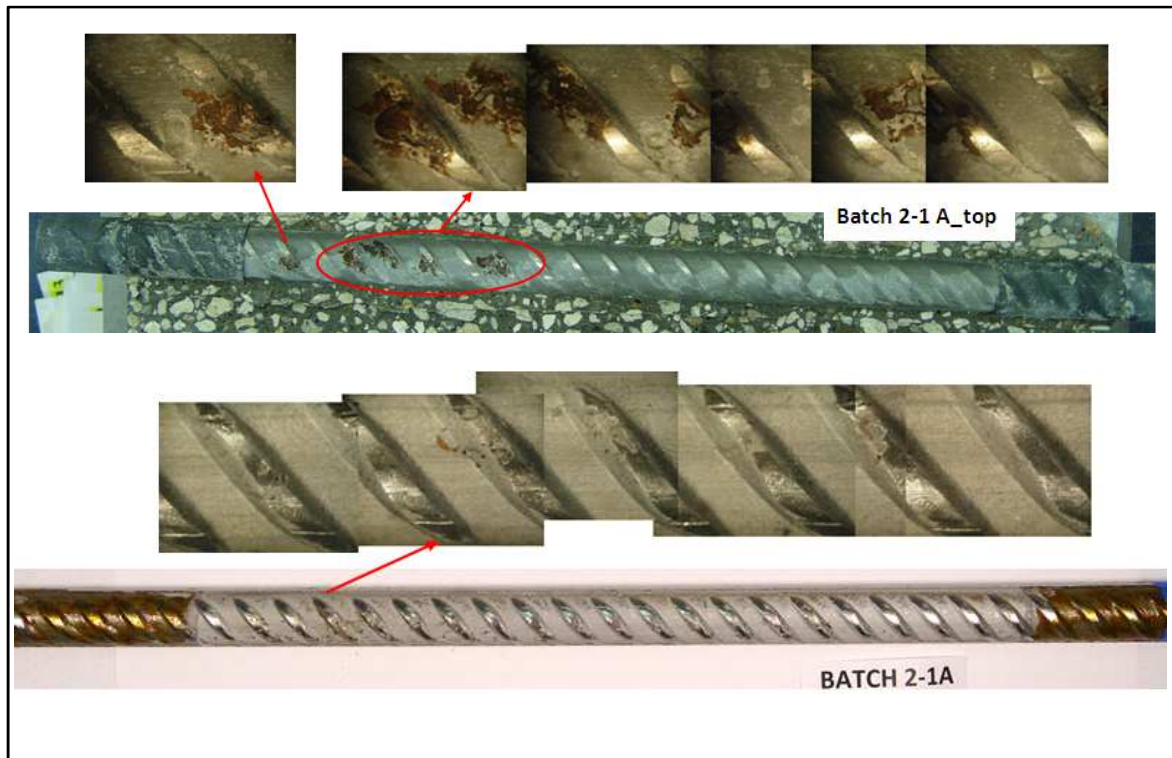


Figure 54 Close-up pictures before and after cleaning for batch 2-1



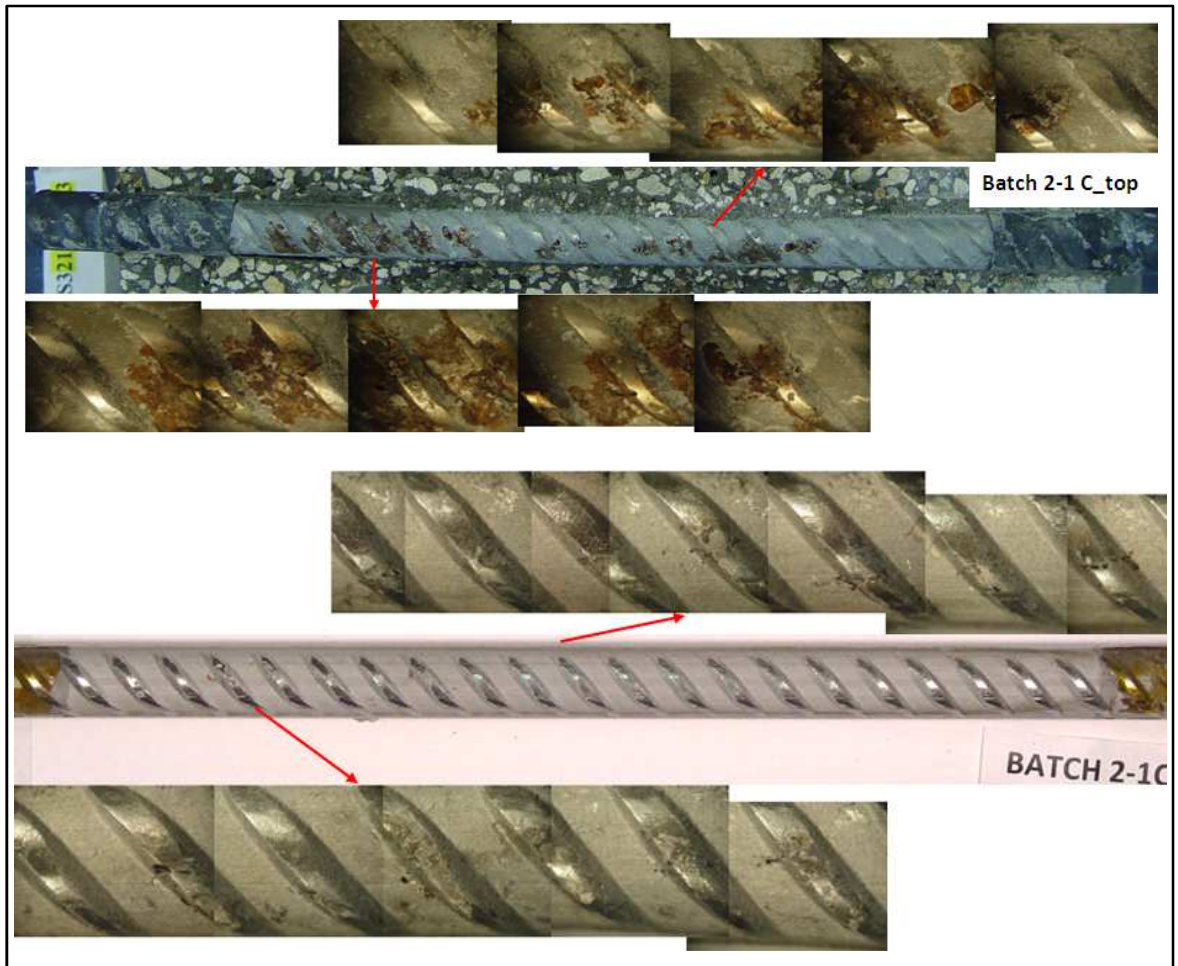
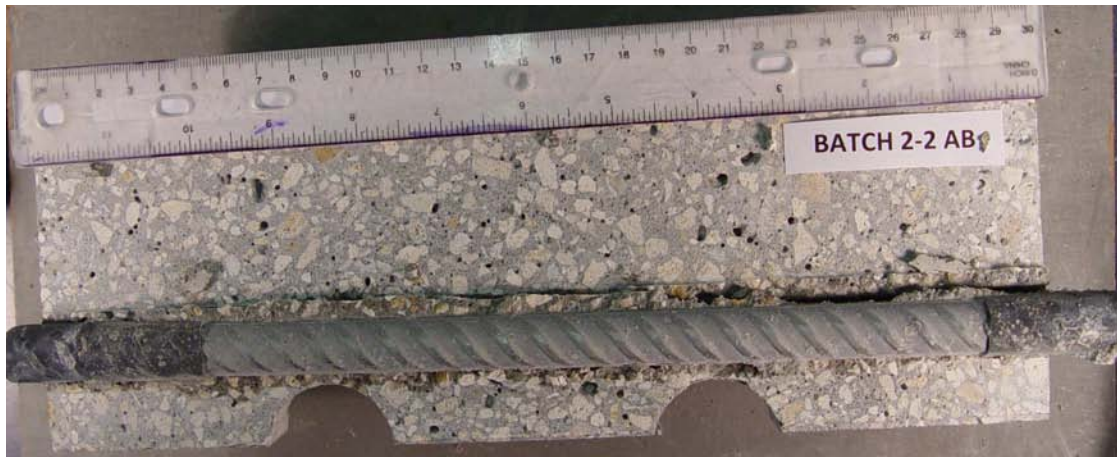


Figure 55 Pictures Autopsy bottom rebars for batch 2-2



7 APPENDIX B.

Chlorite Analysis:

Blank Sample procedures:

1. Fill a 250 mL beaker to 100 mL with DI water.
2. Add 1 mL of low-level ISA solution.
3. Add a magnetic stir stick to the beaker and place on the magnetic stirrer.
4. Place clean electrode in solution.
5. Add 1 mL of 0.01 N Silver-Nitrate and take a reading once stable.
6. Add 0.5 mL of 0.01 N Silver-Nitrate and take a reading.
7. Repeat step 6 three more times.
8. Input the data into Gran's Chloride Analysis program. Reading should be between ± 0.1 mL. If correct "Yes" will be displayed. In the event "No" is displayed repeat steps 1-7.

Titration Procedures of Chloride Concentration:

1. Proper protection gear is to be worn throughout the procedure.
2. Glass-ware, instrumentation, and any other item that will be used shall be cleaned properly.
3. Label all beakers to be used.
4. Weigh 0.9 grams of the sample (for samples that are thought to have lower concentrations of chlorides the sample weight should be increased).
5. Add a small amount (~15mL) of distilled (DI) water to beaker so that the powder is completely submerged.
6. Add 20mL of 1:12 Nitric acid solution to the beakers.
7. Pre-heat hot plate to medium-high.
8. Place beakers on hot-plate with glass lid on top. Constantly monitor the specimens as it will be necessary to add DI water to prevent evaporation.
9. Remove samples from hot-plate when the solution becomes light yellow (~10 min.).
10. Let the samples cool to room temperature.
11. Use DI water to clean the lid and the beaker's walls.
12. Fill the beakers with DI water until the solution reaches 100mL.
13. A stir bar should be added to each beaker.
14. The Dual-Channel reference electrode readout shall be set to absolute mV.
15. Place beaker on stir plate.
16. Place Silver-Sulfide reference electrode in solution.

17. Add Silver-Nitrate solution until the potential ranges between just above the potential found for the blank sample.
18. Add 0.5 mL to the solution and wait for a stable reading.
19. Repeat step 18 four more times.

REFERENCE

- [1] F. Presuel-Moreno, R. G. Powers, W. H. Hartt, "Corrosion Resistant Alloys for Reinforced Concrete," Florida Department of Transportation Research Center, Tallahassee, 2008.
- [2] J. R. S. M. F. Hurley, "Threshold Chloride Concentrations of Selected Corrosion-Resistant Rebar Materials Compared to Carbon Steel," *Corrosion* 62, pp. 892-904, 2006.
- [3] B. Sederholm, J. almqvist, S. Randstrom, "Corrosion Properties of Stainless Steel as Reinforcement in Concrete in Swedish Outdoor Environment," in *NACE International Corrosion 2009 Conference & Expo*, Houston, 2009.
- [4] Jhon R. Scully, M. F. Hurley, "Investigation of the Corrosion Propagation Characteristics of New Metallic Reinforcing Bars," VA Transportation Research Council, Charlottesville, 2007.
- [5] M. Schönning, S. Randström, M. Adair, "Adaption of EN 480-14:2006 as a Test Method for Determining a Critical Chloride Threshold Level for Stainless Steel Rebar," in *Eurocorr 2011*, Stockholm, Sweden, 2011.
- [6] S. Randstrom, M. Amen, R Pettersson, M Adair, "Reproducibility of Critical Chloride Threshold Leves for Stainless Steel Reinforcement," Outokumpu Stainless Ltd., Sweden, 2010.
- [7] E. M. Sanchez, Pitting Potential of High Performance Duplex Stainless Steels Reinforcements, Boca Raton: Florida Atlantic University, 2011.
- [8] Y. Liu, Accelerated Curing of Concrete with High Volume Pozzolans-Resistivity, Diffusivity and Compressive Strength, Boca Raton: Florida Atlantic University, 2012.

- [9] Luca Bertolini, Bernhard Elsener, Pietro Pedferri, Rob P. Polder, "Electrochemical Aspects," in *Corrosion of Steel in Concrete*, Weinheim, WILEY-VCH GmbH & Co. KGaA, 2004, pp. 100 - 123.
- [10] C. Castellote, C. Andrade, C. Alonso, "Accelerated simultaneous determination of the chloride threshold and of the non-stationary diffusion coefficient values," *Corrosion Science*, vol. 44, no. 11, pp. 2409-2424, 2002.
- [11] Luca Bertolini, Bernhard Elsener, Pietro Pedferri, Rob P. Polder, "Transport Processes in Concrete," in *Corrosion of Steel in Concrete*, Weinheim, WILEY-VCH GmbH & Co. KGaA, 2004, pp. 21 - 47.
- [12] S. M. Alvarez, A. Bautista, F. Velasco, "Corrosion behaviour of corrugate lean duplex stainless steel in simulate concrete pore solution," *Corrosion Science*, vol. 53, pp. 1748 - 1755, 2011.
- [13] C. Castellote, C. Andrade, "Assessment of the behavior of concrete in the initiation period of chloride induced corrosion of rebars," in *Concrete Repair, Rehabilitation and Retrofitting II*, 2011.
- [14] S. W. Dean, "Electrochemical Methods of Corrosion Testing," in *Electrochemical Techniques for Corrosion*, Houston, National Association of Corrosion Engineers, 1977, pp. 52 - 57.
- [15] Luca Bertolini, Bernhard Elsener, Pietro Pedferri, Rob P. Polder, "Chloride-induced in Concrete," in *Corrosion of Steel in Concrete*, Weinheim, WILEY-VCH GmbH & Co. KGaA, 2004, pp. 91 - 108.
- [16] R. R. Hussain, T. Ishida, M. Wasim, "Oxygen Transport and Corrosion of Steel in Concrete under Varying Concrete Cover, w/c, and Moisture," *ACI Materials Journal*, vol. 109, no. 1, pp. 3 -10, 2012.
- [17] D. Trejo, R.G. Pillai, "ccelerated Chloride Threshold testing: Part II – Corrosion-Resistant reinforcement," *CI Materials Journal*, vol. 101, no. 1, pp. 57 - 64, 2004.
- [18] D. Trejo, R.G. Pillai, "Accelerated Chloride Threshold testing: Part I – ASTM A 615 and A 706 Reinforcement," *ACI Materials Journal*, vol. 100, no. 6, pp. 519 - 527, 2003.

- [19] F. Presuel-Moreno, "An accelerate approach to study corrosion initiation and propagation on specimens prepared with CRA rebars," in *NACEInternational Corrosion 2013*, Orlando, 2013.
- [20] Nordtest, "492, NT Build, Chloride migration coefficient from non-steady-state migration experiment," Nordtest, Spoo, Finland, 1999.
- [21] FDOT, "Florida Method of Test For Determining Low-Levels of Chloride in Concrete and Raw Material in FM 5-516," FDOT, Florida, 2000.
- [22] Stanley C. Kranc, Alberto A. Sagues, and Francisco J. Presuel-Moreno, "Decreased Corrosion Initiation Time of Steel in Concrete due to Reinforcing Bar Obstruction of Diffusional Flow," *Materials Journal*, vol. 99, no. 1, pp. 51 - 53, 2002.
- [23] L. Bertolini and M. Gastaldi, "Corrosion Resistance of Low Nickel Duplex Stainless Steel Rebars," *Materials and Corrosion*, vol. 62, no. 2, pp. 120 -129, 2011.
- [24] F. Presuel-Moreno, "FHWA/Florida DOT Research on Alternative CRRB's Corrosion Resistant Alloys for Steel Reinforcement in Concrete," in *Corrosion Resistant Reinforcing Bar (CRRB) Seminar, organized by the FHWA and Florida DOT*, Tampa, 2012.
- [25] E. Busba and A.A. Sagues, "Critical localize corrosion penetration of steel reinforcement for concrete cover cracking," in *NACE Corrosion 2013* , Orlando, 2013.
- [26] A. Torres-Acosta and A. A. Sagues, "concrete cracking by localized steel corrosion - geometry effects," *ACI Materials Journal*, vol. 101, no. 6, pp. 501-507, 2004.